Extracellular Delivery of Functional Mitochondria Rescues the Dysfunction of CD4$^+$ T Cells in Aging.

Colwyn A. Headley[1,2,6], Shalini Gautam[1], Angelica Olmo-Fontanez[3], Andreu Garcia-Vilanova[3], Varun Dwivedi[1], Anwari Akhter[3], Alyssa Schami[3], Kevin Chiem[4], Russell Ault[1,2], Hao Zhang[5], Hong Cai[5], Alison Whigham[1], Jennifer Delgado[1], Amberlee Hicks[1], Philip S. Tsao[6], Jonathan Gelfond[7], Luis Martinez-Sobrido[4], Yufeng Wang[5], Jordi B. Torrelles[3] & Joanne Turner[1].

[1] Host-Pathogen Interactions Program, Texas Biomedical Research Institute, San Antonio, Texas 78227, USA
[2] Biomedical Sciences Graduate Program, The Ohio State University, Columbus, Ohio 43201, USA.
[3] Population Health Program, Texas Biomedical Research Institute, San Antonio, Texas, 78227, USA
[4] Disease Intervention & Prevention Program, Texas Biomedical Research Institute, San Antonio, Texas, 78227, USA
[5] Department of Molecular Microbiology and Immunology, South Texas Center for Emerging Infectious Diseases, The University of Texas at San Antonio, San Antonio, TX 78249, USA
[6] Stanford Cardiovascular Institute, Stanford University School of Medicine, Stanford, CA, 94305
[7] UT-Health San Antonio, Department of Epidemiology & Biostatistics, San Antonio, Texas 78229, USA

Correspondence: Dr. Joanne Turner**;** joanneturner@txbiomed.org; Dr. Jordi Torrelles; jtorrelles@txbiomed.org.

Short running title: Mitochondrial transfer boosts the functionality of CD4$^+$ T cells from old mice and the elderly.

Keywords: Aging, Mitochondrial Stress, ROS, CD4$^+$ T cells, Immunometabolism, Oxidative Stress, Immunology, Adaptive Immunity

Abstract

Mitochondrial dysfunction alters cellular metabolism, increases tissue oxidative stress, and may be principal to the dysregulated signaling and function of $CD4^+$ T lymphocytes in the elderly. In this proof of principle study, we investigated whether the transfer of functional mitochondria into $CD4^+$ T cells that were isolated from old mice (aged $CD4^+$ T cells), could abrogate aging-associated mitochondrial dysfunction, and improve the aged $CD4^+$ T cell functionality. Our results show that the delivery of exogenous mitochondria to aged non-activated $CD4^+$ T cells led to significant mitochondrial proteome alterations highlighted by improved aerobic metabolism and decreased cellular mitoROS. Additionally, mito-transferred aged $CD4^+$ T cells showed improvements in activation-induced TCR-signaling kinetics displaying markers of activation (CD25), increased IL-2 production, enhanced proliferation *ex vivo*. Importantly, immune deficient mouse models (RAG-KO) showed that adoptive transfer of mito-transferred naive aged $CD4^+$ T cells, protected recipient mice from influenza A and *Mycobacterium tuberculosis* infections. These findings support mitochondria as targets of therapeutic intervention in aging.

1. Introduction

Biological aging positively correlates with acute and chronic microbial infections and diseases that are of increased severity, poor response to vaccines, increased incidence of autoimmunity, and is accompanied by chronic low-grade inflammation [1-4]. $CD4^+$ T cells bridge communication between innate and adaptive arms of the immune system, and their dysfunction contributes to the aggravation of these aging-associated changes. The collective pool of naïve, memory, and effector $CD4^+$ T cells succumb to aging-associated perturbations. For example, thymic involution stunts the generation of properly educated naïve $CD4^+$ T cells [5-8]. $CD4^+$ memory T cells generated later in life function at subpar levels compared to those generated in younger years [5, 8-10]. Moreover, the kinetics of $CD4^+$ effector T cells (*i.e.* activation and resolution) in aged mice are enervated [11, 12].

Mitochondrial activity orchestrates a significant number of $CD4^+$ T cell signaling events, including shifts in metabolism and ATP production, intracellular Ca^{2+} mobilization, gene induction (NFAT, NF-κB, and AP-1), and production of reactive oxygen species (ROS) [13-23]. Perturbations in T cell intracellular signaling networks are likely central to the collective dysregulation and dysfunction observed in T cells of the elderly [24-27]. Indeed, redox dysregulation due to aging-associated mitochondrial dysfunction might manifest as disturbances in T cell function including homeostasis, activation, proliferation, and their ability to modulate of inflammation [28].

The optimum levels of ROS necessary for the induction of $CD4^+$ T cell signaling cascades are mainly generated as byproducts of oxidative phosphorylation (Ox-Phos). Ox-Phos occurs on the inner membrane of mitochondria via the electron transport chain (ETC) [15, 29-32]. Superoxide anions ($O_2^{\bullet}$-) and hydrogen peroxide (H_2O_2) are the principal mitochondrial ROS (mitoROS) essential for $CD4^+$ T cell redox signaling [15, 23, 33]. Due to its permeability, H_2O_2 serves as a secondary messenger molecule [33-36]. For instance, exposed thiol moieties (-SH) on proteins

can be oxidized by H_2O_2, altering protein conformation to favor either increases or decreases in enzymatic activities [37, 38]. Concurrently, mitoROS contribute to the formation of other increasingly destructive ROS. For example, $O_2^{\bullet}$- can rapidly react with nitric oxide (NO) to form peroxynitrite (ONOO-), while H_2O_2 can react with $O_2^{\bullet}$-, transition metals, lipids, and proteins found within mitochondria and cells, propagating the generation of hydroxyl (OH•), and peroxyl (ROO•) radicals [30-32, 39-42]. Therefore, shifts in the concerted generation and elimination of mitoROS, as seen in many aged cells, tissues, and organs, contribute to abnormal mitochondrial function which in turn perpetuates redox dysregulation and subsequent T cell dysfunction [43, 44].

Cellular energy demand is dynamic, and mitochondria must continually fuse and fragment in response to available nutrients and biological stimuli [45-47]. Increases in mitoROS impact mtDNA stability; continual fusion and fission events may also propagate the inter-mitochondrial dissemination of damaged mtDNA [45, 48-52]. Improper translation and assembly of mtDNA encoded proteins, in turn, hinders proper ETC assembly. Often this is associated with increased mitochondrial electron leaks and excess formation of mitoROS, favoring a pro-oxidant intracellular environment [53-55]. In short, mitochondrial dysfunction manifests as quantifiable abnormalities in the assembly of the ETC, mitochondrial membrane potential, excessive production of mitoROS, and abnormal production of ATP via Ox-Phos [24, 53, 56]. These perturbations impact the metabolic fitness and the redox-sensitive signaling pathways of $CD4^+$ T cells [13, 25, 53, 57-60].

Therapeutic interventions that can simultaneously improve mitochondrial biogenesis and re-establish redox equilibrium in$CD4^+$ T cells may abrogate aging-associated T cell dysfunction [22, 27, 28, 61]. This proof-of-concept study assessed whether the exogenous delivery of functional mitochondria to $CD4^+$ T cells (mito-transfer) from old mice and elderly humans could re-establish the cellular redox balance and positively impact $CD4^+$ T cell function. Compared to non-manipulated $CD4^+$ T cells, mito-transfer remodeled the mitochondrial proteome of $CD4^+$ T cells;

improving their aerobic metabolism resulting in decreased mitoROS. Mito-transferred $CD4^+$ T cells from old mice also displayed enhanced intracellular phosphorylation of key proteins essential to TCR signal transduction, increased cellular production of cytokines including IL-2, increased the number of cells expressing CD25, and improved cellular proliferation after *ex vivo* activation. Importantly, the adoptive transfer of mito-transferred naïve $CD4^+$ T cells from old mice into Rag1-KO mice protected mice against influenza A and *Mycobacterium tuberculosis (M.tb)* infections. These results open the possibility for future translational studies into the immunological and therapeutic implications of directed mito-transfer in aged lymphocytes to re-establish their loss of function.

2. Methods

Mice - Specific pathogen-free C57BL/6 young (2 to 4 months) and old (18 to 24 months) mice were obtained from the National Institute on Aging, Charles River Laboratories (Wilmington, MA, USA), and The Jackson Laboratories (JAX, Bar Harber, ME, USA). Rag1-KO (B6.129S7-Rag1$^{tm1Mom/}$J, 10 weeks old) mice were obtained from JAX. Mice were housed in groups of 5 on individually ventilated cages and fed a standard chow diet, *ad libitum*, for the duration of the study. All procedures were approved by the Texas Biomedical Institutional Laboratory Animal Care and Use Committee (IACUC) under protocols 1608 MU and 1735 MU.

Isolation of $CD4^+$ T cells from mice - Young and old mice were euthanized by CO_2 asphyxiation, and spleens surgically excised. Isolated spleens were individually placed in 6 well plates containing 4 ml of chilled (4°C) complete DMEM and gently hand homogenized using sterile syringe stoppers. Spleen homogenate was passed through a 70 μm microfilter to remove large debris. The resulting single-cell suspensions were centrifuged for 5 min at 300 x *g* at 4°C and suspended in Gey's lysis buffer (8 mM NH_4Cl, 5 mM $KHCO_3$) for 1 min to lyse erythrocytes, and then neutralized with an equivalent volume of complete DMEM. Splenocytes were washed and

suspended in separation buffer (10 mM D-Glucose, 0.5 mM $MgCl_2$, 4.5 mM KCl, 0.7 mM Na_2HPO_4, 1.3 mM NaH_2PO_4, 25 mM $NaHCO_3$, 20 mM HEPES, 5 µM DETC, 25 µM deferoxamine) containing appropriate antibody-magnetic particles for positive selection (α-CD4), or negative selection (α-CD8, α-CD11b, α-CD109, α-CD24, α-CD45, α-CD49b, α-Ly-6G, α-$\chi\delta$ TCR, α-TER-119). The resulting population of $CD4^+$ T cells (85-95% purity) was used for downstream experiments.

Quantitation of intracellular ROS - For flow cytometry-based ROS experiments, $CD4^+$ T cells were incubated in media containing MitoSOX (5 µM) or CellROX (5 µM) for 30 min at 37°C, to measure mitochondrial and cytosolic ROS, respectively. Cells were washed twice with phosphate-buffered saline (PBS, pH 7.4) and stained with antibodies targeting surface proteins of interest (*i.e.* α-CD3, α-CD4, and α-CD69; 25 µg/ml) for 20 min before fixation in 2% paraformaldehyde. Flow cytometry-based ROS and other flow-based quantifications were performed on a BD-LSR II (BD Biosciences, NJ, USA) , BD FACs Symphony, Cyan or CytoFLEX LX (Beckman Coulter, CA, USA) flow cytometers. Data were analyzed using FlowJo (FlowJo LLC- BD, NJ, USA) and GraaphPad Prism ver. 9 (Graphpad Software, CA, USA).

For electron paramagnetic resonance (EPR)-based ROS experiments, $CD4^+$ T cells were probed for mitochondria-specific $O_2^{\bullet}$- (*mt*$O_2^{\bullet}$-) using Mito-Tempo-H. Briefly, $CD4^+$ T cells were incubated in EPR buffer (10 mM D-Glucose, 0.5 mM MgCl, 4.5 mM KCl, 0.7 mM Na_2HPO_4, 1.3 mM NaH_2PO_4, 25 mM $NaHCO_3$, 20 mM HEPES, 5 µM DETC, 25 µM deferoxamine), containing 100 µM Mito-Tempo-H, for ~45 min at 37°C. EPR spectra were obtained on a Bruker EMXnano ESR system (Bruker Corporation, MA, USA) using the following parameters: microwave frequency, 9.6 GHz; center field, 3430.85 G; modulation amplitude, 6 G; microwave power at 25.12 mW; conversion time of 71.12 ms; time constant of 20 ms; sweep width of 100 G; receiver gain at 1.0

x 10^5; and a total number 5 of scans. The Two-Dimensional (2-D) spectra were integrated, baseline corrected, and analyzed using spin-fit and GraphPad software.

Isolation of mouse embryonic fibroblasts - Mouse embryonic fibroblasys (MEFs) were isolated from 12-14 days post-coitum C57BL/6 mice as described [62]. Briefly, mouse embryos were aseptically isolated, minced, and digested in 0.05% trypsin and crude DNase solution for 30 min at 37°C, 5% CO_2, in a humidified incubator. Primary MEFs were cultured in sterile T-150 flasks (Corning, NY, USA), in 50:50 F12/DMEM (Corning) supplemented with 10% FBS, 1% HEPES, 2% NEAA, 1 mM sodium pyruvate, 2 mM L-glutamine, and 100 µg/ml primocin. MEFs were sub-passaged as necessary, with MEFs from passages 2-3 being used for all experiments.

Mitochondrial isolation and transfer - Mitochondria were isolated from donor MEFs and centrifuged into $CD4^+$ T cells using a published protocol [63]. Briefly, MEFs were homogenized in SHE buffer [250 mM sucrose, 20 mM HEPES, 2 mM EGTA, 10 mM KCl, 1.5 mM $MgCl_2$, and 0.1% defatted bovine serum albumin (BSA)], containing complete Minitab protease inhibitor cocktail (Sigma Alrich, MO, US). The cell homogenates weree centrifuged at 800 x *g* for 3 min at 4°C to remove cellular debris. The resulting supernatant was recovered and centrifuged at 10,000 x *g* for 5 min to pellet isolated mitochondria. The $CD4^+$ T cells and isolated mitochondria were suspended in 150 µL cold PBS in V-bottom 96 well plates, and plates were centrifuged at 1,400 x *g* for 5 min at 4°C. After centrifugation, cells were washed 2-3 times with cold PBS before further experimentation. Independent of mito-transfer, all experimental groups were centrifuged accordingly.

Determination of cardiolipin content - Mitochondrial cardiolipin content was determined using a commercially available cardiolipin assay kit (BioVision Inc, CA, USA) per the manufacturer's instructions. Briefly, isolated mitochondria were stained with a cardiolipin-specific fluorometric

probe 1,1,2,2-tetrakis[4-(2-trimethylammonioethoxy)-phenyl]ethene tetrabromide, and quantified against a cardiolipin standard curve.

Transmission electron microscopy (TEM) - $CD4^+$ T cells were fixed in PBS containing 4% glutaraldehyde and 1% paraformaldehyde for 1 h, after which, cells were rinsed in PBS for 20 min. Samples were fixed in 1% Zetterqvist's buffered osmium tetroxide for 30 min followed by an alcohol gradient (70%, 95%, 100%) and propylene oxide dehydration (10 min per solution). Samples were blocked in 1:1 propylene oxide/resin for 30 min, and 100% resin for 30 min (at 25 psi). Samples were then polymerized overnight at 85°C and stained with 1% uracil acetate and alkaline lead citrate. Images were captured using a JEM-1400 transmission electron microscope (JEOL, MA, USA) at 25,000X and 50,000X magnification, and analyzed using FIJI software (ImageJ ver. 1.52p, NIH, MD, USA) [64].

Extracellular flux-based assays - Kinetic analysis of cellular glycolysis and oxygen consumption and the rate of ATP production was accomplished through the use of the Extracellular Flux Analyzer XF^e96 (Agilent/Seahorse, CA, USA). Briefly, 2.5 x 10^5 $CD4^+$ T cells were plated onto poly-D-Lysine pre-coated (0.1 mg/ml) XF^e96 microplates. Using real-time injections, the rates of mitochondrial respiration, glycolysis, and ATP production were measured via oxygen consumption rate (OCR, pmol/min) and extracellular acidification rate (ECAR, mPh/min).

For mitochondrial stress and ATP production assays, cells were placed in XF assay media supplemented with 5.5 mM D-glucose, 2 mM L-glutamine, and 1 mM sodium pyruvate. Sequential injections of oligomycin (1 µM; O), carbonyl cyanide-4-(trifluoromethoxy)phenylhydrazine (1.5 µM; FCCP), and rotenone: antimycin (1 µM, R/A) were used for the mitochondrial stress test, while injections of O and R/A alone were used to determine ATP production rate.

For the glycolysis stress test, cells were assayed in D-Glucose deficient XF media containing L-glutamine, and injections of glucose (10 mM), oligomycin (1 µM), and 2-deoxyglucose (50 mM; 2-DG) were used. For the glycolytic rate assay, cells were assayed in complete XF media and sequential injections of R/A (1 µM) and 2-DG were used.

For acute $CD4^+$ T cell activation assays, cells were placed in XF assay media supplemented with 5.5 mM glucose, 2 mM L-glutamine, and 1 mM sodium pyruvate. Sequential injections of PMA/Ionomycin and 2-DG were used to determine the kinetics of oxygen consumption and extracellular acidification after $CD4^+$ T cell activation.

Fluorescent glucose uptake assay - $CD4^+$ T cells were incubated in D-glucose-free DMEM for 20 min before the addition of complete DMEM supplemented with 50 µM 2-deoxy-2-[(7-nitro-2,1,3-benzoxadiazol-4-yl)amino]-D-glucose (2-NBDG), a fluorescent glucose analog, for 30 min. Cells were washed twice in cold PBS, surface stained (α-CD4, 25 µg/ml), fixed in 2% paraformaldehyde and intracellular levels of 2-NBDG were quantified by flow cytometry.

Cellular ATP levels - Cellular ATP was determined using a commercially available luminescent ATP detection kit (Abcam) per the manufacturer's instructions. Briefly, 0.5×10^6 $CD4^+$ T cells were mixed with the kit's detergent and ATP substrate followed by a 10 min incubation at RT. Samples were read using a luminescence microplate reader (Spectra Max M2, Molecular Devices, CA, USA). Absolute ATP concentrations were calculated using an ATP standard curve.

GLUT-1 expression - Cellular GLUT1 expression was measured by intracellular staining. Briefly, $CD4^+$ T cells were fixed and permeabilized using a commercially available kit (BD Biosciences) before intracellular staining with an anti-GLUT1 antibody (Abcam, ab195020, 1:100 dilution). $CD4^+$ T cells were washed twice and MFI of anti-GLUT1 antibody was detected by flow cytometry.

Quantitation of mitochondrial mass and mitochondrial viability/membrane potential - Cellular mitochondrial mass and potential were determined using commercially available probes MitoView Green (MTV-G; Biotium, CA, USA) and Mitotracker Deep Red (MTDR; Life Technologies, CA, USA), respectively. Antibody labeled (α-CD4) $CD4^+$ T cells were fixed in 2% paraformaldehyde before MTV-G staining (50 nM) for 30 min at RT or $CD4^+$ T cells were stained with MTDR (50 nm) for 20 min before fixation in 2% paraformaldehyde. MFI of MTV-G and $MTDR^+$ $CD4^+$ T cells was determined by flow cytometry.

Proteomics - Cell preparations and extracted mitochondria were lysed in a buffer containing 5% SDS/50 mM triethylammonium bicarbonate (TEAB) in the presence of protease and phosphatase inhibitors (Halt; Thermo Scientific) and nuclease (Pierce™ Universal Nuclease for Cell Lysis; Thermo Scientific). Aliquots normalized to 65 µg protein (EZQ™ Protein Quantitation Kit; Thermo Scientific) were reduced with tris(2-carboxyethyl) phosphine hydrochloride (TCEP), alkylated in the dark with iodoacetamide, and applied to S-Traps (mini; Protifi) for tryptic digestion (sequencing grade; Promega) in 50 mM TEAB. Peptides were eluted from the S-Traps with 0.2% formic acid in 50% aqueous acetonitrile and quantified using Pierce™ Quantitative Fluorometric Peptide Assay (Thermo Scientific).

On-line high-performance liquid chromatography (HPLC) separation was accomplished with an RSLC NANO HPLC system [Thermo Scientific/Dionex: column, PicoFrit™ (New Objective; 75 µm i.d.) packed to 15 cm with C18 adsorbent (Vydac; 218MS 5 µm, 300 Å)], using as mobile phase A, 0.5% acetic acid (HAc)/0.005% trifluoroacetic acid (TFA) in water; and as mobile phase B, 90% acetonitrile/0.5% HAc/0.005% TFA/9.5% water; gradient 3 to 42% B in 120 min; flow rate at 0.4 µl/min. Data-independent acquisition mass spectrometry (DIA-MS) was conducted on an Orbitrap

Fusion Lumos mass spectrometer (Thermo Scientific). A pool was made of all of the HPLC fractions (experimental samples), and 2 µg peptide aliquots were analyzed using gas-phase fractionation and 4-*m/z* windows (120k resolution for precursor scans, 30k for product ion scans, all in the Orbitrap) to create a DIA-MS chromatogram library [65] by searching against a panhuman spectral library [66]. Subsequently, experimental samples were blocked by replicate and randomized within each replicate. Injections of 2 µg of peptides were employed. MS data for experimental samples were also acquired in the Orbitrap using 12-*m/z* windows (staggered; 120k resolution for precursor scans, 30k for product ion scans) and searched against the DIA-MS chromatogram library generated. Scaffold DIA (ver. 1.3.1; Proteome Software) was used for all DIA data processing.

Western blots - Cells or extracted mitochondria were lysed by sonication in RIPA lysis buffer (25 mM Tris-HCl, pH 7.6, 150 mM NaCl, 1% NP-40, 1% sodium deoxycholate, 0.1% SDS, ThermoFisher) containing Minitab protease inhibitors (Sigma). The total protein quantity per sample was determined by BCA assay. Proteins (20 µg/sample) were resolved on 4–15% Mini-PROTEAN® TGX™ Precast Protein Gels (Biorad) and transferred to PVDF membranes (Biorad). To quantify ETC proteins, membranes were incubated overnight with the Total OX-PHOS Rodent Western Blot Antibody Cocktail (Abcam; 1:500) in 1% milk at 4°C. To quantify isolated mitochondria purity, membranes were incubated with Cytochrome C (Cell signaling; 1:500), α-COX IV (Abcam, 1:500), and α-PCNA (Abcam; 1:500). Membranes were washed and incubated with mouse IgG kappa-binding protein conjugated to horseradish peroxidase (m-IgGk-HRP, 1:4000) (Santa Cruz technologies) in 5% milk for 1 h at 4°C. Membranes were then stripped and probed for β-actin levels. Images were captured on a UVP ChemStudio 815 system (Analytik, Jena, DE).

Quantitation of intracellular thiols - Intracellular reduced glutathione levels were determined using commercially available fluorometric thiol probe thiol tracker Violet (Thermo Fisher) and the total glutathione (GSH) Detection Assay Kit (Abcam, MA, USA). $CD4^+$ T cells were stained with thiol-tracker violet (10 µM) for 30 min at 37°C. Cells were washed twice with PBS, stained with surface antibodies of interest (*i.e.* α-CD3, α-CD4, and α-CD69; 25 µg/ml) for 20 min, fixed in 2% paraformaldehyde, and data collected by flow cytometry. The total GSH detection assay was performed according to the manufacturer's directions.

Cytokine detection - The EliSpot and Luminex assays were used to measure the cellular production of cytokines. For the EliSpot assay, 5.0 x 10^4 $CD4^+$ T cells were serially diluted onto either α-IL-2 or α-IFNɣ sterile coated PVDF 96 well plates (BD Biosciences, NJ, USA). The $CD4^+$ T cells were then activated for 24 or 72 h in complete DMEM. After allotted time points, the EliSpot microplates were developed following the manufacturer's protocol and analyzed using an ImmunoSpot analyzer (Cellular Technology Limited, OH, USA). Individual spots are representative of individual cytokine-producing cells.

Briefly, 2.5 x 10^5 $CD4^+$ T cells were cultured in 96 well plates containing PMA/Ionomycin for 24 or 72 h, after which media were collected and measured for the presence of cytokines IL-2, IFNɣ, IL-4, IL-5, IL-10, IL-17/IL-17A, TNFα, and the chemokine CCL5/RANTES following the manufacture's protocol.

Proliferation Assay - $CD4^+$ T cell proliferation was determined by the Click-it EdU detection assay (Thermo Fisher) [67]. Briefly, 2.5 x 10^5 $CD4^+$ purified T cells were activated for 72 h in 600 µL cDMEM containing 50 µM 5-Ethynyl-2´-deoxyuridine (EdU) and αCD28 (0.05 µg/ml), in sterile 48 well plates precoated with 400 µL of αCD3 (0.5 µg/ml in PBS). EdU incorporation into DNA

from proliferating cells was detected by a fluorescent bioconjugate and flow cytometry. The assay was performed per the manufacturer's instructions.

Adoptive transfer of naïve CD4$^+$ T cells and infection of mice with influenza A or *M. tb* - Naïve CD4$^+$ T cells from old mice were isolated by negative magnetic bead selection. Non-manipulated naïve CD4$^+$ T cells or mito-transferred naïve CD4$^+$ T cells (~ 2.0 x 10^6 cells) were tail vein injected into Rag1-KO (n= 4 to 5 mice per group) in a final volume of 200 µl. A control group of Rag1-KO (n= 2 to 4 mice per group) were tail-vein injected with 200 µl of PBS.

Determination of influenza A-induced morbidity and mortality - Before and after infection with influenza A, mice were weighed and monitored daily for body weight change (% morbidity). Mice that lost 20% of their initial body weight were humanely euthanized (% mortality) [68, 69].

Determination of *M. tb* bacterial burden - At 21 days post-*M.tb* infection, the lung (local infection), and spleen (systemic infection) of infected mice were excised and homogenized in sterile PBS (Sigma). Homogenized organs were serially diluted and plated onto 150 mm x 20 mm sterile plates of 7H11 agar supplemented with OADC (oleic acid, albumin, dextrose, catalase) and incubated for 14 to 21 days at 37°C. *M.tb* CFU was counted and expressed as Log_{10} CFU per organ [70, 71].

Confocal Microscopy - *Z*-stack confocal images were obtained on a Leica Stellaris-8 microscope (Leica Camera AG, Wetzlar, GER) equipped with an HC PL APO CS2 63x/1.40 OIL objective. Fluorophores were detected using UV laser diode 405 nm (for α-CD4 Pacific Blue; Biolegend) and solid-state lasers 488nm (for Turbo-GFP tagged hexokinase 1 mitochondria (HK-GFP-mito); Horizon Discovery, MA, USA) and 641 nm (RedDot™2 nuclear stain (RD-2); Biotium), with pinhole set to 5.5 AU, in XYZ scan mode, using a scan speed of 400 Hz, 1x Zoom, and 1.575 µs

pixel dwell time. Post-processing was performed using the LAS X LIGHTNING ver.4.3.0.24308 (Leica Camera AG). Images were processed using ImageJ software.

mt-DNA copy number - The quantification of mitochondrial DNA (mt-DNA) copy number in $CD4^+$ T cells was done using the commercially available mouse mitochondrial DNA copy number kit (Detroid R&D, MI, USA), following the manufacturer's instructions.

Bioinformatic Analysis - Gene ontology analysis was performed using DAVID [72, 73]. The Bonferroni, Benjamini, and false discovery rate (FDR) were used for multiple test corrections[74]. Functional pathway and network analysis of differentially expressed proteins were performed using Ingenuity Pathway Analysis (IPA) (Qiagen, Redwood City, CA, USA). The pathway and network score were based on the hypergeometric distribution and calculated with the right-tailed Fisher's exact test.

3. Results

Mito-centrifugation delivers functional mitochondria to $CD4^+$ T cells.

Our initial experiments determined whether mito-centrifugation could deliver functional donor mitochondria to $CD4^+$ T cells from old mice. Mitochondria isolated from MEFs (5.0×10^6 cells) were pre-stained with Mitotracker Deep Red (MTDR) and transferred into $CD4^+$ T cells isolated from old mice. Approximately 30 min after mito-transfer, $CD4^+$ T cells were probed with MitoSOX Red and MTV-G, surface labeled with α-CD4, fixed in 4% PFA, and analyzed by flow cytometry. No more than 10% of $CD4^+$ T cells from old mice were $MTDR^+$ after mito-transfer indicating that these received donor mitochondria **(Fig. 1. A-C)**. Compared to non-manipulated $CD4^+$ T cells from old mice (*i.e.* $MTDR^-$ $CD4^+$ T cells), the relative MFI of MitoSOX Red in the subset of $CD4^+$ T cells from old mice that received mitochondria via mito-centrifugation significantly decreased, indicating a reduction in mitoROS production **(Fig. 1. D-E).** Further, compared to $MTDR^-$ $CD4^+$ T

cells, the relative MFI of MTV-G in the subset of MTDR$^+$ CD4$^+$ T cells significantly increased, indicating an increase in mitochondrial mass **(Fig. 1. F).** These data suggested that mito-centrifugation transfered functional donor mitochondria to CD4$^+$ T cells. Although the efficiency of this transfer at this volume was low (≤ 10%) **(Fig. 1. A-B),** these initial experiments hinted that mito-transfer significantly decreased mitoROS levels of CD4$^+$ T cells in old mice. Next, we sought to improve and standardize a protocol for mito-transfer to CD4$^+$ T cells.

Standardizing mito-transfer to CD4$^+$ T cells from old mice.

In eukaryotes, the phospholipid cardiolipin (CL) is exclusively localized in mitochondria [75-78], thus, for uniform cell cultures the abundance of CL is thought to accurately reflect the overall mitochondrial content [75, 78, 79]. Our results estimated that approximately 30 nmol of cardiolipin (equivalent to roughly 250 µg of extracted protein) is present in the mitochondrial fraction (*i.e.* supernatant) isolated from 1.0 x 10^7 MEFs **(Fig. 1. G)**. We also assessed whether non-mitochondrial proteins were present in the mitochondrial fraction by detecting PCNA, a nuclear localized protein, PCNA, via western blot. PCNA was present in the mitochondrial fraction, but was comparatively lower than the cytoplasmic fraction that remained after mitochondria isolation **(Supp. Fig. 1)**. These data suggest that the mitochondrial fraction was enriched for mitochondria.

To further optimize mito-transfer efficiency, two volumes of MEF mitochondria based on CL concentrations (1 nmol and 5 nmol CL), were mito-centrifuged into CD4$^+$ T cells. MEF were stained with MTDR before isolation and transfer. After mito-transfer, whole CD4$^+$ T cell populations were analyzed by flow cytometry to quantify frequency of MTDR$^+$ CD4$^+$ T cells, and shifts in MTDR fluorescence (MFI), which are indicative of successful mito-transfer. Both concentrations tested significantly increased the frequencies of MTDR$^+$ CD4$^+$ T cells and shifted the MFI of MTDR (**Fig. 1. H-J**). The MFI of MTDR in CD4$^+$ T cells increased by 5 fold with 1 nmol of cardiolipin, while 5 nmol increased the MFI by 10 fold (**Fig. 1. J**). However, maximum (100%)

mito-transfer efficiency was achieved with 5 nmol CL (**Fig. 1. I**);which was used for subsequent experiments.

We further confirmed successful delivery of mitochondria to $CD4^+$ T cells by quantification and visualization of fluorescent mitochondria (Turbo-GFP tagged hexokinase1; HK-GFP-mito), and transmission electron microscopy (TEM). Various volumes of HK-GFP-mito (0, 20, 40, 80 µL) were mito-centrifuged into $CD4^+$ T cells. The percent of HK-GFP-$mito^+$ $CD4^+$ T cells increased with higher HK-GFP-mito volume **(Fig. 1.K-L)**, indicating increased delivery of functional mitochondria. These data paralleled our initial experiments with MTDR prestained mitochondria **(Fig 1.B, I)**. We further confirmed whether the GFP signal originated from within $CD4^+$ T cells. A 3D volumetric reconstruction of confocal slices (*Z-stacks*) of $CD4^+$ T cells counterstained with αCD4 surface marker and RedDot™2 (RD-2) nuclear stain, indicated that HK-GFP-mito signal was from within the cytosolyc compartment of recipient $CD4^+$ T cells after mito-centrifugation **(Fig.1. M)**.

Immediately after mito-transfer (~5 min), mito-transferred $CD4^+$ T cells from old mice , and non-manipulated $CD4^+$ T cells from young and old mice (controls) were fixed and processed for TEM. Black triangles in TEM micrographs are representative of individual mitochondria **(Fig. 1.N)**. Compared to $CD4^+$ T cells from young mice, the total mitochondrial area **(Fig. 1.O)** and the number of mitochondria **(Fig. 1.P)** per $CD4^+$ T cell micrograph from old mice trended towards a decrease but it was not significant. However, the % ratio of mitochondrial area to cell area **(Fig. 1.Q)** was significantly lower in CD4+ T cells from old mice compared to CD4 T cells from young mice (4.38% vs. 5.33%). After mito-transfer was performed on $CD4^+$ T cells from old mice, there were significant increases in the total mitochondrial area (from 0.92 ± 0.06 to 1.24 ± 0.06 μm^2), the number of mitochondria (from 7.03 ± 0.35 to 8.46 ± 0.46), and % ratio of mitochondria to cell

area (from 4.38 ± 0.24 to 5.88 ± 0.28). Collectively, our flow cytometry, confocal microscopy and TEM data indicate that mitochondria were succeffully delivered into $CD4^+$ T cells from old mice.

Mito-transfer decreases mitochondrial oxidative stress in $CD4^+$ T cells from old mice.

Observations that mito-transfer of MEF mitochondria decreased mitoROS levels in $CD4^+$ T cells from old mice (**Fig. 1.D-E**) warranted further examination of the oxidative stress status of $CD4^+$ T cells from old mice prior to and after mito-transfer. The expression of global antioxidant proteins and proteins related to mitochondrial detoxification were detected by LC-MS/MS in non-manipulated and mito-transferred $CD4^+$ T cells from old mice (i.e. **Fig.2. A**, **O1-O3**), at 4 h after mito-transfer. Compared to non-manipulated $CD4^+$ T cells from old mice, a majority of cellular antioxidants and mitochondrial detoxification proteins were downregulated in mito-transferred $CD4^+$ T cells from old mice (**Fig. 2.A**, **OM1-OM3**, and **Supp. Table 1**). Flow cytometry-based detection of total thiol levels, as indicators of sulfate-based oxidants, showed no significant changes in $CD4^+$ T cells from old mice with or without mito-transfer, as well as $CD4^+$ T cells from young mice **(Fig. 2.B).**

Basal levels of cytoplasmic (cytoROS) and mitochondrial (mitoROS) in old $CD4^+$ T cells was also assessed at 4 h after mito-transfer and compared against non-manipulated $CD4^+$ T cells from young and old mice. No significant difference was detected in cytoROS (relative MFI of CellROX DR) in $CD4^+$ T cells **(Fig. 2.C)**. However, mitoROS levels (relative MFI of MitoSOX Red) in mito-transferred $CD4^+$ T cells from old mice, and non-manipulated $CD4^+$ T cells from young mice were similar, and both were significantly lower than mitoROS levels in non-manipulated $CD4^+$ T cells from old mice **(Fig. 2.D)**. EPR-based detection of Mito-TEMPO• in $CD4^+$ T cells also showed similar results, corroborating results from MitoSOX Red experiments **(Fig. 2.E)**. Overall, these data suggest that mito-transfer reduced the basal levels of mitoROS in $CD4^+$ T cells from old mice to those measured in $CD4^+$ T cells from young mice without affecting cytoROS levels.

Mito-transfer alters mitochondrial gene expression and mitochondrial ultrastructure.

Whether mito-transfer changed the mitochondrial proteome of $CD4^+$ T cells from old mice was investigated through pathway analysis based on the cellular proteome detected by LC-MS/MS. The expression of the majority of proteins in the mitochondrial proteome increased in mito-transferred $CD4^+$ T cells from old mice **(Fig. 3.A, Supp. Table 2.)**. Ingenuity Pathway Analysis (IPA) revealed that the most upregulated pathways were related to mitochondrial function **(Fig. 3.B).** Similar to IPA results, the most upregulated processes identified by Gene Ontology Term enrichment analysis were related to mitochondrial function and ultrastructure **(Fig. 3.C).** To corroborate these findings, and understanding that mitochondria function relies on the inner membrane, we compared the mitochondrial cristae ultrustructure of mito-transferred $CD4^+$ T cells against non-manipulated $CD4^+$ T cells from old mice, at 0.1 h and 4 h after mito-transfer **(Fig. 3.D)**. Compared to non-manipulated $CD4^+$ T cells, mito-transferred $CD4^+$ T cells from old mice had denser mitochondrial cristae evidenced by increased and more pronounced folds/wrinkles **(Fig. 3.D; black arrows)**, indicative of increased inner mitochondrial membrane surface area.

The subset of mitochondrial proteome related to the electron transport chain (ETC) of $CD4^+$ T cells from old mice with and without mito-transfer was also analyzed. After 4 h of mito-transfer, $CD4^+$ T cells from old mice showed significant upregulation (1.5-fold increase in protein expression in mitochondria-transferred old *vs.* old, with adjusted *p*-value <0.1) of proteins related to complexes of the ETC, such as NDUS2, SDHA, COX15, QCR7, ATPK **(Fig. 3.E, Supp. Table 3).** We further examined the expression of selected ETC proteins important at different steps of Ox-Phos (NDUFB8, SDHB, UQCRC2, MTCO1, and ATP5A) in old mouse $CD4^+$ T cells at 30 min and 4 h after mito-transfer, and compared their relative expression against those of $CD4^+$ T cells isolated from young and old mice **(Fig. 3.F-H)**. Compared to $CD4^+$ T cells from young mice, significantly lower levels of UQCRC2, a subunit of CIII of the ETC, and lower levels of ATP5A, a

protein subunit of the ATP synthase machinery, were detected in old mouse $CD4^+$ T cells **(Fig. 3.G-H)**. However, after 4 h of mito-transfer, both ATP5A and UQCRC2 were significantly upregulated in $CD4^+$ T cells from old mice **(Fig. 3.F-H)**. No other differences were noted between the detected ETC proteins of $CD4^+$ T cells from all groups studied. These observed changes in mitochondrial proteome prompted us to consider the impact of mito-transfer on the mtDNA in $CD4^+$ T cells from old mice after mito-transfer. indeed, immediately after mito-transfer, mtDNA copy number significantly increased in $CD4^+$ T cells from old mice and returned to previous levels 4 h after **(Fig. 3.I)**.

To determine the impact on mitochondrial mass, T cells were fixed and then stained with MTV-G at 4 h post mito-transfer. Compared to non-manipulated $CD4^+$ T cells from old mice, mito-transferred $CD4^+$ T cells from old mice had significantly lower MFIs of MTV-G, indicating a decrease in overall mitochondrial mass **(Fig. 3.J)**. Collectively, these data suggest that mito-transfer altered the mitochondrial proteome, ultrastructure, and decreased overall mitochondrial abundance.

Mito-transfer increases aerobic metabolism in $CD4^+$ T cells from old mice.

Extracellular flux analysis (mito-stress test) was used to assess changes in cellular oxygen kinetics (OCR) of non-manipulated and mito-transferred $CD4^+$ T cells from old mice. The OCR of $CD4^+$ T cells from young mice was also measured as a reference **(Fig. 4.A)**. Compared to $CD4^+$ T cells from young mice, $CD4^+$ T cells from old mice had increased maximal respiration, increased proton leak and decreased coupling efficiency **(Fig. 4.A-D)**. No other significant differences were noted in other OCR parameters measured in $CD4^+$ T cells from young and old mice **(Fig. 4.A-D)**. However, mito-transferred $CD4^+$ T cells from old mice had significantly increased basal, maximal, spare respiratory capacity **(Fig. 4.B)**, proton leak, non-mitochondrial oxygen consumption rates, and ATP production **(Fig. 4.C)**. Further, the coupling efficiency of mito-transferred $CD4^+$ T cells

from old mice decreased, indicating an increase in proton leak while maintaining ATP production **(Fig. 4.D)**. ECAR of $CD4^+$ T cells from old mice was significantly higher than that of $CD4^+$ T cells from young mice, and mito-transfer further enhanced ECAR of $CD4^+$ T cells from old mice **(Supp. Fig. 2. A-B)**. Therefore, mito-transfer increased the rates of Ox-Phos in $CD4^+$ T cells from old mice.

Increased glycolysis in $CD4^+$ T cells from old mice after mito-transfer.

Both glycolysis and mitochondrial respiration (β-oxidation, ATPase activity) can contribute to cellular ECAR [80]. We delineated the observed changes in ECAR by performing the glycolysis stress test **(Fig. 4.E)**. Basally, $CD4^+$ T cells from old mice were more glycolytic than $CD4^+$ T cells from young mice and had increased non-glycolytic acidification **(Fig. 4.F)**. Mito-transfer further significantly increased glycolysis, non-glycolytic acidification, and the glycolytic capacity of $CD4^+$ T cells from old mice **(Fig. 4.F)**. No significant differences in the glycolytic reserve were observed between $CD4^+$ T cells from young and old mice. However, after mito-transfer, $CD4^+$ T cells from old mice had significantly lower glycolytic reserves **(Fig. 4.F)**.

The glycolytic rate assay and 2-NDBG glucose analog uptake were also performed to further corroborate results from the glycolysis stress test. The proton efflux rate (PER) obtained from the glycolytic rate assay is a measure of glycolytic flux (glucose →pyruvate). Compared to $CD4^+$ T cells from young mice, $CD4^+$ T cells from old mice had significantly higher glycoPER, which further increased in mito-transferred $CD4^+$ T cells from old mice **(Fig. 4.G).** For 2-NDBG tracing, $CD4^+$ T cells were incubated in DMEM containing 2-NDBG, afterwhich the percent and relative MFIs of 2-$NDBG^+$ cells were quantified. $CD4^+$ T cells from old and young mice had a similar percent of 2-$NDBG^+$ populations **(Fig. 4.H-I)**. After mito-transfer, the percentage of 2-$NDBG^+$ $CD4^+$ T cells significantly increased **(Fig. 4.I)**. These data suggest that mito-transfer increased the glucose uptake of $CD4^+$ T cells in old mice. Further, the relative MFI of 2-$NDBG^+$ $CD4^+$ T cells from young

mice was significantly higher than that of $CD4^+$ T cells from old mice **(Fig. 4.J)**. Mito-transfer further decreased the MFI of 2-NDBG in $CD4^+$ T cells from old mice **(Fig. 4.J)**. This decrease in MFI suggests faster degradation of 2-NDBG, and increased glycolytic rate, which is in agreement with the glycoPER data [81, 82].

We additionally assessed the expression of GLUT-1 in $CD4^+$ T cells after mito-transfer but observed no significant change **(Fig. 4.K-L)**. Collectively, data from seahorse and flow cytometry-based assays suggest that mito-transfer increased glycolysis in $CD4^+$ T cells from old mice.

Increased ATP production in $CD4^+$ T cells from old mice after mito-transfer.

Increased glycolysis and oxygen consumption hinted of an increase in the synthesis of ATP [83, 84]. Through the XF ATP rate assay, we determined whether mito-transfer increased ATP synthesis in $CD4^+$ T cells from old mice, and what were the relative contributions of glycolysis and mitochondrial Ox-Phos. $CD4^+$ T cells from young and old mice had comparable rates of mitochondria-linked ATP production (**Fig. 4.M**). Compared to young mice, $CD4^+$ T cells from old mice showed higher rates of glycolysis-linked ATP production (**Fig. 4.M**). Mito-transfer enhanced both mitochondria and glycolysis-linked ATP production rates of $CD4^+$ T cells from old mice, with a roughly 50% increase in total ATP production (**Fig. 4.M**). We additionally measured the intracellular levels of ATP but noted no significant differences among groups (**Fig. 4.N**).

Mito-transfer improves T cell activation and cytokine production in $CD4^+$ T cells from old mice.

Because mitochondrial fitness impacts T cell activation, we compared TCR signalosome and phosphorylation kinetics of $CD4^+$ T cells from old mice with and without mito-transfer. LC-MS/MS analysis showed that mito-transfer basally downregulated a majority of TCR signalosome proteins

in $CD4^+$ T cells from old mice **(Fig. 5.A-B, Supp. Table 4).** To examine the activation-induced T cell phosphorylation kinetics, $CD4^+$ T cells were stimulated with αCD3/αCD28 for either 15, 30, or 60 min, fixed with 2% PFA and intracellularly stained for phosphorylated proteins (p-SLP76, p-PLCg1, p-ZAP70, and p-LCK). Compared to non-manipulated $CD4^+$ T cells from old mice, the activation-induced phosphorylation of TCR signalosome proteins p-SLP76 and p-PLCg1 were significantly higher in mito-transferred $CD4^+$ T cells from old mice **(Fig. 5.C-D)**, but no significant differences in the phosphorylation kinetics of p-ZAP70, and p-LCK were detected **(Fig. 5.E-F).**

T cell activation-induced switch from Ox-Phos to aerobic glycolysis is concurrent with TCR signalosome phosphorylation events. Since mito-transfer increased basal Ox-Phos in $CD4^+$ T cells from old mice, we questioned how mito-transfer impacted the ability of $CD4^+$ T cells from old mice to undergo an activation-induced switch from Ox-Phos to aerobic glycolysis. The basal OCR of mito-transferred $CD4^+$ T cells from old mice was significantly higher than that of non-manipulated $CD4^+$ T cells from old mice **(Fig. 5.G)**. These data are in agreement with our OCR data (mito-stress test, **Fig. 4.A-B**). After acute injection of PMA/IONO, the peak OCR values of mito-transferred $CD4^+$ T cells were significantly higher than those of non-manipulated $CD4^+$ T cells from old mice **(Fig. 5.H)**. Similar trends were noted for ECAR measurements of mito-transferred $CD4^+$ T cells from old mice **(Fig. 5.I)**. Collectively, these data suggest that mito-transferred $CD4^+$ T cells more rapidly switched from Ox-Phos to aerobic glycolysis.

TCR-induced activation also increases ROS production in $CD4^+$ T cells. Compared to non-manipulated $CD4^+$ T cells from old mice, mito-transferred $CD4^+$ T cells had significantly higher levels of mitoROs **(**mitoSOX fluorescence, **Fig. 5.J)**, and levels of cytoROS **(**CellROX DR fluorescence, **Fig. 5.K)** after activation. These data suggest that mito-transfer improved TCR signaling during T cell activation. Cellular antioxidant levels are important to counterbalance ROS production during T cell activation. Thus, the relative levels of intracellular thiols and total GSH in

the supernatant of activated $CD4^+$ T cells from old mice with or without mito-transfer were compared. The relative MFI of thiol-tracker violet increased by roughly 50% in mito-transferred $CD4^+$ T cells from old mice **(Fig. 5.L).** The total GSH produced by T cells was determined at 24 h and 72 h post-activation. Compared to $CD4^+$ T cells without mito-transfer, at both timepoints, mito-transferred $CD4^+$ T cells from old mice produced significantly higher amounts of GSH **(Fig. 5.M).**

To further examine whether mito-transfer would improve T cell activation, the expression of CD69 and CD25, common markers of T cell activation, were determined 24 h after mitogenic stimulation. Indeed, mito-transfer increased the number of $CD25^+CD69^+$ activated cells by approximately 50% **(Fig. 5.N-O**). Overall, mito-transfer increased the amount of $CD4^+$ T cells from old mice that expressed $CD25^+$ (**Fig. 5.P**), but did not change the proportion of total $CD69^+$ $CD4^+$ T cells after activation (**Fig. 5.Q**).

Previous studies highlight the involvement of mitoROS, specifically H_2O_2, in modulating IL-2 expression in T cells [15]. The *ex vivo* stimulation of mito-transferred $CD4^+$ T cells from old mice led to increased expression of CD25, which is also the high affility IL-2 receptor (IL-2Rα) [85, 86]. Mito-transfer increased the amount of IL-2^+ spots (counted as individual spots) by approximately 50% (**Fig. 5.R-T**). Intracellular IL-2 cytokine staining and flow cytometry analysis further corroborated our EliSPOT results **(Fig. 5.U).**

To determine whether the impact of mito-transfer extended beyond IL-2 production or T helper cell lineage**,** we additionally measured levels of soluble IL-2 and other cytokines (IFNχ, TNFα, IL-4, IL-5, IL-10, IL-17) and the chemokine CCL-5/RANTES, in culture media of activated non-manipulated and mito-transferred $CD4^+$ T cells at 24 h and 72 h post-activation **(Fig. 5.V-W)**. The levels of IL-2 in the media of mito-transferred $CD4^+$ T cells from old mice were significantly lower than that of non-manipulated $CD4^+$ T cells from old mice at 24 h post-activation **(Fig. 5. V-W).** The

media of mito-transferred $CD4^+$ T cells from old mice also contained significantly lower levels of cytokines TNFα and IL-4, significantly higher levels of IL-5, and CCL-5/RANTES, and comparable levels of IFNγ, IL-10, and IL-17 at 24 h post activation. At 72 h post-infection, these cytokine/ chemokine levels shifted with significantly lower IFNγ and IL-4, significantly higher IL-5, IL-10, IL-17a, and CCL-5/RANTES, and comparable IL-2 and TNFα levels (**Fig. 5.V-W**). These data suggest that mito-transfer in old $CD4^+$ T cells impacts broad cytokine production and extends beyond 24 h of activation.

Finally, whether the proliferative capacity of $CD4^+$ T cells from old mice improved after mito-transfer was also examined. $CD4^+$ T cells from old mice were stimulated for 72 h in complete media supplemented with 50 µM EdU, which is incorporated into newly synthesized DNA during cell proliferation. Compared to non-manipulated $CD4^+$ T cells from old mice, $CD4^+$ T cells after mito-transfer had a two-fold increase in the number of Edu^+ cells **(Fig. 5.X).**

Mito-transfer in naïve CD4 T cells from old mice improves the control of infection.

Previous studies suggest that compared to other T cell subpopulations, naïve $CD4^+$ T cells are most impacted by aging-associated dysregulation and immunosenescence [7, 9, 84, 85], and their dysfunction drives susceptibility to several microbial infections in the elderly. To further assess this, the *in vivo* function of mito-transferred naïve $CD4^+$ T cells was evaluated in separate Rag1-KO adoptive transfer models of influenza A virus (IAV, acute) and *Mycobacterium tuberculosis* (*M.tb*, chronic) infections **(Fig. 6.A)**.

Compared to Rag1-KO mice that received either PBS or non-manipulated naïve $CD4^+$ T cells from old mice, Rag1-KO mice that received mito-transferred naïve $CD4^+$ T cells from old mice had a significant delay in IAV-induced morbidity (weight loss) by day 8 post-infection **(Fig. 6.B)**. Rag1-

KO mice that received mito-transferred naïve $CD4^+$ T from old mice also had significantly reduced mortality (13 days median survival), compared to mice that received either PBS or non-manipulated naïve old mouse $CD4^+$ T cells [9 days median survival **(Fig. 6. C)**]. Overall, these data suggest that mito-transferred naïve $CD4^+$ T cells from old mice improved control of infection (morbidity and mortality) over non-manipulated naïve $CD4^+$ T cells from old mice during IAV infection.

In an *M.tb* model of infection, fewer *M.tb* colony forming units (CFUs) were observed in the lungs of Rag1-KO mice that received mito-transferred naïve $CD4^+$ T cells (p = 0.004) or non-manipulated naïve $CD4^+$ T cells from old mice (p = 0.01), compared to control infected Rag1-KO mice **(Fig. 6.D)**. There were, however, no significant differences between the *M.tb* burden in the lung of Rag1-KO mice that received mito-transferred naïve $CD4^+$ T cells and non-manipulated naïve $CD4^+$ T cells from old mice **(Fig. 6.D)**. The *M.tb* burden in the spleen of Rag1-KO mice that received mito-transferred naïve $CD4^+$ T cells was significantly lower than that of Rag1-KO mice that received non-manipulated naïve $CD4^+$ T cells from old mice (p = 0.016) or PBS (control, p = 0.019) **(Fig. 6.D)**. There were no significant differences in *M.tb* burden in the spleen of Rag1-KO mice that received non-manipulated naïve $CD4^+$ T cells or PBS **(Fig. 6.D)**. *M.tb* studies were repeated using half the amount of adoptively transferred cells (1.0×10^6) and while similar trends were observed, only the lungs of mice that received mito-transferred naïve $CD4^+$ T cells from old mice had a statistically lower *M.tb* burden (p = 0.002) than control mice that received PBS or were infected with *M.tb*. **(Supp. Fig. 5)**. These data suggest that mito-transferred naïve T cells from old mice are capable of developing effector responses and responding to *M.tb* infection but on a Rag1-KO background, absent other essential immune cells, these responses had minimal effect.

4. Discussion

Mitochondria are indispensable for proper T cell homeostasis [13, 15, 17, 20, 27], and aging-associated decline in adaptive immunity is linked to mitochondrial dysfunction and redox imbalance [6, 17, 87-89]. The restoration of redox balance through the reconstitution of mitochondrial fitness (mito-transfer) in lymphocytes from old mice and the elderly humans has not been thoroughly examined. Our results support our hypothesis that restoration via mito-transfer would improve immunological $CD4^+$ T cell functions.

In our experiments using $CD4^+$ T cells from old mice, mito-transfer altered the basal levels of mitoROS and a majority of antioxidant proteins, shifting cells towards lower basal levels of intracellular ROS. Proteomic analysis (IPA and GO term enrichment) of mito-transferred $CD4^+$ T cells from old mice showed that the most upregulated cellular pathways and processes were related to mitochondrial remodeling and Ox-Phos. Visually, this was corroborated by qualitative EM images, where the cristae ultrastructure of mito-transferred CD4 T cells was much denser than non-manipulated $CD4^+$ T cells. This is in accordance with studies showing that increased mitochondrial cristae density does not always reflect an overall increased in mitochondrial mass, but increased cristae density correlates with elevated oxygen consumption [90].

Moreover, extracellular flux analysis of mito-transferred $CD4^+$ T cells showed enhanced aerobic respiration, which is supported by our proteomic data. Our data on mitochondrial mass and mtDNA copy number hint that mito-transfer perhaps transiently increased mitochondrial mass before or during the cellular reprogramming process. At a minimum, the increased mitochondrial activity can be attributed to the increased expression of proteins related to ETC. This also is likely the reason behind the concurrent rise in glycolysis in mito-transferred $CD4^+$ T cells, as the amount of acetyl-CoA needed for the TCA cycle significantly increased. Acetyl-CoA is primarily generated either through β-oxidation of intracellular fatty acids or glycolysis [91]. We did not assess the

preferential utilization of lipids in this study, and the medium preparation used to perform the metabolic analysis did not contain a significant amount of lipids. In line with Le Chatelier's principles of substrate equilibrium, it can be argued that after mito-transfer, $CD4^+$ T cells from old mice upregulated glycolysis to compensate for lagging intracellular levels of acetyl-CoA. Additionally, the ATP production rate of $CD4^+$ T cells isolated from old mice rose by 40% in comparison to non-manipulated $CD4^+$ T cells. Primary information regarding T cell metabolism in the context of aging is still sparse [92]. As of now, it seems the impact of mito-transfer on the metabolism of $CD4^+$ T cells differs from the Warburg phenomenon, as there was no bias towards glycolysis, and mito-transfer decreased mitoROS in the $CD4^+$ T cells from old mice. Moreover, these data collectively suggest that the mitochondrial cristae of $CD4^+$ T cells restructured after mito-transfer, favoring increased cristae density per mitochondria rather than an increase in mitochondrial mass.

Increased cristae density would also explain why the level of mitoROS was significantly higher than that of non-manipulated $CD4^+$ T cells after mito-transferred $CD4^+$ from old mice were activated with PMA/IONO. We also noted that the switch from Ox-Phos to aerobic glycolysis in mito-transferred $CD4^+$ T cells was much faster than that of non-manipulated $CD4^+$ T cells from old mice. Beyond the observed impact on ROS and metabolism, there were other improved T cell functions. Indeed, we identified significant improvements in TCR-signaling kinetics, expression of a T cell activation marker (CD25), cytokine production, and an increase in activation-induced proliferation. Compared to non-manipulated $CD4^+$ T cells, the proportion of activated T cells expressing $CD25^+$ and $CD69^+$ doubled after mito-transfer and 24 h of activating stimulus. We also noted a concomitant doubling of $CD4^+$ T cells producing IL-2, which correlated with increased cell proliferation and contributed to the alteration of cytokine profiles.

The IL-2 signaling pathway is immunomodulatory [93-95], and while $CD4^+$ T cells, $CD8^+$ T cells, NK cells, NK T cells, and dendritic cells are all capable of secreting IL-2, activated $CD4^+$ T cells are its largest producer [85, 93, 96]. Previous research has shown that $CD4^+$ T cells from elderly humans and mice produce insufficient amounts of IL-2, as well as insufficiently express the high-affinity IL-2 receptor IL-2Rα (CD25) necessary for signal transduction [97, 98], and the current consensus is that aging-associated defects in IL-2 signaling can dynamically shift the architecture of adaptive immune responses or even promote T cell anergy [5, 97, 99]. The underlying mechanics regarding blunted IL-2 production and related signaling in the elderly are still unclear [5, 99, 100]. Intracellular IL-2 signaling transduction occurs through the Janus kinase/signal transducer and activation of transcription factor (JAK/STAT), phosphoinositide-3-kinase (PI3K), and mitogen-activated kinase (MAPK) pathways, all of which are sensitive to oxidative modifications [101, 102]. Previous studies have also characterized the role of redox equilibrium in maintaining proper lymphocyte function, and mitoROS, specifically H_2O_2, modulates IL-2 expression in T cells [15, 103]. Supplementation with the antioxidant vitamin E improved the ability of T cells from the elderly to produce IL-2 and proliferate [104]. However, maintaining the intracellular redox balance is delicate [23, 37, 38], and excess antioxidants can hinder proper T cell activation and cytokine production as others have described [105, 106].

Our *in vivo* IAV and *M.tb* infection outcomes highlight the potential of mito-transfer as an immune-booster in the elderly. We demonstrated that mito-transfer can enhance control of viral and non-viral pathogen infections *in vivo,* and the enhanced protection is likely related to the preferential generation of antigen-specific effector memory $CD4^+$ T cells*.* As little as 2.0×10^6 naïve mito-transferred $CD4^+$ T cells from old mice were capable of differentiating into either IAV or *M.tb* specific effector $CD4^+$ T cells that had a physiological impact on IAV-induced morbidity and mortality and on *M.tb* burden. This study could not fully delineate whether antigen-specific effector $CD4^+$ T cell quality (antigen-specific) and or quantity (proliferative capacity) was preferentially

enhanced by mito-transfer. Based on our collective data, we hypothesize that both parameters (i.e. antigen specificity and proliferative capacity) might improve *in vivo*, and consider that improved disease outcomes should be achievable with an increase in the quantity of mito-transferred naïve T cells injected into mice.

The capacity to upscale the process of mito-transfer from *in vitro/ex vivo* towards *in vivo* models is likely limited by available techniques to perform MRT and the number of viable mitochondria or mtDNA needed to revert a specific mitochondrial metabolic abnormality in an organism [107, 108]. Mitochondrial encapsulation or injections can facilitate *in vivo* studies [109, 110] and Chang *et al.* showed that cell-penetrating peptide (pep-1) mediated delivery of healthy mitochondria to MCF-7 breast cancer cells reversed Warburg metabolism, decreased oxidative stress, and increased cancer cell susceptibility to chemotherapeutics [109].

Nevertheless, mito-transfer is an especially promising avenue for the immunological landscape, partly because it is plausibly easy to isolate and re-insert autologous and allogeneic lymphocytes/leukocytes in a clinic or lab setting. This could have transformative impact on aging-associated immune dysregulations and on immune based dysregulation that generally involve mitochondrial dysfunction. For example, work by Vaena *et al*. showed that anti-tumor T cells from aged individuals succumb to ceramide accumulation-induced mitochondrial dysfunction and this consequently inhibits anti-tumor T cell responses [111]. It would be interesting to assess whether mito-transferred anti-tumor $CD8^+$ T cells from aged mice and elderly can mitigate ceramide induce mito-dysfunction and promote anti-tumor activity. Guo *et al*. and team also demonstrated that mitochondrial reprograming through upregulation of mitochondrial pyruvate carrier was essential to restoring the functionality of exhausted $CD8^+$ T cells, and this improved their anti-tumor capacities [112]. Undoubtedly, future studies will need to investigate the full potential of mito-transfer on anti-tumor immunity.

In conclusion, under our experimental conditions, mito-transfer decreased mitochondrial dysfunction, improved activation, cytokine production, and proliferation of $CD4^+$ T cells from old mice. Importantly, mito-transfer had a physiological impact on IAV-induced morbidity and mortality, and on *M.tb* burden *in vivo*. In addition to mitoROS mediated redox signaling [113-117], calcium mobilization and buffering in coordination with the endoplasmic reticulum (ER) [13, 23, 45, 118], cytochrome c mediated apoptosis [119-123], NAD^+ mediated epigenetic regulation (sirtuins) [124, 125], as well as protein transport and degradation [126, 127], are all interdependent on proper mitochondrial form and function. We suspect that the impact of mito-transfer on other aspects of T cell function were also improved. More in-depth mechanistic studies outside the scope of this current study are warranted to elucidate the specific means by which mito-transfer altered the pathways in $CD4^+$ T cells in old mice and the elderly.

Acknowledgments

We would like to acknowledge the thoughtful discussions with Drs. Susan Weintraub, Larry S. Schlesinger, Douglas Green & James Stambulli that have strengthened this manuscript. We would also like to acknowledge Drs. Gourav Choudhury and Marcel Daadi for sharing their MEF isolation protocol. Finally we would like to acknowledge Ms. Kimberley Olsen for her technical and administrative assistance throughout the duration of this project.

Funding

Research reported in this publication was supported by the National Institute On Aging of the National Institutes of Health (NIH/NIA) under the award number P01AG051428 (to JT). The content is solely the responsibility of the authors and does not necessarily represent the official views of the National Institutes of Health. CAH was supported in part by the Douglass Foundation Graduate Student Fellowship, the Texas Biomed Post-Doctoral Forum Grant, and National Heart,

Lung, and Blood Institute (1T32HL098049), and Stanford University Propel Post-Doctoral Fellowship. KC was partially supported by the Douglass Foundation Graduate Student Fellowship at Texas Biomed. AOF was supported by a NIH/NIA F99/K00 fellowship (F99AG079802). Research reported in this publication was supported by the Office Of The Director, National Institutes Of Health of the National Institutes of Health under Award Number S10OD028653. The content is solely the responsibility of the authors and does not necessarily represent the official views of the National Institutes of Health.

Conflict of interest

The authors declare no competing interests.

Author Contributions

This project was conceived by CAH & JT; CAH designed the experiments; CAH, AM, AV, SG, VD, AW, AA, JD, AH, RA, KC, HZ, and HC performed experiments; CAH and JG performed the statistical analysis, CAH wrote the manuscript; CAH, PS, LMS, YW, JBT and JT edited the manuscript.

Data Availability

The authors declare that the data supporting the findings of this study are available within the paper and its supplementary information files. Reagents are available upon request.

References

1. Orme, I.M., *Aging and immunity to tuberculosis: increased susceptibility of old mice reflects a decreased capacity to generate mediator T lymphocytes.* J Immunol, 1987. **138**(12): p. 4414-8.
2. Weyand, C.M. and J.J. Goronzy, *Aging of the Immune System. Mechanisms and Therapeutic Targets.* Ann Am Thorac Soc, 2016. **13 Suppl 5**: p. S422-S428.
3. Herndler-Brandstetter, D., *How aging affects T lymphocyte-mediated immunity.* Front Immunol, 2013. **4**: p. 296.
4. Akbar, A.N., S.M. Henson, and A. Lanna, *Senescence of T Lymphocytes: Implications for Enhancing Human Immunity.* Trends Immunol, 2016. **37**(12): p. 866-876.
5. Donnini, A., et al., *Age-related susceptibility of naive and memory CD4 T cells to apoptosis induced by IL-2 deprivation or PHA addition.* Biogerontology, 2005. **6**(3): p. 193-204.
6. Mattoo, H., et al., *Naive CD4 T cells from aged mice show enhanced death upon primary activation.* Int Immunol, 2009. **21**(11): p. 1277-89.
7. Lefebvre, J.S. and L. Haynes, *Aging of the CD4 T Cell Compartment.* Open Longev Sci, 2012. **6**: p. 83-91.
8. Nikolich-Zugich, J., *Aging of the T cell compartment in mice and humans: from no naive expectations to foggy memories.* J Immunol, 2014. **193**(6): p. 2622-9.
9. Haynes, L., et al., *CD4 T cell memory derived from young naive cells functions well into old age, but memory generated from aged naive cells functions poorly.* Proc Natl Acad Sci U S A, 2003. **100**(25): p. 15053-8.
10. Yanes, R.E., et al., *Metabolic reprogramming in memory CD4 T cell responses of old adults.* Clin Immunol, 2019. **207**: p. 58-67.
11. Pieren, D.K.J., et al., *Response kinetics reveal novel features of ageing in murine T cells.* Sci Rep, 2019. **9**(1): p. 5587.
12. Mirza, N., et al., *Comparative kinetic analyses of gene profiles of naive CD4+ and CD8+ T cells from young and old animals reveal novel age-related alterations.* Aging Cell, 2011. **10**(5): p. 853-67.
13. Nagy, G., A. Koncz, and A. Perl, *T cell activation-induced mitochondrial hyperpolarization is mediated by Ca2+- and redox-dependent production of nitric oxide.* J Immunol, 2003. **171**(10): p. 5188-97.
14. Quintana, A., et al., *T cell activation requires mitochondrial translocation to the immunological synapse.* Proc Natl Acad Sci U S A, 2007. **104**(36): p. 14418-23.
15. Kaminski, M.M., et al., *Mitochondrial reactive oxygen species control T cell activation by regulating IL-2 and IL-4 expression: mechanism of ciprofloxacin-mediated immunosuppression.* J Immunol, 2010. **184**(9): p. 4827-41.
16. Fracchia, K.M., C.Y. Pai, and C.M. Walsh, *Modulation of T Cell Metabolism and Function through Calcium Signaling.* Front Immunol, 2013. **4**: p. 324.
17. Ron-Harel, N., A.H. Sharpe, and M.C. Haigis, *Mitochondrial metabolism in T cell activation and senescence: a mini-review.* Gerontology, 2015. **61**(2): p. 131-8.
18. Leavy, O., *T Cell responses: Defective mitochondria disrupt CD8(+) T cells.* Nat Rev Immunol, 2016. **16**(9): p. 534-5.
19. Buck, M.D., et al., *Mitochondrial Dynamics Controls T Cell Fate through Metabolic Programming.* Cell, 2016. **166**(1): p. 63-76.
20. Almeida, L., et al., *Metabolic pathways in T cell activation and lineage differentiation.* Semin Immunol, 2016. **28**(5): p. 514-524.
21. Dimeloe, S., et al., *T-cell metabolism governing activation, proliferation and differentiation; a modular view.* Immunology, 2017. **150**(1): p. 35-44.

22. Patel, C.H. and J.D. Powell, *Targeting T cell metabolism to regulate T cell activation, differentiation and function in disease.* Curr Opin Immunol, 2017. **46**: p. 82-88.
23. Desdin-Mico, G., G. Soto-Heredero, and M. Mittelbrunn, *Mitochondrial activity in T cells.* Mitochondrion, 2018. **41**: p. 51-57.
24. Perl, A., R. Hanczko, and E. Doherty, *Assessment of mitochondrial dysfunction in lymphocytes of patients with systemic lupus erythematosus.* Methods Mol Biol, 2012. **900**: p. 61-89.
25. Bhargava, A., et al., *Role of mitochondrial oxidative stress on lymphocyte homeostasis in patients diagnosed with extra-pulmonary tuberculosis.* Cell Biol Int, 2016. **40**(2): p. 166-76.
26. Sanderson, S.L. and A.K. Simon, *In aged primary T cells, mitochondrial stress contributes to telomere attrition measured by a novel imaging flow cytometry assay.* Aging Cell, 2017. **16**(6): p. 1234-1243.
27. Fisicaro, P., et al., *Targeting mitochondrial dysfunction can restore antiviral activity of exhausted HBV-specific CD8 T cells in chronic hepatitis B.* Nat Med, 2017. **23**(3): p. 327-336.
28. Desdin-Mico, G., et al., *T cells with dysfunctional mitochondria induce multimorbidity and premature senescence.* Science, 2020. **368**(6497): p. 1371-1376.
29. Adam-Vizi, V. and C. Chinopoulos, *Bioenergetics and the formation of mitochondrial reactive oxygen species.* Trends Pharmacol Sci, 2006. **27**(12): p. 639-45.
30. Murphy, M.P., *How mitochondria produce reactive oxygen species.* Biochem J, 2009. **417**(1): p. 1-13.
31. Venditti, P., L. Di Stefano, and S. Di Meo, *Mitochondrial metabolism of reactive oxygen species.* Mitochondrion, 2013. **13**(2): p. 71-82.
32. Zorov, D.B., M. Juhaszova, and S.J. Sollott, *Mitochondrial reactive oxygen species (ROS) and ROS-induced ROS release.* Physiol Rev, 2014. **94**(3): p. 909-50.
33. Gill, T. and A.D. Levine, *Mitochondria-derived hydrogen peroxide selectively enhances T cell receptor-initiated signal transduction.* J Biol Chem, 2013. **288**(36): p. 26246-55.
34. Kim, H.J., et al., *Exogenous Hydrogen Peroxide Induces Lipid Raft-Mediated STAT-6 Activation in T Cells.* Cell Physiol Biochem, 2017. **42**(6): p. 2467-2480.
35. Reth, M., *Hydrogen peroxide as second messenger in lymphocyte activation.* Nat Immunol, 2002. **3**(12): p. 1129-34.
36. Ball, J.A., et al., *Hydrogen Peroxide Triggers a Dual Signaling Axis To Selectively Suppress Activated Human T Lymphocyte Migration.* J Immunol, 2017. **198**(9): p. 3679-3689.
37. Yarosz, E.L. and C.H. Chang, *The Role of Reactive Oxygen Species in Regulating T Cell-mediated Immunity and Disease.* Immune Netw, 2018. **18**(1): p. e14.
38. Belikov, A.V., B. Schraven, and L. Simeoni, *T cells and reactive oxygen species.* J Biomed Sci, 2015. **22**: p. 85.
39. Poderoso, J.J., *The formation of peroxynitrite in the applied physiology of mitochondrial nitric oxide.* Arch Biochem Biophys, 2009. **484**(2): p. 214-20.
40. Rimessi, A., et al., *Mitochondrial reactive oxygen species and inflammation: Molecular mechanisms, diseases and promising therapies.* Int J Biochem Cell Biol, 2016. **81**(Pt B): p. 281-293.
41. Davies, M.J., *Protein oxidation and peroxidation.* Biochem J, 2016. **473**(7): p. 805-25.
42. Dan Dunn, J., et al., *Reactive oxygen species and mitochondria: A nexus of cellular homeostasis.* Redox Biol, 2015. **6**: p. 472-85.
43. Spinelli, J.B. and M.C. Haigis, *The multifaceted contributions of mitochondria to cellular metabolism.* Nat Cell Biol, 2018. **20**(7): p. 745-754.
44. De Gaetano, A., et al., *Mitophagy and Oxidative Stress: The Role of Aging.* Antioxidants (Basel), 2021. **10**(5).
45. Osellame, L.D., T.S. Blacker, and M.R. Duchen, *Cellular and molecular mechanisms of mitochondrial function.* Best Pract Res Clin Endocrinol Metab, 2012. **26**(6): p. 711-23.

46. Mills, E.L., B. Kelly, and L.A.J. O'Neill, *Mitochondria are the powerhouses of immunity.* Nat Immunol, 2017. **18**(5): p. 488-498.
47. Lanna, A. and M.L. Dustin, *Mitochondrial fusion fuels T cell memory.* Cell Res, 2016. **26**(9): p. 969-70.
48. Czajka, A., et al., *Altered Mitochondrial Function, Mitochondrial DNA and Reduced Metabolic Flexibility in Patients With Diabetic Nephropathy.* EBioMedicine, 2015. **2**(6): p. 499-512.
49. Zsurka, G., et al., *Is There Still Any Role for Oxidative Stress in Mitochondrial DNA-Dependent Aging?* Genes (Basel), 2018. **9**(4).
50. Ziada, A.S., et al., *Mitochondrial DNA somatic mutation burden and heteroplasmy are associated with chronological age, smoking, and HIV infection.* Aging Cell, 2019. **18**(6): p. e13018.
51. Mikhed, Y., A. Daiber, and S. Steven, *Mitochondrial Oxidative Stress, Mitochondrial DNA Damage and Their Role in Age-Related Vascular Dysfunction.* Int J Mol Sci, 2015. **16**(7): p. 15918-53.
52. Lagouge, M. and N.G. Larsson, *The role of mitochondrial DNA mutations and free radicals in disease and ageing.* J Intern Med, 2013. **273**(6): p. 529-43.
53. Brand, M.D. and D.G. Nicholls, *Assessing mitochondrial dysfunction in cells.* Biochem J, 2011. **435**(2): p. 297-312.
54. Brookes, P.S., *Mitochondrial H(+) leak and ROS generation: an odd couple.* Free Radic Biol Med, 2005. **38**(1): p. 12-23.
55. Suski, J., et al., *Relation Between Mitochondrial Membrane Potential and ROS Formation.* Methods Mol Biol, 2018. **1782**: p. 357-381.
56. Georgieva, E., et al., *Detection of Redox Imbalance in Normal Lymphocytes with Induced Mitochondrial Dysfunction - EPR Study.* Anticancer Res, 2016. **36**(10): p. 5273-5279.
57. Lichtenfels, R., et al., *Comparative expression profiling of distinct T cell subsets undergoing oxidative stress.* PLoS One, 2012. **7**(7): p. e41345.
58. Holmdahl, R., et al., *Hydrogen peroxide as an immunological transmitter regulating autoreactive T cells.* Antioxid Redox Signal, 2013. **18**(12): p. 1463-74.
59. Jitschin, R., et al., *Mitochondrial metabolism contributes to oxidative stress and reveals therapeutic targets in chronic lymphocytic leukemia.* Blood, 2014. **123**(17): p. 2663-72.
60. Franchina, D.G., C. Dostert, and D. Brenner, *Reactive Oxygen Species: Involvement in T Cell Signaling and Metabolism.* Trends Immunol, 2018. **39**(6): p. 489-502.
61. Agrawal, A. and U. Mabalirajan, *Rejuvenating cellular respiration for optimizing respiratory function: targeting mitochondria.* Am J Physiol Lung Cell Mol Physiol, 2016. **310**(2): p. L103-13.
62. A, E.M., *Isolation and propagation of mouse embryonic fibroblasts and preparation of mouse embryonic feeder layer cells.* Curr Protoc Stem Cell Biol, 2007. **Chapter 1**: p. Unit1C 3.
63. Kim, M.J., et al., *Delivery of exogenous mitochondria via centrifugation enhances cellular metabolic function.* Sci Rep, 2018. **8**(1): p. 3330.
64. Schindelin, J., et al., *Fiji: an open-source platform for biological-image analysis.* Nat Methods, 2012. **9**(7): p. 676-82.
65. Searle, B.C., et al., *Chromatogram libraries improve peptide detection and quantification by data independent acquisition mass spectrometry.* Nat Commun, 2018. **9**(1): p. 5128.
66. Rosenberger, G., et al., *A repository of assays to quantify 10,000 human proteins by SWATH-MS.* Sci Data, 2014. **1**: p. 140031.
67. Sun, X., et al., *Flow cytometric analysis of T lymphocyte proliferation in vivo by EdU incorporation.* Int Immunopharmacol, 2016. **41**: p. 56-65.
68. Burkholder, T., et al., *Health Evaluation of Experimental Laboratory Mice.* Curr Protoc Mouse Biol, 2012. **2**: p. 145-165.
69. Ullman-Cullere, M.H. and C.J. Foltz, *Body condition scoring: a rapid and accurate method for assessing health status in mice.* Lab Anim Sci, 1999. **49**(3): p. 319-23.

70. Beamer, G.L., et al., *CBA/J mice generate protective immunity to soluble Ag85 but fail to respond efficiently to Ag85 during natural Mycobacterium tuberculosis infection.* Eur J Immunol, 2012. **42**(4): p. 870-9.
71. Cyktor, J.C., et al., *IL-10 inhibits mature fibrotic granuloma formation during Mycobacterium tuberculosis infection.* J Immunol, 2013. **190**(6): p. 2778-90.
72. Huang da, W., B.T. Sherman, and R.A. Lempicki, *Systematic and integrative analysis of large gene lists using DAVID bioinformatics resources.* Nat Protoc, 2009. **4**(1): p. 44-57.
73. Sherman, B.T., et al., *DAVID: a web server for functional enrichment analysis and functional annotation of gene lists (2021 update).* Nucleic Acids Res, 2022.
74. Benjamini, Y. and Y. Hochberg, *Controlling the False Discovery Rate: A Practical and Powerful Approach to Multiple Testing.* Journal of the Royal Statistical Society: Series B (Methodological), 1995. **57**(1): p. 289-300.
75. Leung, C.W., et al., *Superior fluorescent probe for detection of cardiolipin.* Anal Chem, 2014. **86**(2): p. 1263-8.
76. Dudek, J., *Role of Cardiolipin in Mitochondrial Signaling Pathways.* Front Cell Dev Biol, 2017. **5**: p. 90.
77. Paradies, G., et al., *Oxidative stress, mitochondrial bioenergetics, and cardiolipin in aging.* Free Radic Biol Med, 2010. **48**(10): p. 1286-95.
78. Paradies, G., et al., *Functional role of cardiolipin in mitochondrial bioenergetics.* Biochim Biophys Acta, 2014. **1837**(4): p. 408-17.
79. Osman, C., D.R. Voelker, and T. Langer, *Making heads or tails of phospholipids in mitochondria.* J Cell Biol, 2011. **192**(1): p. 7-16.
80. Mookerjee, S.A., et al., *The contributions of respiration and glycolysis to extracellular acid production.* Biochim Biophys Acta, 2015. **1847**(2): p. 171-181.
81. Yoshioka, K., et al., *Intracellular fate of 2-NBDG, a fluorescent probe for glucose uptake activity, in Escherichia coli cells.* Biosci Biotechnol Biochem, 1996. **60**(11): p. 1899-901.
82. Kim, W.H., et al., *Visualizing sweetness: increasingly diverse applications for fluorescent-tagged glucose bioprobes and their recent structural modifications.* Sensors (Basel), 2012. **12**(4): p. 5005-27.
83. Bonora, M., et al., *ATP synthesis and storage.* Purinergic Signal, 2012. **8**(3): p. 343-57.
84. Mookerjee, S.A., et al., *Quantifying intracellular rates of glycolytic and oxidative ATP production and consumption using extracellular flux measurements.* J Biol Chem, 2017. **292**(17): p. 7189-7207.
85. Malek, T.R. and I. Castro, *Interleukin-2 receptor signaling: at the interface between tolerance and immunity.* Immunity, 2010. **33**(2): p. 153-65.
86. Shatrova, A.N., et al., *Time-Dependent Regulation of IL-2R alpha-Chain (CD25) Expression by TCR Signal Strength and IL-2-Induced STAT5 Signaling in Activated Human Blood T Lymphocytes.* PLoS One, 2016. **11**(12): p. e0167215.
87. Pattabiraman, G., et al., *Aging-associated dysregulation of homeostatic immune response termination (and not initiation).* Aging Cell, 2017. **16**(3): p. 585-593.
88. Ron-Harel, N., et al., *Defective respiration and one-carbon metabolism contribute to impaired naive T cell activation in aged mice.* Proc Natl Acad Sci U S A, 2018. **115**(52): p. 13347-13352.
89. Ghatreh-Samani, M., et al., *Oxidative stress and age-related changes in T cells: is thalassemia a model of accelerated immune system aging?* Cent Eur J Immunol, 2016. **41**(1): p. 116-24.
90. Nielsen, J., et al., *Plasticity in mitochondrial cristae density allows metabolic capacity modulation in human skeletal muscle.* J Physiol, 2017. **595**(9): p. 2839-2847.
91. Shi, L. and B.P. Tu, *Acetyl-CoA and the regulation of metabolism: mechanisms and consequences.* Curr Opin Cell Biol, 2015. **33**: p. 125-31.

92. Quinn, K.M., et al., *The clock is ticking: the impact of ageing on T cell metabolism.* Clin Transl Immunology, 2019. **8**(11): p. e01091.
93. Ross, S.H. and D.A. Cantrell, *Signaling and Function of Interleukin-2 in T Lymphocytes.* Annu Rev Immunol, 2018. **36**: p. 411-433.
94. Gaffen, S.L. and K.D. Liu, *Overview of interleukin-2 function, production and clinical applications.* Cytokine, 2004. **28**(3): p. 109-23.
95. Busse, D., et al., *Competing feedback loops shape IL-2 signaling between helper and regulatory T lymphocytes in cellular microenvironments.* Proc Natl Acad Sci U S A, 2010. **107**(7): p. 3058-63.
96. Liao, W., J.X. Lin, and W.J. Leonard, *Interleukin-2 at the crossroads of effector responses, tolerance, and immunotherapy.* Immunity, 2013. **38**(1): p. 13-25.
97. Pahlavani, M.A. and A. Richardson, *The effect of age on the expression of interleukin-2.* Mech Ageing Dev, 1996. **89**(3): p. 125-54.
98. Thoman, M.L. and W.O. Weigle, *Lymphokines and aging: interleukin-2 production and activity in aged animals.* J Immunol, 1981. **127**(5): p. 2102-6.
99. Haynes, L., et al., *Interleukin 2, but not other common gamma chain-binding cytokines, can reverse the defect in generation of CD4 effector T cells from naive T cells of aged mice.* J Exp Med, 1999. **190**(7): p. 1013-24.
100. Gardner, E.M. and D.M. Murasko, *Age-related changes in Type 1 and Type 2 cytokine production in humans.* Biogerontology, 2002. **3**(5): p. 271-90.
101. Simeoni, L. and I. Bogeski, *Redox regulation of T-cell receptor signaling.* Biol Chem, 2015. **396**(5): p. 555-68.
102. Kesarwani, P., et al., *Redox regulation of T-cell function: from molecular mechanisms to significance in human health and disease.* Antioxid Redox Signal, 2013. **18**(12): p. 1497-534.
103. Sena, L.A., et al., *Mitochondria are required for antigen-specific T cell activation through reactive oxygen species signaling.* Immunity, 2013. **38**(2): p. 225-36.
104. Marko, M.G., et al., *Age-associated decline in effective immune synapse formation of CD4(+) T cells is reversed by vitamin E supplementation.* J Immunol, 2007. **178**(3): p. 1443-9.
105. Previte, D.M. and J.D. Piganelli, *Reactive Oxygen Species and Their Implications on CD4(+) T Cells in Type 1 Diabetes.* Antioxid Redox Signal, 2017.
106. Previte, D.M., et al., *Reactive oxygen species are required for driving efficient and sustained aerobic glycolysis during CD4+ T cell activation.* PLoS One, 2017. **12**(4): p. e0175549.
107. Patananan, A.N., et al., *Modifying the Mitochondrial Genome.* Cell Metab, 2016. **23**(5): p. 785-96.
108. Caicedo, A., et al., *Artificial Mitochondria Transfer: Current Challenges, Advances, and Future Applications.* Stem Cells Int, 2017. **2017**: p. 7610414.
109. Chang, J.C., et al., *Mitochondrial transplantation regulates antitumour activity, chemoresistance and mitochondrial dynamics in breast cancer.* J Exp Clin Cancer Res, 2019. **38**(1): p. 30.
110. Chen, W., et al., *Mitochondrial Surface Engineering for Multidrug Resistance Reversal.* Nano Lett, 2019. **19**(5): p. 2905-2913.
111. Vaena, S., et al., *Aging-dependent mitochondrial dysfunction mediated by ceramide signaling inhibits antitumor T cell response.* Cell Rep, 2021. **35**(5): p. 109076.
112. Guo, Y., et al., *Metabolic reprogramming of terminally exhausted CD8(+) T cells by IL-10 enhances anti-tumor immunity.* Nat Immunol, 2021. **22**(6): p. 746-756.
113. Kang, J. and S. Pervaiz, *Mitochondria: redox metabolism and dysfunction.* Biochem Res Int, 2012. **2012**: p. 896751.
114. Case, A.J., et al., *Mitochondrial Superoxide Signaling Contributes to Norepinephrine-Mediated T-Lymphocyte Cytokine Profiles.* PLoS One, 2016. **11**(10): p. e0164609.
115. Moldovan, L. and N.I. Moldovan, *Oxygen free radicals and redox biology of organelles.* Histochem Cell Biol, 2004. **122**(4): p. 395-412.

116. Handy, D.E. and J. Loscalzo, *Redox regulation of mitochondrial function.* Antioxid Redox Signal, 2012. **16**(11): p. 1323-67.
117. Mailloux, R.J., S.L. McBride, and M.E. Harper, *Unearthing the secrets of mitochondrial ROS and glutathione in bioenergetics.* Trends Biochem Sci, 2013. **38**(12): p. 592-602.
118. Bertero, E. and C. Maack, *Calcium Signaling and Reactive Oxygen Species in Mitochondria.* Circ Res, 2018. **122**(10): p. 1460-1478.
119. Redza-Dutordoir, M. and D.A. Averill-Bates, *Activation of apoptosis signalling pathways by reactive oxygen species.* Biochim Biophys Acta, 2016. **1863**(12): p. 2977-2992.
120. Giorgi, C., et al., *Mitochondrial Ca(2+) and apoptosis.* Cell Calcium, 2012. **52**(1): p. 36-43.
121. Zhong, H., et al., *Mitochondrial control of apoptosis through modulation of cardiolipin oxidation in hepatocellular carcinoma: A novel link between oxidative stress and cancer.* Free Radic Biol Med, 2017. **102**: p. 67-76.
122. Kim, H.J. and A.E. Nel, *The role of phase II antioxidant enzymes in protecting memory T cells from spontaneous apoptosis in young and old mice.* J Immunol, 2005. **175**(5): p. 2948-59.
123. Petrosillo, G., F.M. Ruggiero, and G. Paradies, *Role of reactive oxygen species and cardiolipin in the release of cytochrome c from mitochondria.* FASEB J, 2003. **17**(15): p. 2202-8.
124. Braidy, N., et al., *Age related changes in NAD+ metabolism oxidative stress and Sirt1 activity in wistar rats.* PLoS One, 2011. **6**(4): p. e19194.
125. Christian, B.E. and G.S. Shadel, *Aging: it's SIRTainly possible to restore mitochondrial dysfunction.* Curr Biol, 2014. **24**(5): p. R206-8.
126. Mishra, P. and D.C. Chan, *Metabolic regulation of mitochondrial dynamics.* J Cell Biol, 2016. **212**(4): p. 379-87.
127. Mohanty, A., R. Tiwari-Pandey, and N.R. Pandey, *Mitochondria: the indispensable players in innate immunity and guardians of the inflammatory response.* J Cell Commun Signal, 2019. **13**(3): p. 303-318.

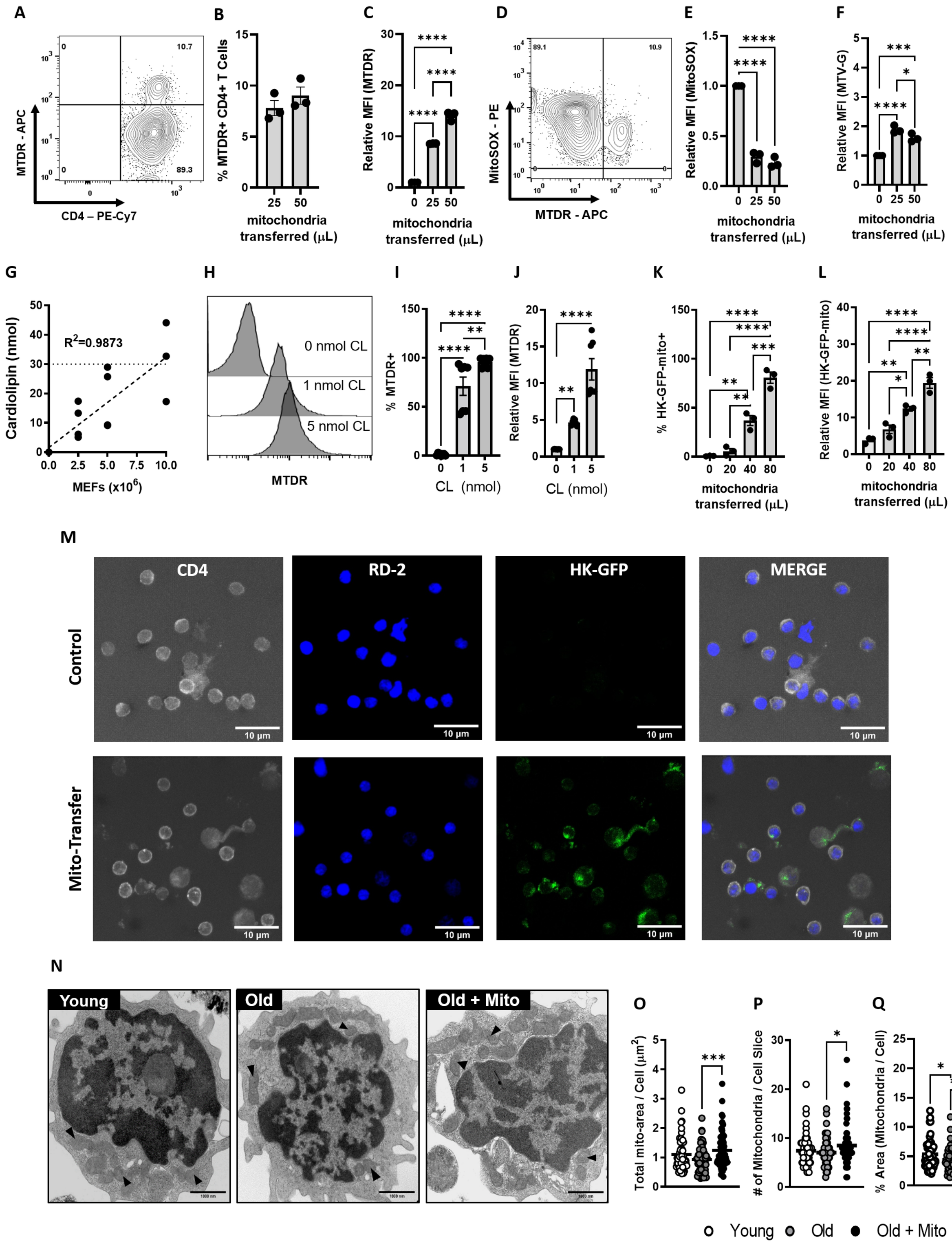
A
MTDR - APC
CD4 – PE-Cy7
10.7
89.3
B
% MTDR+ CD4+ T Cells
mitochondria transferred (μL)
C
Relative MFI (MTDR)
mitochondria transferred (μL)
D
MitoSOX - PE
MTDR - APC
89.1
10.9
E
Relative MFI (MitoSOX)
mitochondria transferred (μL)
F
Relative MFI (MTV-G)
mitochondria transferred (μL)
G
Cardiolipin (nmol)
R2=0.9873
MEFs (x106)
H
0 nmol CL
1 nmol CL
5 nmol CL
MTDR
I
% MTDR+
CL (nmol)
J
Relative MFI (MTDR)
CL (nmol)
K
% HK-GFP-mito+
mitochondria transferred (μL)
L
Relative MFI (HK-GFP-mito)
mitochondria transferred (μL)
M
CD4
RD-2
HK-GFP
MERGE
Control
Mito-Transfer
10 μm
N
Young
Old
Old + Mito
O
Total mito-area / Cell (μm2)
P
# of Mitochondria / Cell Slice
Q
% Area (Mitochondria / Cell)
Young
Old
Old + Mito

Fig. 1. Mito-centrifugation efficiently delivers mitochondria to CD4$^+$ T cells. (**A – F)** Donor mitochondria were prestained with Mito-tracker Deep Red (MTDR) and then transplanted into CD4$^+$ T cells isolated from old mice via mito-centrifugation. After mito-transfer, cells were probed with MitoSOX to determine mitoROS production and MTV-G to determine relative mitochondrial mass. **A)** Representative Contour plot and scatter bar graphs of **B)** the percent MTDR$^+$ CD4$^+$ T cells and **C)** the relative fold change in MFI of MTDR$^+$ CD4$^+$ T cells after mito-transfer. **D)** Representative Contour plot and scatter bar graphs of **E)** relative MFI of MitoSOX Red and **F)** MTV-G in CD4$^+$ T cells from old mice after mito-transfer. **G**) Cardiolipin concentration curve of isolated mitochondria from MEFs. Cardiolipin experiments were repeated twice with 3-4 mice/group. **H)** Flow cytometry histograms and scatter bar graphs of **I)** percent MTDR$^+$ CD4$^+$ T cells, and **J**) relative MFI of MTDR$^+$ CD4$^+$ T cells after mito-transfer, based on cardiolipin concentration. Flow cytometry scatter bar graphs of **K)** percent HK-GFP$^+$ CD4$^+$ T cells, and **L)** the relative MFI of HK-GFP$^+$ CD4$^+$ T cells after mito-transfer. **M)** Confocal images of CD4$^+$ T cells with or without donor mitochondria (HK-GFP$^+$). **N)** TEM images mitochondrial distributions (black arrows) in CD4$^+$ T cells (young, old, and old+mito). Quantifications of **O)** total mitochondrial area, **P**) the number of mitochondria, and **Q)** percent area of mitochondria per cell area (in image slice) of CD4$^+$ T cells isolated from young and old mice, and old mice ~5-6 min after mito-transfer. TEM images were obtained from 2 mice/groups. All other experiments were done with at minimum 3 biological replicates (n=3). $p \leq 0.05$ = *, $p \leq 0.01$ = **, $p \leq 0.001$ = *** and $p \leq 0.001$ = **** , using unpaired Student's *t*-test, or one-way-ANOVA where appropriate.

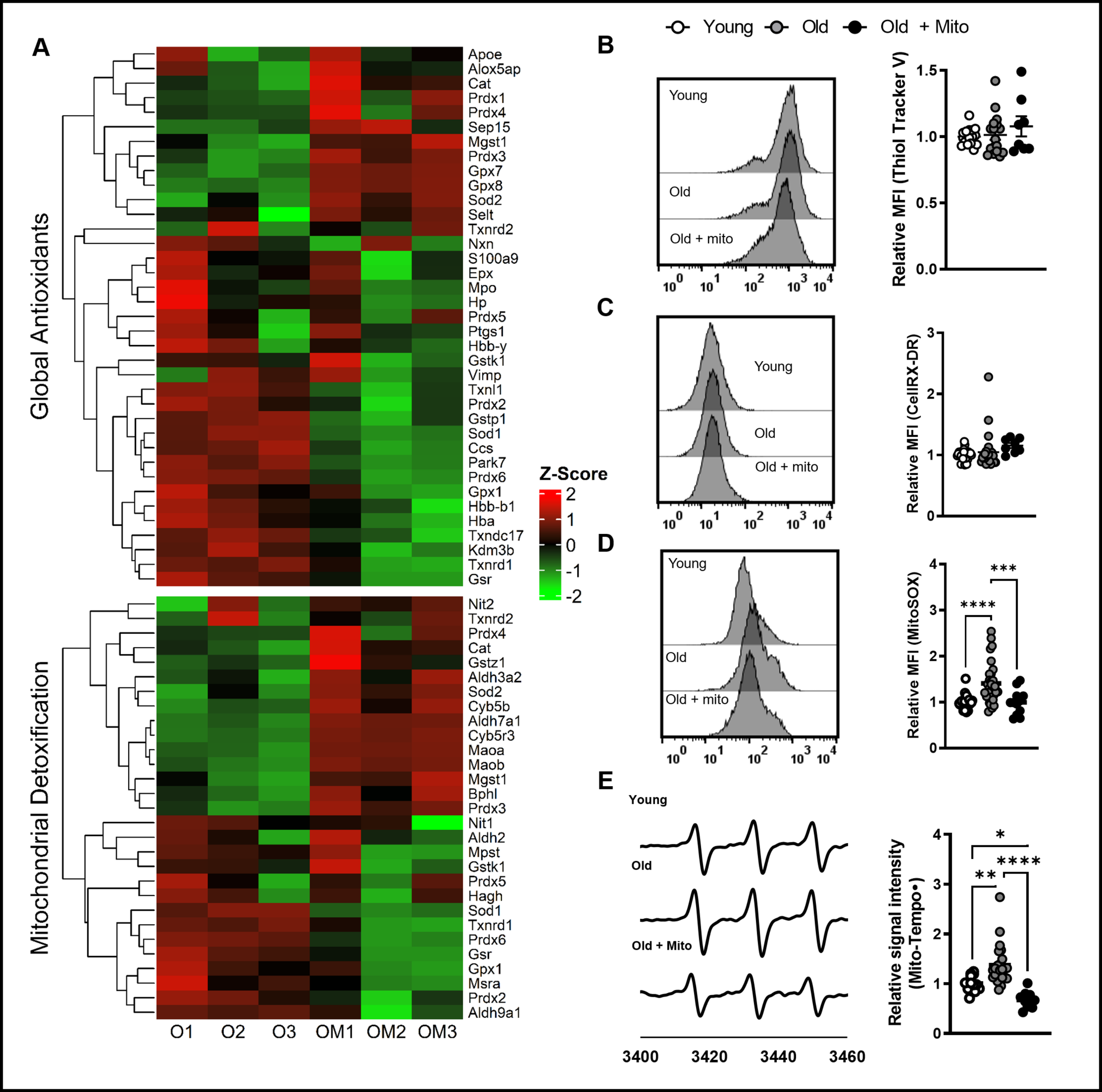
A
Global Antioxidants
Apoe
Alox5ap
Cat
Prdx1
Prdx4
Sep15
Mgst1
Prdx3
Gpx7
Gpx8
Sod2
Selt
Txnrd2
Nxn
S100a9
Epx
Mpo
Hp
Prdx5
Ptgs1
Hbb-y
Gstk1
Vimp
Txnl1
Prdx2
Gstp1
Sod1
Ccs
Park7
Prdx6
Gpx1
Hbb-b1
Hba
Txndc17
Kdm3b
Txnrd1
Gsr
Mitochondrial Detoxification
Nit2
Txnrd2
Prdx4
Cat
Gstz1
Aldh3a2
Sod2
Cyb5b
Aldh7a1
Cyb5r3
Maoa
Maob
Mgst1
Bphl
Prdx3
Nit1
Aldh2
Mpst
Gstk1
Prdx5
Hagh
Sod1
Txnrd1
Prdx6
Gsr
Gpx1
Msra
Prdx2
Aldh9a1
O1
O2
O3
OM1
OM2
OM3
Z-Score
2
1
0
-1
-2
Young
Old
Old + Mito
B
Young
Old
Old + mito
Relative MFI (Thiol Tracker V)
1.5
1.0
0.5
0.0
C
Young
Old
Old + mito
Relative MFI (CellRX-DR)
3
2
1
0
D
Young
Old
Old + mito
Relative MFI (MitoSOX)
4
3
2
1
0
***
****
E
Young
Old
Old + Mito
3400
3420
3440
3460
Relative signal intensity (Mito-Tempo•)
4
3
2
1
0
*
**
****

Fig 2. Mito-transfer decreases oxidative stress in $CD4^+$ T cells from old mice. A) Heatmap of proteins related to cellular antioxidants and mitochondrial detoxification in $CD4^+$ T cells from old mice with and without mito-transfer (4h). Flow cytometry histograms and scatter plots of the relative MFI of **B)** thiol-tracker violet, **C)** CellROX Deep Red, and **D)** MitoSOX Red stained $CD4^+$ T cells from young, old mice and $CD4^+$ T cells from old mice after mito-transfer. **E**) EPR spectrum and H) bar graphs of CD4+ T cells probed with Mito-Tempo-H. 4-5 mice per group, with experiments repeated at least once, $p \leq 0.05$ = *, $p \leq 0.01$ = **, $p \leq 0.001$ = *** and $p \leq 0.001$ = **** , using one-way-ANOVA where appropriate.

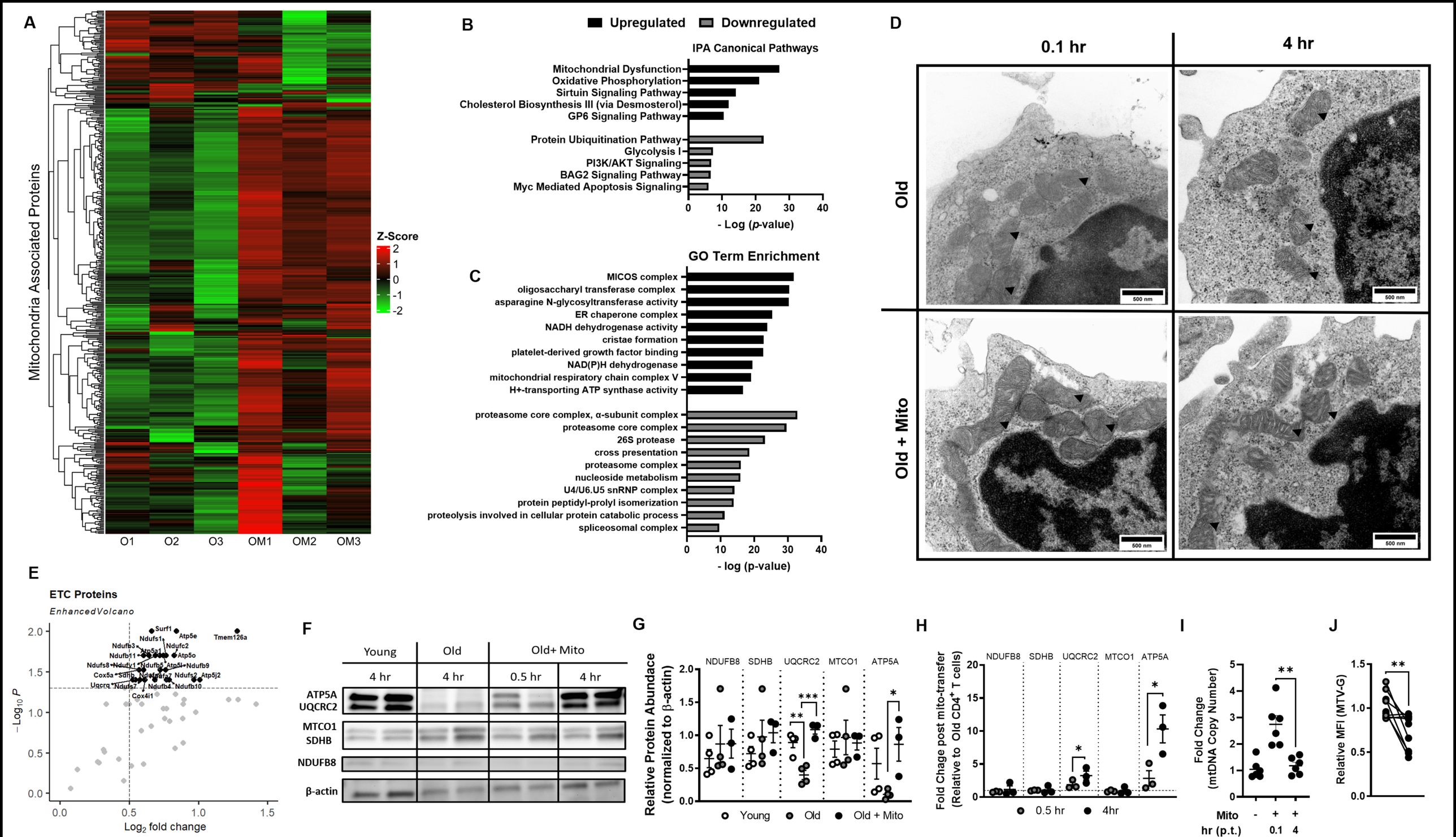
A
Mitochondria Associated Proteins
Z-Score
2
1
0
-1
-2
O1
O2
O3
OM1
OM2
OM3
B
Upregulated
Downregulated
IPA Canonical Pathways
Mitochondrial Dysfunction
Oxidative Phosphorylation
Sirtuin Signaling Pathway
Cholesterol Biosynthesis III (via Desmosterol)
GP6 Signaling Pathway
Protein Ubiquitination Pathway
Glycolysis I
PI3K/AKT Signaling
BAG2 Signaling Pathway
Myc Mediated Apoptosis Signaling
0
10
20
30
40
- Log (p-value)
C
GO Term Enrichment
MICOS complex
oligosaccharyl transferase complex
asparagine N-glycosyltransferase activity
ER chaperone complex
NADH dehydrogenase activity
cristae formation
platelet-derived growth factor binding
NAD(P)H dehydrogenase
mitochondrial respiratory chain complex V
H+-transporting ATP synthase activity
proteasome core complex, α-subunit complex
proteasome core complex
26S protease
cross presentation
proteasome complex
nucleoside metabolism
U4/U6.U5 snRNP complex
protein peptidyl-prolyl isomerization
proteolysis involved in cellular protein catabolic process
spliceosomal complex
0
10
20
30
40
- log (p-value)
D
0.1 hr
4 hr
Old
Old + Mito
500 nm
E
ETC Proteins
EnhancedVolcano
Surf1
Atp5e
Tmem126a
Ndufs1
Ndufb3
Ndufc2
Atp5a1
Ndufb11
Atp5o
Ndufs8
Ndufv1
Ndufb5
Atp5l
Ndufb9
Cox5a
Sdhb
Ndufaf7
Ndufs2
Atp5j2
Uqcrq
Ndufs7
Ndufb4
Ndufb10
Cox4i1
2.0
1.5
1.0
0.5
0.0
$-Log_{10}$ P
0.0
0.5
1.0
1.5
Log_2 fold change
F
Young
Old
Old+ Mito
4 hr
4 hr
0.5 hr
4 hr
ATP5A
UQCRC2
MTCO1
SDHB
NDUFB8
β-actin
G
NDUFB8
SDHB
UQCRC2
MTCO1
ATP5A
Relative Protein Abundace (normalized to β-actin)
2.0
1.5
1.0
0.5
0.0
**
***
*
Young
Old
Old + Mito
H
NDUFB8
SDHB
UQCRC2
MTCO1
ATP5A
Fold Chage post mito-transfer (Relative to Old CD4+ T cells)
20
15
10
5
0
*
*
0.5 hr
4hr
I
Fold Change (mtDNA Copy Number)
5
4
3
2
1
0
**
Mito
-
+
+
hr (p.t.)
0.1
4
J
Relative MFI (MTV-G)
1.5
1.0
0.5
0.0
**

Fig 3. Mito-transfer alters mitochondrial gene expression and mitochondrial ultrastructure. **A)** Heatmap of the mitochondrial proteome in $CD4^+$ T cells from old mice with and without mito-transfer. **B)** Top 5 upregulated and downregulated Canonical pathways (IPA) and the **C)** top 10 upregulated and downregulated GO Term enrichment of old CD4+ T cells after mito-transfer**. D)** TEM images of mitochondrial cristae morphology in $CD4^+$ T cells from old mice with and without mito-transfer at ~5 mins and 4 h after mito-transfer. **E)** Volcano plot of electron transport chain (ETC) proteome detected in $CD4^+$ T cells from old mice with and without mito-transfer, 4 h after mito-transfer. **F)** Western blot images and, **G)** relative protein abundance in $CD4^+$ T cells isolated from young and old mice, and $CD4^+$ T cells from old mice 4 h after mito-transfer. **H)** Fold change in ETC proteins in $CD4^+$ T cells from old mice after mito-transfer (at 30 min and 4 h). Proteomic experiments were performed once with 3 mice/group and internally normalized to β-actin. **I)** Fold change in mtDNA copy number in $CD4^+$ from old mice after mito-transfer (at 5 min and 4 h). **J)** Relative MFI of MTV-G in $CD4^+$ T cells from old mice (grey) and $CD4^+$ T cells from old mice (4h) after mito-transfer. $p \leq 0.05$ = * or $p \leq 0.01$ = **, using paired and unpaired Students' *t*-test where appropriate.

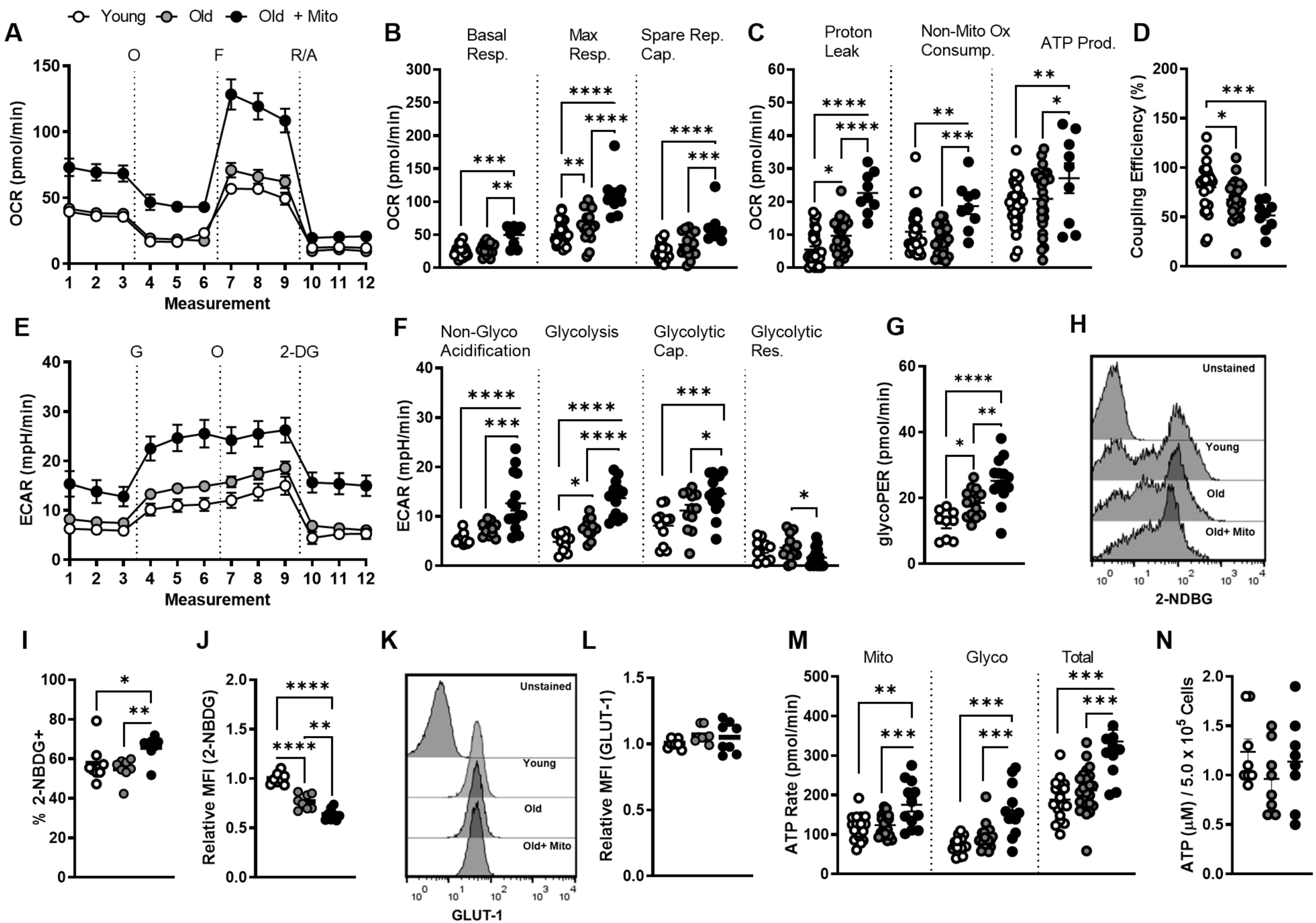
A
Young
Old
Old + Mito
O
F
R/A
OCR (pmol/min)
Measurement
B
Basal Resp.
Max Resp.
Spare Rep. Cap.
OCR (pmol/min)
C
Proton Leak
Non-Mito Ox Consump.
ATP Prod.
OCR (pmol/min)
D
Coupling Efficiency (%)
E
G
O
2-DG
ECAR (mpH/min)
Measurement
F
Non-Glyco Acidification
Glycolysis
Glycolytic Cap.
Glycolytic Res.
ECAR (mpH/min)
G
glycoPER (pmol/min)
H
Unstained
Young
Old
Old+ Mito
2-NDBG
I
% 2-NBDG+
J
Relative MFI (2-NBDG)
K
Unstained
Young
Old
Old+ Mito
GLUT-1
L
Relative MFI (GLUT-1)
M
Mito
Glyco
Total
ATP Rate (pmol/min)
N
ATP (μM) / 5.0 x 10^5 Cells

Fig. 4. Mito-transfer increases aerobic metabolism in $CD4^+$ T cells from old mice. $CD4^+$ T cells (2.5×10^5) were plated onto poly-D-lysine coated 96-well microplates, after which O_2 consumption (OCR) and extracellular acidification rates (ECAR) were measured under basal conditions and in response to the mito-stress test. **A)** Representative mito stress test kinetic graph, **B)** quantitation of basal, maximal, and spare respiratory capacity, **C)** proton leak, non-mitochondrial oxygen consumption, and ATP production rate, and **D)** coupling efficiency. **E)** Representative glycolysis stress test kinetic graph, and quantitations of **F)** non-glycolytic acidification, glycolysis, glycolytic capacity, glycolytic reserve and **G)** GlycoPER of $CD4^+$ T cells. **H)** Flow cytometry histograms and **I-J)** dot plots of 2-NBDG uptake in $CD4^+$ T cells from young and old mice, and $CD4^+$ T cells from old mice after mito- transfer. **K)** Flow cytometry histograms and **L)** dot plots of GLUT1 expression in $CD4^+$ T cells from young and old mice, and $CD4^+$ T cells from old mice after mito-transfer. **M)** Rates of glycolytic and mitochondrial-derived ATP, and total ATP production, and **N)** cellular levels of ATP in $CD4^+$ T cells from young and old mice, and $CD4^+$ T cells from old mice after mito-transfer; 3 to 4 mice were used per group and experiments were repeated at least once ($n \geq 2$), $p \leq 0.05$ = *, $p \leq 0.01$ = **, $p \leq 0.001$ = *** and $p \leq 0.001$ = **** , using one-way-ANOVA.

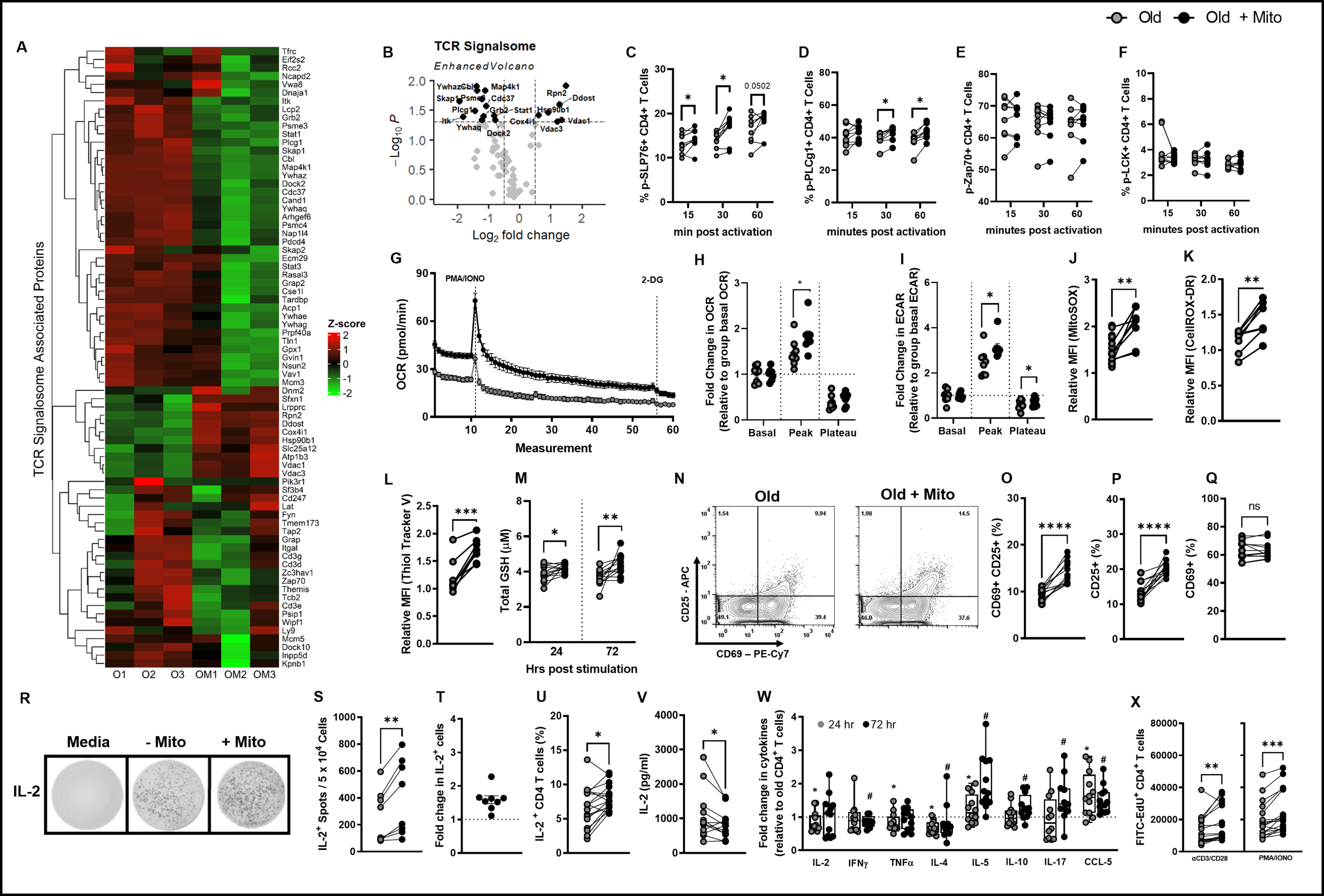

Old
Old + Mito
A
TCR Signalosome Associated Proteins
Z-score
O1 O2 O3 OM1 OM2 OM3
B
TCR Signalsome
EnhancedVolcano
Log2 fold change
C
% p-SLP76+ CD4+ T Cells
min post activation
D
% p-PLCg1+ CD4+ T Cells
minutes post activation
E
p-Zap70+ CD4+ T Cells
minutes post activation
F
% p-LCK+ CD4+ T Cells
minutes post activation
G
PMA/IONO
2-DG
OCR (pmol/min)
Measurement
H
Fold Change in OCR (Relative to group basal OCR)
Basal Peak Plateau
I
Fold Change in ECAR (Relative to group basal ECAR)
Basal Peak Plateau
J
Relative MFI (MitoSOX)
K
Relative MFI (CellROX-DR)
L
Relative MFI (Thiol Tracker V)
M
Total GSH (μM)
Hrs post stimulation
N
Old
Old + Mito
CD25 - APC
CD69 – PE-Cy7
O
CD69+ CD25+ (%)
P
CD25+ (%)
Q
CD69+ (%)
R
Media
- Mito
+ Mito
IL-2
S
IL-2+ Spots / 5 x 10^4 Cells
T
Fold chage in IL-2+ cells
U
IL-2 + CD4 T cells (%)
V
IL-2 (pg/ml)
W
24 hr
72 hr
Fold change in cytokines (relative to old CD4+ T cells)
IL-2 IFNγ TNFα IL-4 IL-5 IL-10 IL-17 CCL-5
X
FITC-EdU+ CD4+ T cells
αCD3/CD28
PMA/IONO

Fig 5. Mito-transfer improves T cell activation and cytokine production in $CD4^+$ T cells from old mice. The $CD4^+$ T cells from old mice with and without mito-transfer were evaluated for activation capabilities. **A)** Heatmap and **B)** volcano plot of TCR signalosome proteome detected in $CD4^+$ T cells isolated from old mice with or without mito-transfer. The phosphorylation kinetics of TCR-related proteins **C)** SLP76, **D)** PLCg1, **E)** Zap70 and **F)** LCK in $CD4^+$ T cells from old mice with or without mito-transfer, at 15, 30, and 60 min post activation with αCD3/αCD28 stimulation. **G)** OCR micrograph of $CD4^+$ T cells from old mice with or without mito-transfer, after acute activation with PMA/IONO. The relative fold changes in **H)** OCR and **I)** ECAR of $CD4^+$ T cells isolated from old mice with or without mito-transfer after acute activation with PMA/Ionomycin. The relative MFI of **J)** MitoSOX Red and **K)** CellROX Deep Red stained $CD4^+$ T cells from old mice with or without mito-transfer, after stimulation PMA/ Ionomycin (4h). **L)** Thiol-tracker violet and the **M)** total GSH produced by $CD4^+$ T cells from old mice with or without mito-transfer after stimulation with PMA/IONO.**N)** Contour plots of CD25 v CD69 expression on $CD4^+$ T cells with and without mito-transfer, after PMA/ Ionomycin stimulation (24 h). The percent of **O)** $CD25^+$ $CD69^+$, **P)** $CD25^+$ and, **Q)** $CD69^+$ $CD4^+$ T cells from old mice with or without mito-transfer, at stimulation with PMA/ Ionomycin (24h). **R)** Representative EliSpot images, the **S)** number IL-2^+ producing T cells and the **T)** fold change in IL-2^+ producing $CD4^+$ T cells from old mice with or without mito-transfer, after stimulation with PMA/Ionomycin (24hr). The **U)** percent of IL-2^+ $CD4^+$ T cells via intracellular cytokine staining, in $CD4^+$ T cells from old mice with or without mito-transfer, after stimulation with PMA/Ionomycin (4h). **V)** Soluble IL-2 detected in the supernatants of PMA/Ionomycin- stimulated (24 h) $CD4^+$ T cells from old mice with or without mito-transfer. The relative fold change in cytokine production of PMA/Ionomycin- stimulated $CD4^+$ T cells from old mice with or without mito-transfer, at 24 & 72 h after stimulation. **X)** Number of EdU^+ cells in αCD3/αCD28 or PMA/Ionomycin-stimulated $CD4^+$ T cell cultures from old mice with or without mito-transfer. All experiments were at least repeated (n=2), $p \leq 0.05$ = *, $p \leq 0.01$ = **, or $p \leq 0.001$ = *** using paired Student's *t*-test.

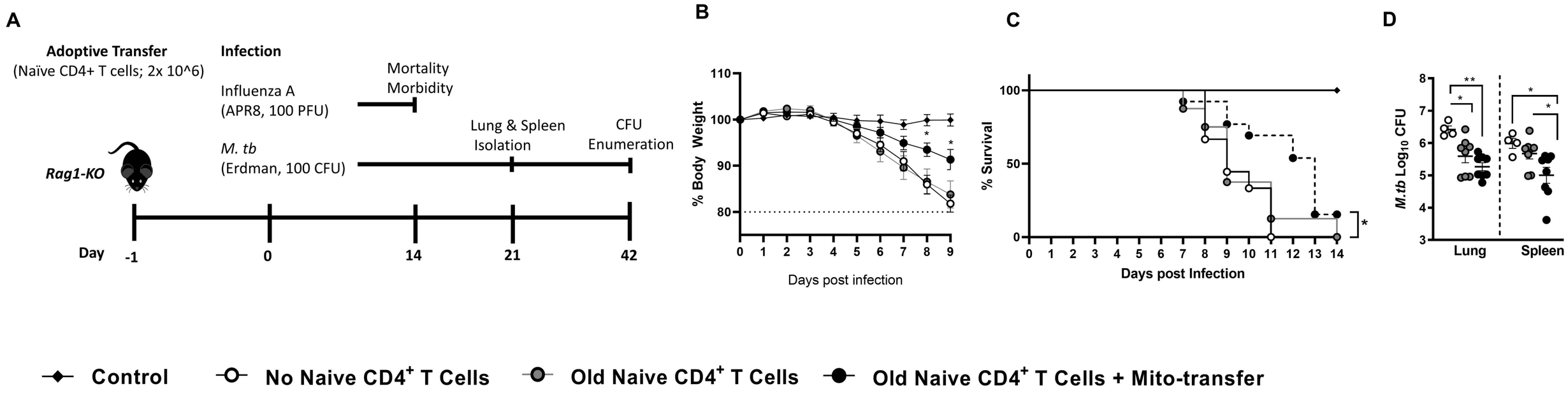
A
Adoptive Transfer
(Naïve CD4+ T cells; 2x 10^6)
Infection
Influenza A
(APR8, 100 PFU)
Mortality
Morbidity
M. tb
(Erdman, 100 CFU)
Lung & Spleen
Isolation
CFU
Enumeration
Rag1-KO
Day
-1
0
14
21
42
B
% Body Weight
Days post infection
C
% Survival
Days post Infection
D
M.tb Log10 CFU
Lung
Spleen
Control
No Naive CD4+ T Cells
Old Naive CD4+ T Cells
Old Naive CD4+ T Cells + Mito-transfer

Fig 6. Mito-transfer in naïve CD4 T cells from old mice protects mice against pathogens & promotes protective T cell phenotypes. A) 2.0 x 10^6 naïve $CD4^+$ T cells from old mice with or without mito-transfer, or PBS were tail vein injected in Rag1-KO mice that were subsequently infected with either IAV or *M.tb*. Rag1-KO mice infected with IAV were monitored for **B)** disease body weight (morbidity) and **C)** survival (mortality). After 21 days of infection, **D)** lung and spleen of Rag1-KO mice infected with *M.tb* were processed to determine M.tb burden.

Supplementary figures.

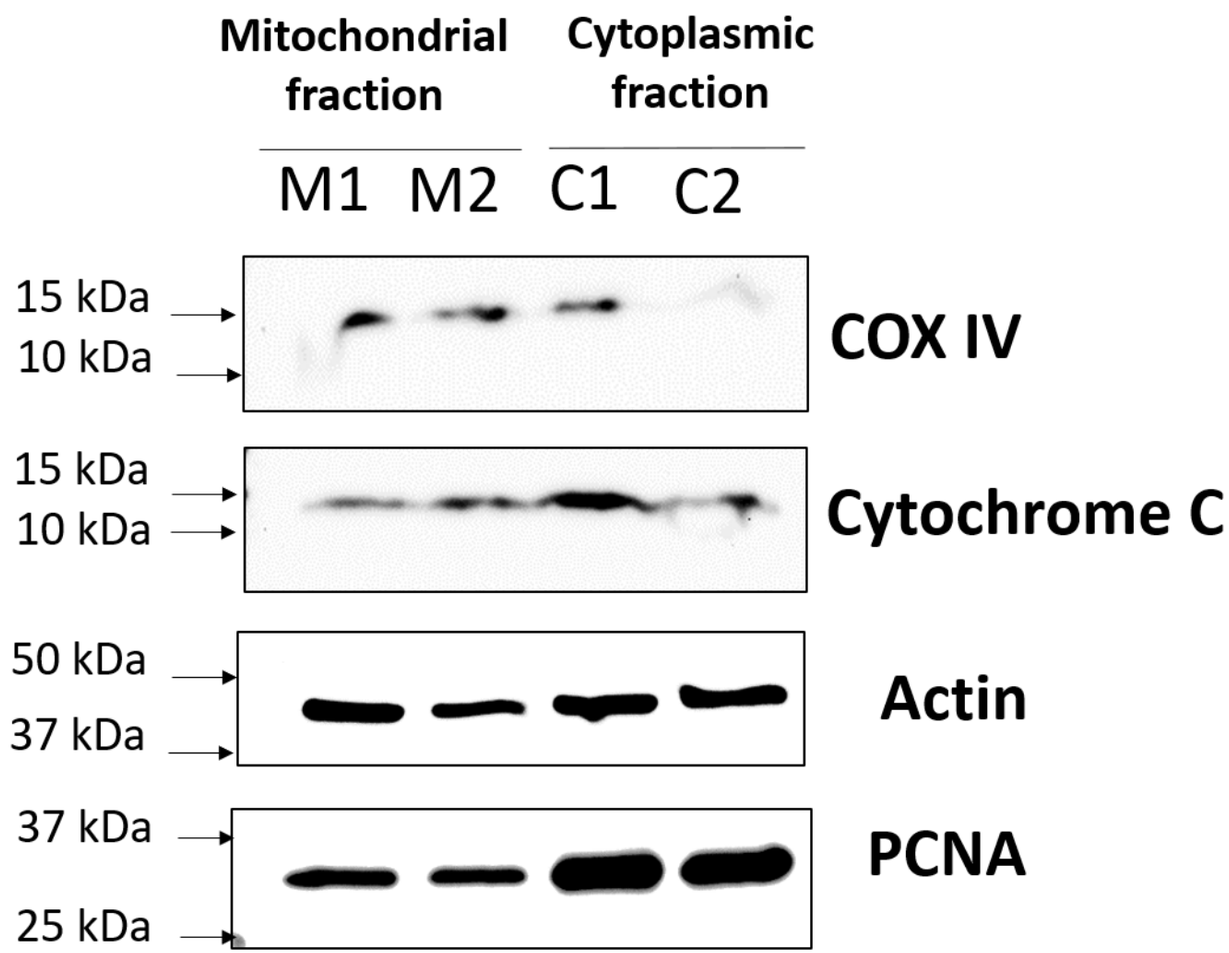
Mitochondrial fraction
Cytoplasmic fraction
M1
M2
C1
C2
15 kDa
10 kDa
COX IV
15 kDa
10 kDa
Cytochrome C
50 kDa
37 kDa
Actin
37 kDa
25 kDa
PCNA

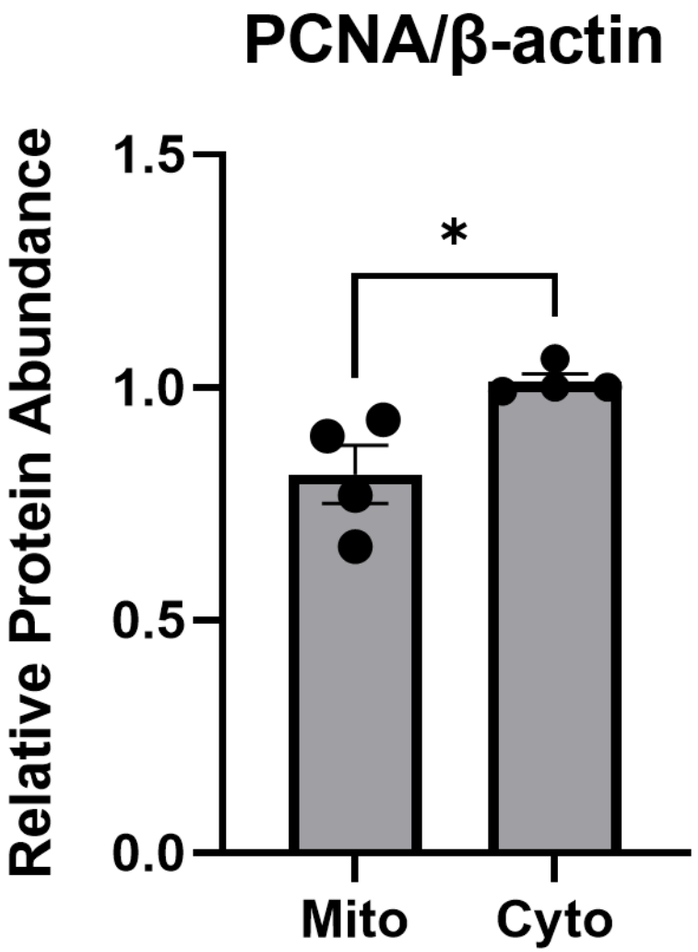
PCNA/β-actin
Relative Protein Abundance
1.5
1.0
0.5
0.0
*
Mito
Cyto

Supp. Fig. 1. Purity of mitochondrial isolation. A) Representative wester blot images of probed mitochondrial and nuclear proteins in the mitochondrial fraction and cell fragments/unlysed cells after mitochondrial isolation. **B)** Relative amount of PCNA normalized to B-actin. (n=4), $p<0.05$=significant (*) using unpaired Student's t-test.

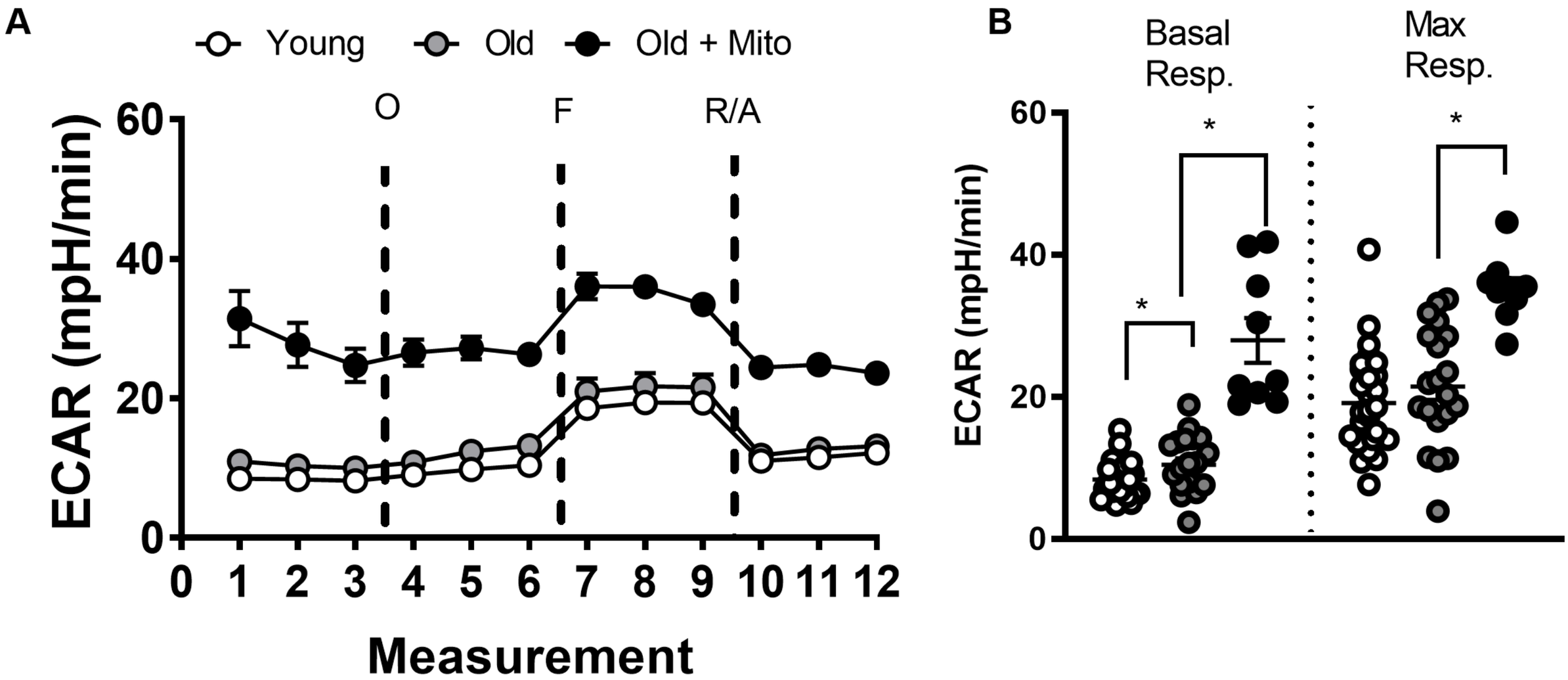
A
Young
Old
Old + Mito
O
F
R/A
ECAR (mpH/min)
60
40
20
0
0 1 2 3 4 5 6 7 8 9 10 11 12
Measurement
B
Basal Resp.
Max Resp.
ECAR (mpH/min)
60
40
20
0
*
*
*

Supp. Fig. 2. Mito-transfer increases ECAR of $CD4^+$ T cells from old mice. A) Kinetic curve of ECAR collected from mito-stress test assay, **B)** ECAR corresponding to basal and maximal respiration of $CD4^+$ T cells. 3-4 mice were used per group and experiments were replicated twice (n=3), $p<0.05$=significant (*) using unpaired Student's t-test.

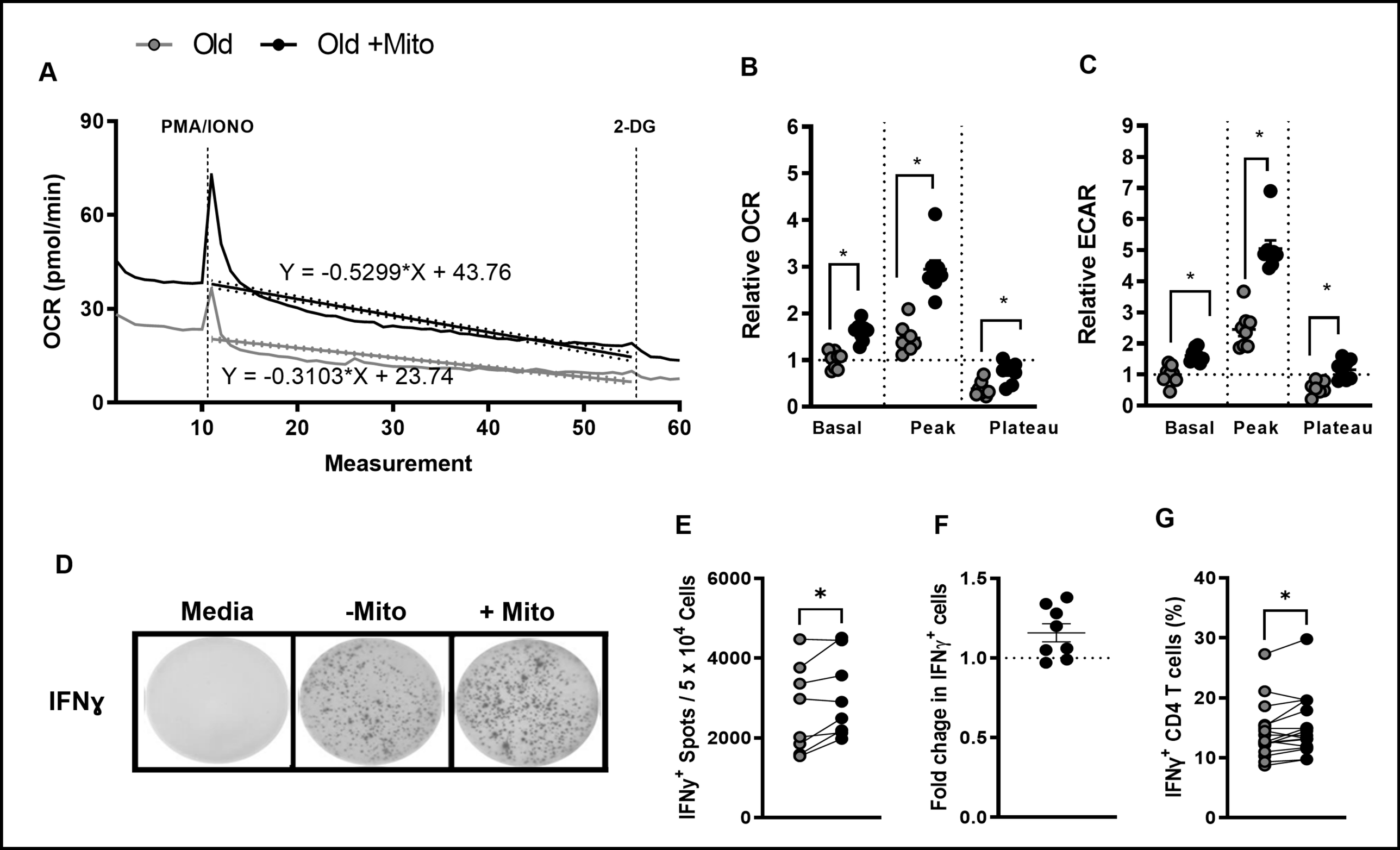
Old
Old +Mito
A
PMA/IONO
2-DG
OCR (pmol/min)
Y = -0.5299*X + 43.76
Y = -0.3103*X + 23.74
Measurement
B
Relative OCR
Basal
Peak
Plateau
C
Relative ECAR
Basal
Peak
Plateau
D
Media
-Mito
+ Mito
IFNγ
E
IFNγ+ Spots / 5 x 10^4 Cells
F
Fold chage in IFNγ+ cells
G
IFNγ+ CD4 T cells (%)

Supp. Fig. 3. Mito-transfer enhaced T cell activation induced metabolic switch and increased IFNγ$^+$ CD4$^+$ T cells. A) The slope of OCR depression after acute injection of PMA/IONO in mito-transferred and non-manipulated CD4+ T cells from old mice. The relative change in **B)** OCR and **C)** ECAR of activated T cells (non-normalized to group). **D-G)** CD4$^+$ T cells from old mice with or without mito-transfer were stimulated with PMA/Ionomycin, after which various assays were used to quantify IFNγ production. **D)** Representative EliSpot images, **E)** the number IFNγ$^+$ producing T cells, and **F)** the fold change in IFNγ$^+$ producing CD4$^+$ T cells from old mice with or without mito-transfer, after stimulation with PMA/Ionomycin (24hr). The **G)** percent of IFNγ$^+$ CD4$^+$ T cells via intracellular cytokine staining, in CD4$^+$ T cells from old mice with or without mito-transfer, after stimulation with PMA/Ionomycin (4h). 3-4 mice per group, repeated at least once ($n \geq 2$). $p < 0.05$ = significant (*) using paired Student's *t*-test.

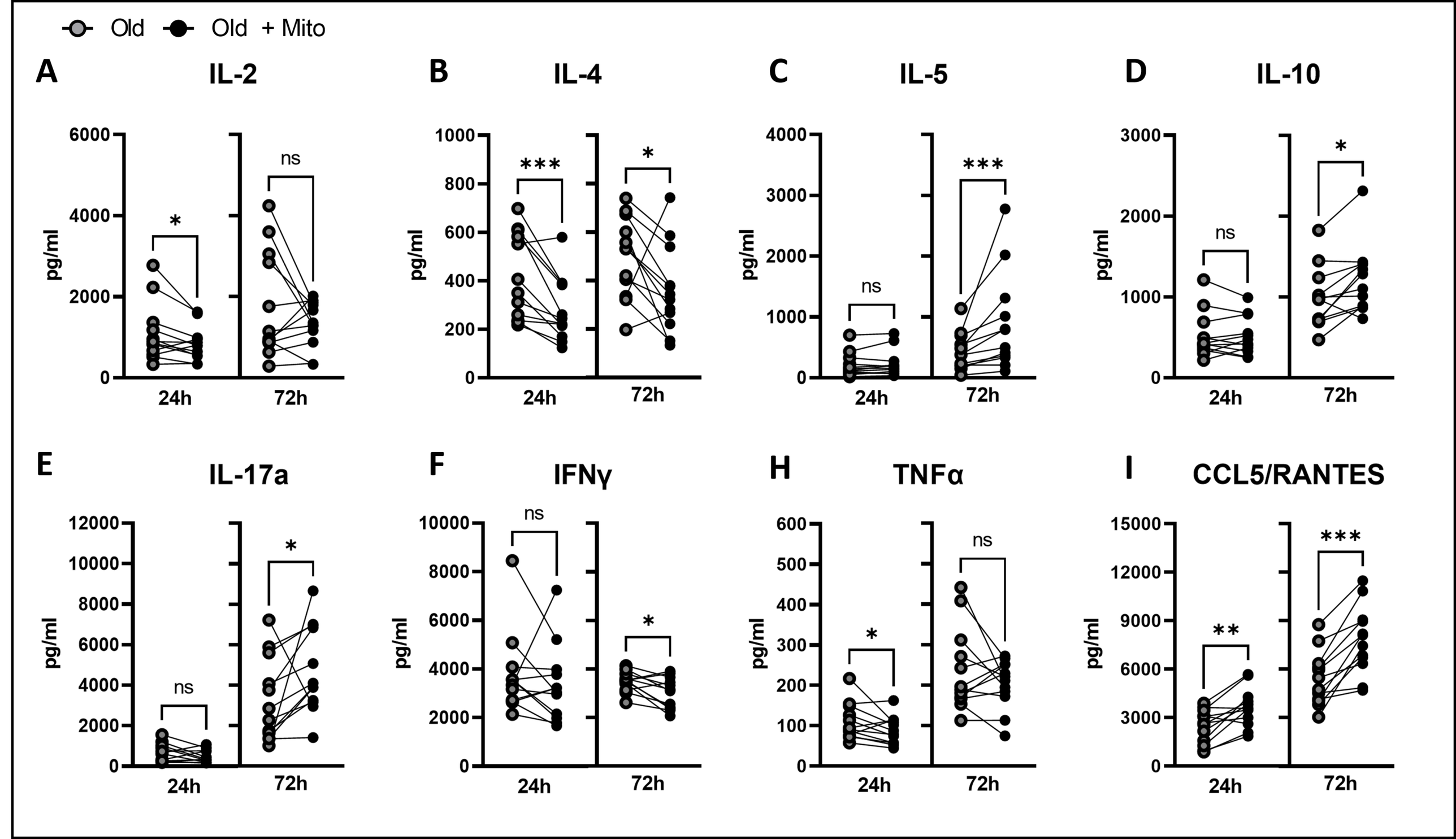
Old
Old + Mito
A
IL-2
B
IL-4
C
IL-5
D
IL-10
E
IL-17a
F
IFNγ
H
TNFα
I
CCL5/RANTES
pg/ml
24h
72h
ns
*
**
***

Supp. Fig. 4. Mito-transfer alters T cell activation & cytokine production of $CD4^+$ T cells in old mice. $CD4^+$ T cells from old mice with or without mito-transfer were stimulated with PMA/Ionomycin. After 24 and 72 h of stimulation with PMA/Ionomycin, the supernatants were examined by Luminex array for cytokines produced. $p \leq 0.05$ = *, $p \leq 0.01$ = **, or $p \leq 0.001$ = *** using paired Student's *t*-test.

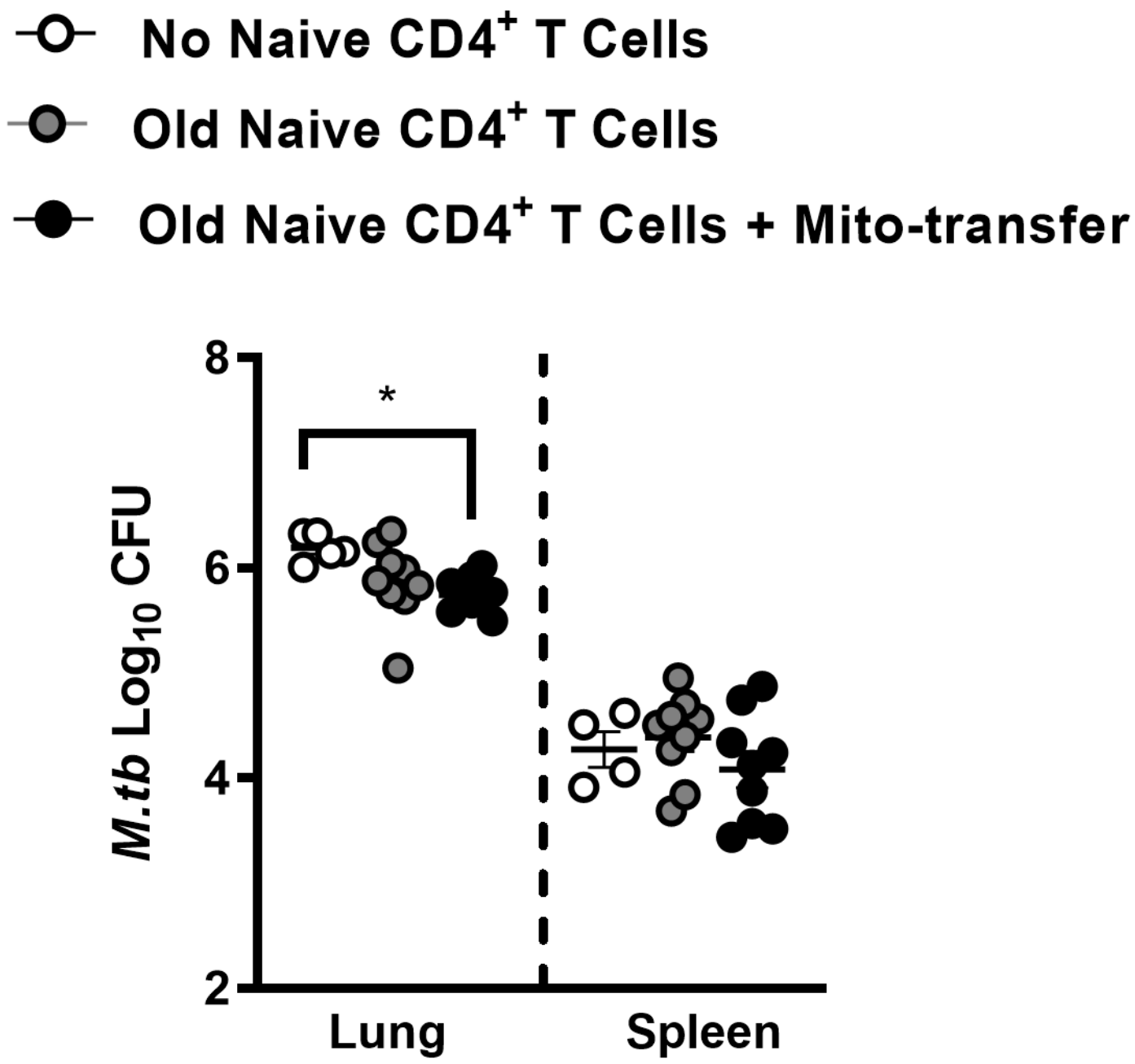
No Naive CD4+ T Cells
Old Naive CD4+ T Cells
Old Naive CD4+ T Cells + Mito-transfer
M.tb Log10 CFU
8
6
4
2
*
Lung
Spleen

Supp. Fig. 5. Mito-transfer in naïve CD4 T cells from old mice protected mice against pathogens. Naïve $CD4^+$ T cells from old mice with or without mito-transfer, or PBS were tail vein injected in Rag1-KO mice that were subsequently infected with *M.tb*. Lung and spleen CFU burden after 21 days of *M.tb* infection in Rag1-KO mice adoptively treated with $1x\ 10^6$ naïve $CD4^+$ T cells from old mice with or without mito-transfer. 4-8 mice per group, with $p \leq 0.05$ = *, using unpaired Student's *t*-test.

Uniprot ID	Gene ID	P.Val	FDR	O1	O2	O3	OM1	OM2	OM3
P24270	Cat	0.046	0.148	0.177	0.000	-0.253	1.040	0.403	0.494
Q99LX0	Park7	0.001	0.015	0.016	-0.257	0.000	-1.140	-1.450	-1.350
P11247	Mpo	0.459	0.719	1.480	0.000	-0.328	0.674	-0.715	-0.546
Q9JMH6	Txnrd1	0.030	0.114	0.000	-0.115	0.093	-0.408	-1.270	-1.320
P08228	Sod1	0.000	0.013	-0.224	0.010	0.000	-1.080	-1.290	-1.170
Q9ERR7	Sep15	0.054	0.164	0.000	0.000	0.112	0.582	0.658	0.160
O08709	Prdx6	0.003	0.031	0.085	0.000	-0.156	-1.090	-1.810	-1.670
P19157	Gstp1	0.004	0.036	-0.138	0.000	0.106	-1.050	-1.380	-0.809
Q8CDN6	Txnl1	0.008	0.051	0.000	0.040	-0.283	-0.969	-1.380	-0.821
P11352	Gpx1	0.131	0.294	0.457	0.000	-0.235	-0.028	-0.804	-0.877
P99029	Prdx5	0.996	1.000	0.234	0.000	-0.266	0.051	-0.201	0.121
Q61171	Prdx2	0.040	0.134	0.089	0.000	-0.208	-0.353	-0.755	-0.402
P09671	Sod2	0.023	0.096	-0.061	0.348	0.000	0.715	0.476	0.682
P02088	Hbb-b1	0.050	0.155	0.499	0.000	-0.660	-1.080	-1.670	-3.060
P35700	Prdx1	0.130	0.293	0.028	0.000	-0.030	0.421	-0.006	0.325
Q99LJ6	Gpx7	0.000	0.012	0.150	-1.130	0.000	5.360	4.910	5.340
Q9D7B7	Gpx8	0.000	0.007	0.000	0.540	-0.171	5.920	5.450	5.940
P31725	S100a9	0.374	0.622	1.930	0.000	-0.136	0.985	-2.240	-0.397
P01942	Hba	0.040	0.135	0.473	0.000	-0.794	-0.999	-1.950	-2.470
P49290	Epx	0.465	0.724	1.320	-0.368	0.000	0.885	-1.770	-0.395
P22437	Ptgs1	0.902	1.000	0.376	0.000	-0.608	0.313	-0.174	-0.239
P62342	Selt	0.115	0.270	0.000	0.100	-0.390	0.284	0.120	0.255
Q91VS7	Mgst1	0.030	0.113	0.999	0.000	-0.245	1.580	1.500	2.410
P47791	Gsr	0.018	0.084	0.341	0.000	-0.118	-0.466	-1.080	-1.080
Q9JLT4	Txnrd2	0.839	1.000	0.000	0.351	-0.041	0.125	0.030	0.247
Q6ZPY7	Kdm3b	0.027	0.107	0.000	0.495	-0.124	-0.530	-1.600	-1.240
Q9CQM5	Txndc17	0.008	0.055	-0.143	0.362	0.000	-1.500	-1.760	-2.830
P08226	Apoe	0.508	0.772	0.861	-0.299	0.000	0.960	0.161	0.360
P20108	Prdx3	0.006	0.046	0.214	-0.058	0.000	0.778	0.509	0.675
Q61646	Hp	0.202	0.399	1.520	-0.351	0.000	0.109	-1.160	-0.961
O08807	Prdx4	0.256	0.470	0.038	0.000	-0.002	0.439	-0.070	0.262
Q9DCM2	Gstk1	0.701	0.977	0.010	0.000	-0.212	0.377	-0.571	-0.378
Q9BCZ4	Vimp	0.732	1.000	-0.386	0.179	0.000	0.206	-0.445	-0.249
Q9WU84	Ccs	0.004	0.036	-0.087	0.000	0.263	-0.735	-1.230	-1.050
P30355	Alox5ap	0.424	0.678	0.786	0.000	-0.301	1.160	0.291	0.218
P02104	Hbb-y	0.451	0.708	0.641	0.000	-2.510	-0.842	-1.560	-2.020
P97346	Nxn	0.333	0.570	0.333	0.000	-1.090	-2.170	0.304	-1.790

Uniprot	Gene ID	P.Val	FDR	O1	O2	O3	OM1	OM2	OM3
P24270	Cat	0.046	0.148	0.177	0.000	-0.253	1.040	0.403	0.494
P47738	Aldh2	0.815	1.000	0.398	0.000	-0.923	0.773	-0.269	-0.602

Q8VDK1	Nit1	0.269	0.488	0.029	0.000	-0.100	-0.074	-0.053	-0.391
P47740	Aldh3a2	0.057	0.169	0.000	0.097	-0.121	0.310	0.102	0.328
Q9JMH6	Txnrd1	0.030	0.114	0.000	-0.115	0.093	-0.408	-1.270	-1.320
P08228	Sod1	0.000	0.013	-0.224	0.010	0.000	-1.080	-1.290	-1.170
Q99J99	Mpst	0.334	0.571	0.163	0.000	-0.160	0.378	-0.932	-0.891
Q9JHW2	Nit2	0.309	0.542	-0.141	0.431	0.000	0.296	0.245	0.362
O08709	Prdx6	0.003	0.031	0.085	0.000	-0.156	-1.090	-1.810	-1.670
P11352	Gpx1	0.131	0.294	0.457	0.000	-0.235	-0.028	-0.804	-0.877
P99029	Prdx5	0.996	1.000	0.234	0.000	-0.266	0.051	-0.201	0.121
Q61171	Prdx2	0.040	0.134	0.089	0.000	-0.208	-0.353	-0.755	-0.402
P09671	Sod2	0.023	0.096	-0.061	0.348	0.000	0.715	0.476	0.682
Q64133	Maoa	0.000	0.011	0.151	0.000	-0.761	3.640	3.580	3.770
Q8R164	Bphl	0.031	0.114	0.197	0.000	-0.133	0.714	0.305	0.778
Q9DBF1	Aldh7a1	0.000	0.009	0.000	0.318	-0.191	2.700	2.460	2.520
Q9WVL0	Gstz1	0.112	0.265	0.000	0.163	-0.024	1.190	0.487	0.239
Q9DCN2	Cyb5r3	0.000	0.005	0.000	0.161	-0.051	2.080	1.950	2.120
Q8BW75	Maob	0.000	0.013	0.667	0.000	-0.370	4.120	3.720	4.010
Q9CQX2	Cyb5b	0.013	0.071	-0.164	0.064	0.000	0.975	0.423	0.947
Q99KB8	Hagh	0.754	1.000	0.142	0.000	-0.442	-0.018	-0.512	-0.014
Q9JLJ2	Aldh9a1	0.081	0.213	0.030	-0.088	0.000	-0.239	-1.410	-0.779
Q91VS7	Mgst1	0.030	0.113	0.999	0.000	-0.245	1.580	1.500	2.410
P47791	Gsr	0.018	0.084	0.341	0.000	-0.118	-0.466	-1.080	-1.080
Q9JLT4	Txnrd2	0.839	1.000	0.000	0.351	-0.041	0.125	0.030	0.247
P20108	Prdx3	0.006	0.046	0.214	-0.058	0.000	0.778	0.509	0.675
O08807	Prdx4	0.256	0.470	0.038	0.000	-0.002	0.439	-0.070	0.262
Q9D6Y7	Msra	0.068	0.189	0.549	-0.217	0.000	-0.252	-0.768	-0.814
Q9DCM2	Gstk1	0.701	0.977	0.010	0.000	-0.212	0.377	-0.571	-0.378

Supp. Table 1. Antioxidant & mitochondrial detoxification proteins were detected in $CD4^+$ T cells isolated from old mice after mito-transfer and in non-manipulated $CD4^+$ T cells from old mice. $CD4^+$ T cells from young and old mice, and from old mice after mito-transfer were cultured for 4 h before processing for mass spectrometry analysis. Data expressed as median protein Log2 fold change of $CD4^+$ T cells from old mice, from 3 individual old mice (paired experiment)

Uniprot ID	Gene ID	P. Val	FDR	O1	O2	O3	OM1	OM2	OM3
Q9JIK9	Mrps34	0.049	0.154	0.000	0.757	-0.497	1.210	1.140	1.010
Q8K1Z0	Coq9	0.032	0.117	0.000	0.186	-0.023	0.862	0.388	0.472
P97450	Atp5j	0.033	0.121	0.000	0.125	-0.630	1.010	0.420	1.140

Q9D0K2	Oxct1	0.000	0.012	0.000	0.092	-0.243	1.760	1.440	1.670
P52825	Cpt2	0.312	0.545	0.000	0.208	-0.370	1.210	0.043	0.051
Q9D6J6	Ndufv2	0.049	0.154	0.000	0.342	-0.183	0.718	0.363	0.856
O08734	Bak1	0.010	0.060	0.000	0.028	-0.547	0.687	0.764	0.655
P24270	Cat	0.046	0.148	0.177	0.000	-0.253	1.040	0.403	0.494
Q8BJZ4	Mrps35	0.007	0.051	0.062	0.000	-0.636	1.340	1.050	0.901
D3Z7P3	Gls	0.500	0.765	0.000	0.006	-0.037	0.732	-0.191	0.043
Q9JI39	Abcb10	0.138	0.303	0.860	-0.266	0.000	1.480	0.456	1.190
Q9CQJ8	Ndufb9	0.003	0.033	-0.196	0.220	0.000	0.740	0.744	0.811
P97742	Cpt1a	0.015	0.076	0.000	0.296	-0.452	0.925	0.756	0.903
P47738	Aldh2	0.815	1.000	0.398	0.000	-0.923	0.773	-0.269	-0.602
Q9Z2I8	Suclg2	0.566	0.835	0.026	0.000	-0.159	0.510	-0.235	0.016
Q9DCX2	Atp5h	0.025	0.101	0.000	0.466	-0.336	1.070	1.120	0.719
Q8VE22	Mrps23	0.006	0.044	-0.054	0.132	0.000	0.889	0.501	0.810
Q9D404	Oxsm	0.917	1.000	0.000	0.611	-0.220	0.234	0.026	0.045
Q99JB2	Stoml2	0.007	0.048	0.000	0.206	-0.196	0.991	0.626	0.828
P59017	Bcl2l13	0.118	0.274	0.000	-0.077	0.194	-0.067	-0.784	-0.362
Q8BGH2	Samm50	0.000	0.013	0.000	0.083	-0.194	0.973	0.871	0.934
Q9CZR8	Tsfm	0.707	0.983	0.245	0.000	-0.207	0.426	-0.475	-0.282
Q6PB66	Lrpprc	0.035	0.125	0.000	0.121	-0.292	0.941	0.428	0.430
O09111	Ndufb11	0.001	0.018	0.019	-0.197	0.000	0.578	0.575	0.648
Q9D6R2	Idh3a	0.546	0.814	0.000	0.280	-0.166	0.748	-0.097	0.040
Q9CQ92	Fis1	0.078	0.209	0.240	-0.067	0.000	-0.226	-0.500	-0.127
Q78PY7	Snd1	0.431	0.687	0.121	0.000	-0.224	0.151	-0.543	-0.309
P29758	Oat	0.001	0.018	0.000	0.170	-0.473	1.810	1.920	2.200
O08749	Dld	0.005	0.039	0.000	0.188	-0.179	0.904	0.625	0.763
P38647	Hspa9	0.072	0.196	0.035	0.000	-0.356	1.510	0.407	0.498
P63038	Hspd1	0.006	0.044	0.000	0.119	-0.240	1.090	0.650	0.822
Q9DBL1	Acadsb	0.001	0.022	0.000	0.020	-0.201	1.980	1.390	1.380
Q9Z2I0	Letm1	0.002	0.025	0.000	0.057	-0.198	0.565	0.495	0.591
Q07813	Bax	0.323	0.559	-0.110	0.000	0.085	0.671	-0.114	0.210
Q99JY0	Hadhb	0.462	0.721	-0.070	0.350	0.000	0.625	-0.024	0.237
Q9Z110	Aldh18a1	0.109	0.261	0.000	0.052	-0.331	1.350	0.197	0.449
Q8VDK1	Nit1	0.269	0.488	0.029	0.000	-0.100	-0.074	-0.053	-0.391
Q9CPY7	Lap3	0.806	1.000	0.158	0.000	-0.383	0.568	-0.516	0.000
Q8BH59	Slc25a12	0.037	0.127	-0.084	0.153	0.000	0.368	0.204	0.480
Q9R0X4	Acot9	0.058	0.171	0.000	0.694	-0.021	1.030	0.770	0.829
Q8BWT1	Acaa2	0.089	0.228	0.000	0.088	-0.212	0.592	0.136	0.245
Q99N84	Mrps18b	0.001	0.019	-0.100	0.262	0.000	1.290	1.020	1.220
Q99LX0	Park7	0.001	0.015	0.016	-0.257	0.000	-1.140	-1.450	-1.350
Q9CQ06	Mrpl24	0.031	0.115	0.158	0.000	-0.175	0.302	0.820	0.865
P47740	Aldh3a2	0.057	0.169	0.000	0.097	-0.121	0.310	0.102	0.328
Q9CPV4	Glod4	0.023	0.096	0.000	0.150	-0.049	-0.326	-0.824	-0.470
Q9D0L7	Armc10	0.027	0.107	-0.131	0.052	0.000	-0.301	-0.431	-0.208
Q9CR61	Ndufb7	0.020	0.088	0.000	-0.043	0.113	0.717	0.435	1.080

Q9DC69	Ndufa9	0.004	0.037	-0.072	0.102	0.000	0.741	0.442	0.635
Q9CQN1	Trap1	0.459	0.719	0.170	0.000	-0.139	0.175	-0.335	-0.254
Q9Z2Z6	Slc25a20	0.006	0.043	0.161	0.000	-0.081	0.953	0.633	0.619
Q921H8	Acaa1a	0.168	0.349	0.077	0.000	-0.377	0.732	-0.098	0.503
Q9ERS2	Ndufa13	0.056	0.168	0.038	-0.179	0.000	0.652	0.143	0.876
P19783	Cox4i1	0.004	0.038	0.100	-0.024	0.000	0.711	0.422	0.696
Q9CZ42	Naxd	0.001	0.018	0.148	0.000	-0.050	1.030	0.765	0.960
Q99LC3	Ndufa10	0.006	0.047	0.000	0.010	-0.249	0.718	0.460	0.860
Q8R2Y8	Ptrh2	0.015	0.077	-0.265	0.190	0.000	1.240	1.150	2.290
Q8R4N0	Clybl	0.061	0.177	0.182	0.000	-0.138	0.704	0.176	0.694
O88696	Clpp	0.016	0.078	0.000	0.043	-0.364	0.863	0.401	0.665
Q80Y81	Elac2	0.624	0.899	0.000	-0.208	0.155	0.131	-0.831	0.116
Q9CRD0	Ociad1	0.184	0.372	-0.379	0.247	0.000	-0.636	-0.622	-0.097
Q64105	Spr	0.003	0.033	-0.370	0.096	0.000	-1.650	-1.710	-1.160
P09528	Fth1	0.085	0.220	0.442	-0.233	0.000	-0.225	-1.190	-0.715
Q9DB77	Uqcrc2	0.140	0.306	0.000	0.125	-0.097	0.556	0.046	0.312
Q61425	Hadh	0.375	0.623	-0.733	0.214	0.000	0.578	0.284	-0.255
Q99MN9	Pccb	0.003	0.032	0.000	0.238	-0.023	0.894	0.712	1.040
Q8BMS1	Hadha	0.932	1.000	0.027	0.000	-0.269	0.492	-0.475	-0.178
P38060	Hmgcl	0.061	0.177	0.000	0.148	-0.178	0.592	0.202	0.328
Q9CZ13	Uqcrc1	0.015	0.076	0.081	0.000	-0.051	0.660	0.292	0.464
Q922W5	Pycr1	0.000	0.014	0.208	0.000	-0.219	2.510	1.920	2.420
P97287	Mcl1	0.225	0.427	0.197	0.000	-0.777	0.487	-0.153	1.300
P50544	Acadvl	0.245	0.456	0.000	0.061	-0.285	0.866	-0.022	0.132
Q8CAQ8	Immt	0.003	0.032	0.000	0.109	-0.145	0.915	0.583	0.795
P56480	Atp5b	0.009	0.057	0.000	0.258	-0.162	0.723	0.568	0.808
Q9CYG7	Tomm34	0.013	0.071	-0.013	0.210	0.000	-0.338	-0.800	-0.588
O35857	Timm44	0.016	0.078	0.231	0.000	-0.162	0.827	0.450	0.765
Q8CC88	Vwa8	0.942	1.000	0.000	0.045	-0.313	0.847	-0.752	-0.481
Q91VD9	Ndufs1	0.002	0.025	0.000	0.197	-0.065	0.847	0.648	0.786
Q8BFR5	Tufm	0.440	0.697	0.165	0.000	-0.339	0.256	-0.698	-0.598
Q14C51	Ptcd3	0.001	0.019	0.000	0.011	-0.187	0.717	0.554	0.741
Q9QX60	Dguok	0.708	0.984	-0.077	0.150	0.000	0.044	-0.050	0.196
Q9JJL8	Sars2	0.446	0.703	0.281	0.000	-0.050	0.559	-0.022	0.196
Q99JR1	Sfxn1	0.018	0.083	0.000	0.180	-0.179	0.403	0.408	0.393
Q80Y14	Glrx5	0.112	0.265	0.079	0.000	-0.218	0.910	0.185	0.266
P50136	Bckdha	0.099	0.243	0.030	0.000	-0.341	0.421	0.014	0.389
P54071	Idh2	0.004	0.036	0.054	0.000	-0.276	1.440	0.889	0.986
Q9WTP7	Ak3	0.037	0.129	-0.146	0.101	0.000	0.809	0.233	0.598
Q6NVE9	Pptc7	0.557	0.825	0.000	-0.054	0.016	0.205	-0.490	-0.140
Q7TMF3	Ndufa12	0.011	0.064	-0.161	0.000	0.141	0.792	0.547	1.110
O35465	Fkbp8	0.521	0.786	0.000	0.167	-0.029	0.317	-0.227	-0.452
Q60932	Vdac1	0.006	0.046	0.000	0.313	-0.052	1.240	1.010	1.700
Q60597	Ogdh	0.007	0.048	0.000	0.044	-0.239	0.747	0.432	0.587
Q78IK4	Apool	0.010	0.060	-0.061	0.205	0.000	0.712	0.459	0.823

Q91YT0	Ndufv1	0.001	0.019	0.000	0.034	-0.076	0.817	0.553	0.688
Q91ZA3	Pcca	0.004	0.037	0.000	0.273	-0.086	0.822	0.667	0.847
Q3UV70	Pdp1	0.009	0.056	-0.168	0.000	0.071	0.763	0.401	0.775
P51174	Acadl	0.039	0.132	0.000	0.343	-0.012	0.526	0.424	0.475
Q8K4Z3	Naxe	0.013	0.071	0.012	0.000	-0.125	0.324	0.340	0.156
Q99KI0	Aco2	0.135	0.299	0.000	0.042	-0.166	0.553	0.087	0.138
P26443	Glud1	0.007	0.048	-0.208	0.207	0.000	0.756	0.579	0.813
Q8BMF4	Dlat	0.002	0.025	0.000	0.245	-0.070	1.060	0.823	1.080
Q9Z2I9	Sucla2	0.144	0.311	0.045	0.000	-0.226	0.968	0.063	0.320
Q9DCS9	Ndufb10	0.006	0.043	0.000	0.250	-0.106	0.628	0.918	0.805
Q99MN1	Kars	0.095	0.237	0.000	0.246	-0.487	-0.474	-0.558	-0.660
Q8R123	Flad1	0.186	0.376	0.107	0.000	-0.001	-0.107	-0.914	-0.144
Q9JMH6	Txnrd1	0.030	0.114	0.000	-0.115	0.093	-0.408	-1.270	-1.320
Q9D2G2	Dlst	0.003	0.033	0.000	0.150	-0.204	0.862	0.626	0.867
Q80ZK0	Mrps10	0.027	0.107	0.000	0.562	-0.484	1.350	0.904	1.690
Q9CRB9	Chchd3	0.005	0.039	-0.052	0.233	0.000	0.868	0.646	1.000
Q9DAM5	Slc25a19	0.512	0.776	0.000	0.235	-0.215	0.146	0.162	-1.530
Q99J39	Mlycd	0.122	0.280	0.000	0.662	-0.127	0.733	0.678	0.583
P08228	Sod1	0.000	0.013	-0.224	0.010	0.000	-1.080	-1.290	-1.170
Q99LC5	Etfa	0.310	0.542	0.000	0.213	-0.198	0.705	-0.164	0.467
Q8BH04	Pck2	0.009	0.056	0.068	0.000	-0.323	1.320	0.741	0.823
Q9Z0V7	Timm17b	0.705	0.982	0.000	-0.059	0.096	0.339	-0.298	0.243
Q9WTQ8	Timm23	0.001	0.017	0.000	0.198	-0.057	0.799	0.774	0.865
P28352	Apex1	0.028	0.107	0.000	-0.288	0.047	-0.452	-0.881	-0.582
Q80XN0	Bdh1	0.208	0.404	0.000	0.147	-0.057	0.047	-0.615	-0.246
Q8BVI4	Qdpr	0.149	0.319	0.000	-0.293	0.016	-0.220	-0.562	-0.276
Q9CQ62	Decr1	0.431	0.687	-0.053	0.110	0.000	0.728	-0.038	0.024
Q9WV85	Nme3	0.093	0.234	0.001	-0.129	0.000	-0.343	-0.578	-0.122
Q99J99	Mpst	0.334	0.571	0.163	0.000	-0.160	0.378	-0.932	-0.891
Q3UQ84	Tars2	0.008	0.053	0.000	0.010	-0.095	0.543	0.329	0.293
Q8CD10	Micu2	0.000	0.014	-0.023	0.080	0.000	1.030	0.770	0.952
Q8JZN5	Acad9	0.215	0.412	0.000	0.153	-0.210	0.571	0.123	0.083
Q91V61	Sfxn3	0.006	0.043	-0.166	0.192	0.000	0.721	0.546	0.762
Q91WD5	Ndufs2	0.006	0.045	0.000	0.406	-0.118	0.946	0.914	1.040
Q8BKZ9	Pdhx	0.019	0.086	0.000	0.072	-0.571	0.880	0.548	0.654
Q8VCF0	Mavs	0.900	1.000	-0.276	0.000	0.068	-0.034	-0.283	0.051
Q60930	Vdac2	0.002	0.023	0.000	0.161	-0.063	1.040	0.946	1.360
Q8K009	Aldh1l2	0.000	0.014	0.838	0.000	-0.233	4.520	3.900	4.030
Q3UJU9	Rmdn3	0.332	0.570	0.215	0.000	-0.020	-0.077	-0.868	0.115
Q61941	Nnt	0.000	0.013	1.030	-0.638	0.000	5.910	5.440	5.700
Q9D0S9	Hint2	0.816	1.000	0.000	1.130	-1.100	-0.268	1.220	-0.316
Q921S7	Mrpl37	0.249	0.462	0.174	0.000	-0.144	0.783	-0.030	0.302
Q3V3R1	Mthfd1l	0.570	0.839	0.201	0.000	-0.215	0.497	-0.751	-0.501
Q8K411	Pitrm1	0.003	0.030	0.219	0.000	-0.224	1.320	0.923	1.190
Q9D1L0	Chchd2	0.596	0.869	-0.345	0.000	0.075	0.112	-1.140	0.029

Q9QYR9	Acot2	0.001	0.018	-0.148	0.041	0.000	0.854	0.676	0.934
Q9JHW2	Nit2	0.309	0.542	-0.141	0.431	0.000	0.296	0.245	0.362
Q9DB20	Atp5o	0.001	0.019	0.000	0.129	-0.067	0.904	0.673	0.901
O08709	Prdx6	0.003	0.031	0.085	0.000	-0.156	-1.090	-1.810	-1.670
Q8BIJ6	Iars2	0.008	0.053	0.000	0.073	-0.104	0.819	0.408	0.655
Q9DC61	Pmpca	0.012	0.068	0.000	0.351	-0.158	1.180	0.802	0.788
Q99L13	Hibadh	0.000	0.014	0.000	0.215	-0.163	1.320	1.240	1.450
Q03265	Atp5a1	0.002	0.025	0.000	0.050	-0.113	0.804	0.540	0.809
Q9QXX4	Slc25a13	0.004	0.038	-0.014	0.047	0.000	0.518	0.393	0.699
O35855	Bcat2	0.331	0.569	0.049	0.000	-0.484	0.516	-0.134	0.039
Q9CQC7	Ndufb4	0.005	0.039	0.000	0.250	-0.034	0.719	0.760	0.569
Q8CGK3	Lonp1	0.159	0.335	0.242	0.000	-0.158	1.280	0.204	0.415
Q8VEM8	Slc25a3	0.001	0.019	0.000	0.026	-0.130	1.170	0.803	0.950
Q9D051	Pdhb	0.332	0.570	0.000	0.004	-0.255	0.792	-0.134	0.064
Q9CYR0	Ssbp1	0.351	0.592	0.000	0.077	0.000	0.385	-0.069	0.185
Q64521	Gpd2	0.010	0.061	0.000	0.125	-0.395	0.903	0.600	0.693
Q9Z0X1	Aifm1	0.917	1.000	0.000	0.036	-0.025	0.160	-0.134	0.015
Q8K1R3	Pnpt1	0.333	0.571	0.128	0.000	-0.456	1.050	0.609	-0.428
Q91V92	Acly	0.836	1.000	0.521	0.000	-0.217	0.528	-0.126	0.096
Q9WUM5	Suclg1	0.579	0.850	0.279	0.000	-0.064	1.160	-0.031	-0.140
Q8K2B3	Sdha	0.017	0.081	0.000	0.002	-0.204	0.722	0.297	0.454
P67778	Phb	0.003	0.033	0.000	0.017	-0.309	0.843	0.579	0.735
Q922Q4	Pycr2	0.016	0.078	0.102	0.000	-0.106	1.190	0.520	0.764
Q61102	Abcb7	0.585	0.857	-0.410	0.169	0.000	0.145	-0.268	0.316
P47802	Mtx1	0.295	0.522	0.000	0.014	-0.282	0.283	-0.076	0.042
P08249	Mdh2	0.023	0.096	-0.067	0.250	0.000	0.700	0.373	0.737
P42125	Eci1	0.192	0.384	0.000	0.429	-0.075	0.361	0.416	0.326
O35143	Atpif1	0.013	0.069	0.259	0.000	-0.321	1.590	1.150	0.813
P84084	Arf5	0.092	0.233	0.000	0.100	-0.067	-0.116	-1.250	-0.806
O35972	Mrpl23	0.003	0.033	0.000	0.107	-0.240	0.886	0.665	0.669
Q9D0D3	Mtpap	0.039	0.134	-0.042	0.000	0.411	0.553	0.544	0.831
Q9D6S7	Mrrf	0.086	0.223	0.000	0.433	-0.651	0.785	0.917	0.434
Q9CXT8	Pmpcb	0.017	0.082	0.000	0.156	-0.441	1.050	0.643	0.643
Q8CHT0	Aldh4a1	0.875	1.000	0.335	-0.067	0.000	1.090	-0.715	-0.397
Q9D1N9	Mrpl21	0.001	0.019	0.000	0.089	-0.218	0.892	0.811	1.010
Q8QZT1	Acat1	0.050	0.156	0.000	0.181	-0.006	0.765	0.228	0.592
Q9DCS3	Mecr	0.121	0.279	0.000	0.207	-0.206	1.210	0.269	0.392
Q3ULD5	Mccc2	0.004	0.036	0.000	0.315	-0.197	1.080	0.893	0.981
Q9DCC8	Tomm20	0.641	0.917	-0.090	0.350	0.000	0.068	0.058	0.398
P55096	Abcd3	0.092	0.232	0.042	0.000	-0.929	1.360	1.060	0.053
P32020	Scp2	0.103	0.248	0.172	0.000	-0.126	0.611	0.091	0.465
P19096	Fasn	0.558	0.826	0.157	0.000	-0.066	0.282	-0.464	-0.161
Q8BH95	Echs1	0.035	0.124	0.000	0.240	-0.097	0.915	0.414	0.524
P56391	Cox6b1	0.015	0.076	0.029	0.000	-0.083	0.406	0.174	0.409
Q99N96	Mrpl1	0.091	0.231	0.000	-1.980	0.201	0.820	0.852	1.270

Q99KE1	Me2	0.952	1.000	0.000	0.140	-0.205	0.190	-0.212	-0.072
Q60931	Vdac3	0.007	0.050	0.000	0.252	-0.058	1.080	0.902	1.570
P09925	Surf1	0.000	0.013	0.069	0.000	-0.073	0.682	0.590	0.722
Q8BMD8	Slc25a24	0.023	0.096	-0.447	0.176	0.000	0.526	0.574	0.757
P11352	Gpx1	0.131	0.294	0.457	0.000	-0.235	-0.028	-0.804	-0.877
P54116	Stom	0.556	0.825	0.677	0.000	-0.243	0.446	-0.539	-0.245
P99029	Prdx5	0.996	1.000	0.234	0.000	-0.266	0.051	-0.201	0.121
Q07417	Acads	0.730	1.000	0.089	0.000	-0.125	0.435	-0.537	-0.263
P12787	Cox5a	0.002	0.028	0.000	0.139	-0.028	0.629	0.454	0.629
Q9D0M3	Cyc1	0.192	0.384	0.243	0.000	-0.038	0.016	0.587	0.597
Q80X85	Mrps7	0.051	0.158	0.000	0.066	-0.627	0.765	0.358	0.418
P35486	Pdha1	0.264	0.482	0.044	0.000	-0.235	0.792	0.073	-0.010
Q1HFZ0	Nsun2	0.102	0.247	0.289	0.000	-0.086	-0.029	-1.110	-0.849
Q61171	Prdx2	0.040	0.134	0.088	0.000	-0.208	-0.353	-0.755	-0.402
Q8K3A0	Hscb	0.378	0.627	0.020	0.000	-7.410	-0.071	0.082	-0.054
Q9D6K5	Synj2bp	0.056	0.167	0.000	0.262	-0.061	0.573	0.279	0.805
Q61576	Fkbp10	0.000	0.014	0.444	-0.772	0.000	4.040	3.680	3.950
Q9QZD8	Slc25a10	0.003	0.030	0.000	0.214	-0.415	1.190	1.260	1.510
Q61733	Mrps31	0.132	0.296	0.000	0.114	-0.108	0.841	-0.005	0.687
Q9CQH3	Ndufb5	0.003	0.032	0.000	0.202	-0.151	0.682	0.684	0.812
Q9Z1J3	Nfs1	0.866	1.000	0.239	0.000	-0.042	0.878	-0.349	-0.124
P58059	Mrps21	0.054	0.163	0.000	0.089	-0.066	0.647	0.140	0.589
P53395	Dbt	0.046	0.149	0.000	0.286	-0.049	0.968	0.326	0.859
Q9ESW4	Agk	0.183	0.372	0.000	-0.572	0.077	0.527	-0.141	0.703
O89110	Casp8	0.012	0.067	0.166	-0.032	0.000	-1.050	-1.120	-2.060
Q9CZ83	Mrpl55	0.003	0.031	0.173	0.000	-0.267	0.903	0.758	0.928
Q9DCT2	Ndufs3	0.021	0.090	-0.343	0.080	0.000	0.597	0.506	1.070
P51660	Hsd17b4	0.034	0.122	0.027	0.000	-0.287	1.110	0.293	0.795
Q8VCW8	Acsf2	0.374	0.623	0.347	-0.053	0.000	0.597	-1.130	-0.804
Q8K1J6	Trnt1	0.089	0.227	-0.056	0.000	0.076	-0.250	-0.666	-0.153
Q9CPR5	Mrpl15	0.032	0.119	0.144	-1.190	0.000	1.030	0.900	1.190
Q9DCW4	Etfb	0.322	0.558	0.252	0.000	-0.128	0.867	-0.052	0.291
Q8VD26	Tmem143	0.001	0.022	-0.252	0.062	0.000	0.775	0.891	1.040
Q9CQ54	Ndufc2	0.001	0.022	0.044	0.000	-0.180	0.889	0.645	0.923
Q9CQ75	Ndufa2	0.016	0.078	-0.063	0.189	0.000	0.742	0.367	0.640
P09671	Sod2	0.023	0.096	-0.061	0.348	0.000	0.715	0.476	0.682
P08074	Cbr2	0.001	0.019	0.000	0.042	-1.580	5.280	4.340	4.610
Q99LP6	Grpel1	0.003	0.030	0.000	0.185	-0.177	1.010	0.736	0.977
Q9CR62	Slc25a11	0.026	0.105	0.013	0.000	-0.081	0.658	0.233	0.369
P45952	Acadm	0.441	0.697	0.020	0.000	-0.423	0.852	-0.186	-0.129
Q80ZS3	Mrps26	0.050	0.155	-0.354	0.562	0.000	0.950	0.666	0.952
Q9Z2Q5	Mrpl40	0.003	0.031	0.154	-0.056	0.000	0.713	0.525	0.546
Q924T2	Mrps2	0.014	0.073	0.000	0.348	-0.330	0.736	1.060	0.937
Q9CQA3	Sdhb	0.005	0.042	0.000	0.126	-0.143	0.648	0.433	0.552
Q9D3P8	Plgrkt	0.012	0.069	-0.004	0.232	0.000	0.479	0.379	0.528

P05202	Got2	0.002	0.028	0.000	0.188	-0.073	0.799	0.617	0.665
O08756	Hsd17b10	0.087	0.224	-0.012	0.447	0.000	0.862	0.393	0.563
Q64133	Maoa	0.000	0.011	0.151	0.000	-0.761	3.640	3.580	3.770
P22315	Fech	0.179	0.364	0.378	-1.300	0.000	1.010	0.491	0.277
Q9CPQ8	Atp5l	0.001	0.022	-0.234	0.085	0.000	0.683	0.763	0.798
Q3UMR5	Mcu	0.004	0.038	0.000	0.207	-0.231	0.923	0.701	0.918
Q9WUR2	Eci2	0.392	0.641	-0.002	0.400	0.000	0.637	0.088	0.274
Q61578	Fdxr	0.099	0.243	0.000	0.172	-0.061	-0.043	-0.801	-0.540
Q8JZQ2	Afg3l2	0.015	0.076	0.000	0.089	-0.109	0.828	0.358	0.590
Q9D880	Timm50	0.034	0.123	0.000	0.165	-0.056	0.558	0.221	0.486
Q9D855	Uqcrb	0.013	0.069	0.000	0.173	-0.233	0.669	0.448	0.554
Q5M8N4	Sdr39u1	0.975	1.000	-0.090	1.850	0.000	-0.753	1.040	1.390
P19536	Cox5b	0.287	0.512	-0.201	0.104	0.000	0.204	-0.054	0.216
Q791V5	Mtch2	0.007	0.048	0.000	0.565	-0.017	1.160	1.140	1.190
Q8BFP9	Pdk1	0.386	0.634	0.043	0.000	-0.101	0.101	-0.625	-0.165
Q9EQ20	Aldh6a1	0.368	0.615	0.300	0.000	-0.150	1.460	-0.061	0.226
Q8K2M0	Mrpl38	0.002	0.024	0.114	0.000	-0.089	0.995	0.671	0.855
P16125	Ldhb	0.000	0.013	-0.212	0.132	0.000	-1.330	-1.570	-1.550
Q9DC50	Crot	0.119	0.276	0.000	-0.124	0.034	-0.050	-0.367	-0.340
O35435	Dhodh	0.072	0.196	0.000	0.359	-1.330	0.638	1.240	1.160
O88441	Mtx2	0.276	0.496	0.000	0.113	-0.108	0.703	-0.135	0.393
Q8BJ03	Cox15	0.015	0.075	0.000	-0.638	0.346	1.240	1.100	1.810
Q8R164	Bphl	0.031	0.114	0.197	0.000	-0.133	0.714	0.305	0.778
Q920E5	Fdps	0.104	0.252	1.020	0.000	-0.336	1.880	0.878	1.120
Q9DBF1	Aldh7a1	0.000	0.009	0.000	0.318	-0.191	2.700	2.460	2.520
Q99MR8	Mccc1	0.382	0.631	0.014	0.000	-0.317	0.811	-0.251	0.108
Q9WVL0	Gstz1	0.112	0.265	0.000	0.163	-0.024	1.190	0.487	0.239
Q922H2	Pdk3	0.193	0.385	0.065	0.000	-0.219	0.781	-0.001	0.229
Q9JMA2	Qtrt1	0.001	0.019	0.000	0.059	-0.158	-0.700	-0.758	-0.891
Q8VCX5	Micu1	0.567	0.836	-0.165	0.177	0.000	1.300	-0.698	0.513
Q99M87	Dnaja3	0.029	0.112	0.003	0.000	-0.329	0.713	0.216	0.625
Q9CQ40	Mrpl49	0.092	0.233	0.339	0.000	-0.837	0.637	0.883	0.445
Q8R3F5	Mcat	0.181	0.368	0.020	0.000	-0.178	0.816	-0.052	0.333
Q9DCN2	Cyb5r3	0.000	0.005	0.000	0.161	-0.051	2.080	1.950	2.120
Q9DB15	Mrpl12	0.006	0.044	0.000	0.110	-0.240	0.803	0.551	0.609
Q99NB1	Acss1	0.101	0.247	0.000	0.064	-0.261	-0.149	-0.573	-0.593
Q9EQI8	Mrpl46	0.017	0.081	0.194	0.000	-0.083	1.000	0.471	0.691
Q8C163	Exog	0.071	0.194	-0.225	0.654	0.000	0.703	0.765	1.070
Q5U458	Dnajc11	0.066	0.185	0.771	-0.042	0.000	1.780	1.580	0.657
O08600	Endog	0.058	0.171	-0.172	0.406	0.000	-0.439	-0.313	-0.402
O35459	Ech1	0.045	0.146	0.000	0.120	-0.262	0.291	0.279	0.264
P47968	Rpia	0.160	0.337	0.718	-0.577	0.000	-0.741	-2.220	-0.389
Q8VDC0	Lars2	0.390	0.640	0.288	0.000	-4.090	0.945	-0.292	-0.213
Q3UHB1	Nt5dc3	0.001	0.014	0.000	0.448	-0.077	2.160	2.160	2.560
Q9DCJ5	Ndufa8	0.075	0.202	0.000	1.300	-0.142	1.220	1.620	2.010

Q9R257	Hebp1	0.892	1.000	0.000	0.167	-1.940	1.520	-2.900	-1.030
Q921G7	Etfdh	0.009	0.055	0.011	0.000	-0.217	0.785	0.394	0.573
Q9JHS4	Clpx	0.557	0.825	0.335	0.000	-0.328	1.540	-0.635	0.363
Q8BK72	Mrps27	0.012	0.068	0.000	0.528	-0.256	1.200	1.050	1.510
Q8BW75	Maob	0.000	0.013	0.667	0.000	-0.370	4.120	3.720	4.010
Q922S4	Pde2a	0.073	0.199	0.280	-0.058	0.000	-0.909	-2.760	-0.790
P48962	Slc25a4	0.000	0.013	0.000	0.359	-0.136	2.120	1.860	2.070
Q9CQX2	Cyb5b	0.013	0.071	-0.164	0.064	0.000	0.975	0.423	0.947
Q9CPQ3	Tomm22	0.010	0.061	-0.029	0.000	0.186	1.040	0.523	0.946
P70349	Hint1	0.003	0.030	-0.064	0.000	0.148	-1.010	-1.670	-1.260
P18155	Mthfd2	0.034	0.122	0.000	0.357	-0.941	0.795	1.290	1.380
Q9DCZ4	Apoo	0.004	0.037	0.000	0.124	-0.197	0.733	0.566	0.860
Q9DCM0	Ethe1	0.636	0.912	0.000	0.137	-0.820	0.135	-0.445	0.180
Q99N93	Mrpl16	0.172	0.355	0.000	0.020	-0.274	0.737	-0.068	0.326
P62897	Cycs	0.205	0.401	0.000	0.081	-0.533	-0.300	-0.469	-0.708
Q9D964	Gatm	0.821	1.000	0.770	0.000	-0.380	0.678	0.053	-0.044
P31786	Dbi	0.001	0.019	0.000	0.100	-0.167	-1.290	-1.720	-1.290
Q9DCU6	Mrpl4	0.041	0.138	0.000	0.039	-0.885	0.969	0.968	0.394
Q9CR58	Slc25a30	0.011	0.062	0.000	0.243	-0.162	0.866	0.561	0.664
Q791T5	Mtch1	0.001	0.019	0.000	0.409	-0.005	1.910	1.480	1.660
Q9DB70	Fundc1	0.256	0.470	-0.517	1.650	0.000	2.470	0.712	1.270
Q9CXZ1	Ndufs4	0.012	0.067	-0.105	0.323	0.000	0.881	0.660	1.120
Q9JK81	Myg1	0.012	0.068	-0.941	0.000	0.003	-1.670	-1.890	-1.610
Q9CQN7	Mrpl41	0.001	0.019	-0.057	0.242	0.000	1.080	0.872	1.000
O35129	Phb2	0.003	0.030	0.000	0.062	-0.164	0.922	0.591	0.718
P97823	Lypla1	0.168	0.350	0.000	-0.250	0.196	0.058	-1.140	-0.961
Q9CXW2	Mrps22	0.536	0.803	0.837	-1.070	0.000	1.960	1.660	-1.400
Q91VT4	Cbr4	0.890	1.000	0.000	0.188	-0.136	0.418	-0.152	-0.122
Q9JKF7	Mrpl39	0.494	0.759	0.000	-3.790	0.010	1.100	-0.144	-1.440
Q91VR2	Atp5c1	0.035	0.125	0.127	0.000	-0.028	1.150	0.535	0.475
Q62425	Ndufa4	0.219	0.419	-0.214	0.210	0.000	0.195	0.073	0.541
Q9D5T0	Atad1	0.387	0.636	0.005	-0.010	0.000	0.504	-0.072	0.068
Q9JKX6	Nudt5	0.000	0.014	0.033	-0.029	0.000	-1.110	-1.520	-1.260
Q8QZS1	Hibch	0.404	0.655	0.000	0.318	-0.092	0.156	0.135	0.318
Q99L04	Dhrs1	0.470	0.729	0.040	0.000	-0.227	0.315	-0.898	-0.478
Q99KB8	Hagh	0.754	1.000	0.142	0.000	-0.442	-0.018	-0.512	-0.014
Q9JLJ2	Aldh9a1	0.081	0.213	0.030	-0.088	0.000	-0.239	-1.410	-0.779
Q91VS7	Mgst1	0.030	0.113	0.999	0.000	-0.245	1.580	1.500	2.410
Q91VM9	Ppa2	0.070	0.193	-0.028	0.474	0.000	0.613	0.457	0.874
Q9D8P4	Mrpl17	0.062	0.179	-0.135	0.609	0.000	0.806	0.896	0.632
P47791	Gsr	0.018	0.084	0.341	0.000	-0.118	-0.466	-1.080	-1.080
Q9JLT4	Txnrd2	0.839	1.000	0.000	0.351	-0.041	0.125	0.029	0.247
Q9CQ69	Uqcrq	0.004	0.038	0.000	0.165	-0.022	0.638	0.470	0.464
Q9CZU6	Cs	0.005	0.041	0.000	0.137	-0.034	0.868	0.509	0.669
O88967	Yme1l1	0.017	0.081	0.000	-0.237	0.021	0.822	0.328	0.838

Q811U4	Mfn1	0.420	0.674	0.000	1.260	-0.739	2.090	1.140	-0.275
Q99J47	Dhrs7b	0.010	0.059	0.000	0.380	-0.485	1.100	1.150	1.120
Q9D6J5	Ndufb8	0.039	0.132	-0.884	0.149	0.000	0.958	0.797	0.597
Q8BJ64	Chdh	0.375	0.623	0.970	-0.135	0.000	0.659	-1.190	-0.567
Q9CQN6	Tmem14c	0.066	0.186	0.146	0.000	-0.210	0.760	0.282	0.302
Q9CQL5	Mrpl18	0.012	0.067	-0.027	0.185	0.000	0.925	0.512	1.060
Q8R2Q4	Gfm2	0.142	0.309	0.000	0.144	-0.128	0.042	-1.100	-0.903
Q8JZU2	Slc25a1	0.000	0.012	0.000	0.212	-0.083	1.600	1.430	1.730
Q8BU88	Mrpl22	0.017	0.080	0.003	-0.068	0.000	0.895	0.346	0.595
P53702	Hccs	0.001	0.022	-0.130	0.313	0.000	1.420	1.460	1.860
P36552	Cpox	0.116	0.271	0.330	0.000	-0.246	-0.140	-0.571	-0.479
Q9D0G0	Mrps30	0.012	0.068	0.000	0.044	-0.091	1.010	0.479	0.609
Q9QYA2	Tomm40	0.010	0.059	0.000	0.202	-0.235	1.300	0.723	0.891
Q8BYM8	Cars2	0.412	0.665	0.076	0.000	-0.350	0.743	-0.258	0.119
Q8BTX9	Hsdl1	0.769	1.000	0.000	0.163	-0.252	0.135	-0.129	0.040
Q8JZN7	Rhot2	0.010	0.061	0.084	0.000	-0.204	0.554	0.327	0.480
Q9CXJ4	Abcb8	0.014	0.074	0.000	0.642	-0.065	1.350	1.020	1.280
Q91WS0	Cisd1	0.396	0.646	-0.215	1.180	0.000	0.469	0.808	0.987
O09174	Amacr	0.030	0.113	0.000	0.612	-0.235	1.240	0.949	0.900
Q9D7N3	Mrps9	0.122	0.280	0.267	-0.306	0.000	1.060	0.047	1.140
Q8BWM0	Ptges2	0.946	1.000	-1.850	2.870	0.000	1.240	0.282	-0.189
Q99PU8	Dhx30	0.416	0.670	0.000	0.380	-0.875	1.330	-0.133	-0.053
Q3URS9	Ccdc51	0.007	0.048	0.194	0.000	-0.221	0.635	0.568	0.670
Q9DC70	Ndufs7	0.005	0.040	0.000	0.110	-0.184	0.684	0.466	0.575
Q9EP89	Lactb	0.009	0.055	0.000	0.227	-0.004	0.611	0.438	0.673
Q9D3D9	Atp5d	0.126	0.287	-0.224	0.095	0.000	0.573	0.056	0.267
O88986	Gcat	0.640	0.917	-0.398	0.000	0.308	0.250	-0.442	-0.349
Q9JHI5	Ivd	0.333	0.571	0.000	0.127	-0.011	0.544	-0.052	0.212
Q9CPP6	Ndufa5	0.245	0.456	-0.536	0.555	0.000	0.694	0.147	0.649
O55125	Nipsnap1	0.039	0.134	-0.109	0.000	0.160	0.335	0.199	0.384
Q8BX10	Pgam5	0.212	0.409	-0.303	0.066	0.000	0.400	-0.081	0.256
P48410	Abcd1	0.804	1.000	0.401	-0.082	0.000	0.518	-0.244	0.258
Q9WTP6	Ak2	0.009	0.057	0.187	0.000	-0.011	-0.394	-0.833	-0.616
Q8BG51	Rhot1	0.015	0.076	0.000	0.146	-0.220	0.857	0.556	0.462
Q60759	Gcdh	0.450	0.708	0.000	0.355	-0.371	0.773	-0.053	0.092
P20108	Prdx3	0.006	0.046	0.214	-0.058	0.000	0.778	0.509	0.675
Q3U2A8	Vars2	0.089	0.227	0.000	0.110	-0.376	0.144	0.368	0.307
Q80YD1	Supv3l1	0.046	0.149	0.000	0.195	-0.039	0.533	0.318	0.254
Q99KK9	Hars2	0.327	0.564	0.000	0.815	-0.658	0.593	0.065	1.500
Q91V12	Acot7	0.020	0.089	-0.038	0.193	0.000	0.736	0.449	0.396
Q8BHF7	Pgs1	0.017	0.080	0.000	1.120	-0.175	2.030	1.790	2.010
Q8K3J1	Ndufs8	0.002	0.025	0.000	0.081	-0.026	0.747	0.504	0.553
Q64433	Hspe1	0.001	0.018	0.000	0.100	-0.080	1.090	0.779	0.991
Q8K0D5	Gfm1	0.253	0.467	0.000	0.253	-0.248	1.020	0.078	0.217
Q99N94	Mrpl9	0.093	0.234	0.142	0.000	-0.854	1.030	0.602	0.221

Q8C3X2	Ccdc90b	0.005	0.040	-0.005	0.303	0.000	1.660	1.020	1.250
Q99N87	Mrps5	0.000	0.012	0.039	0.000	-0.040	1.140	0.934	0.888
P51881	Slc25a5	0.203	0.400	0.000	1.090	-0.121	0.477	1.260	1.440
Q8R1S0	Coq6	0.178	0.364	0.000	0.621	-0.148	0.936	0.515	0.414
Q9DBL7	Coasy	0.134	0.298	7.440	-0.978	0.000	7.090	7.330	7.010
Q5HZI9	Slc25a51	0.018	0.083	-0.031	0.632	0.000	1.200	0.956	1.100
Q91VC9	Ghitm	0.003	0.030	0.000	0.088	-0.147	1.130	0.700	0.953
Q8CAK1	Iba57	0.322	0.558	0.036	0.000	-0.449	0.439	-0.205	0.176
Q9D6K8	Fundc2	0.013	0.071	0.000	0.474	-0.255	1.690	1.410	0.958
O08807	Prdx4	0.256	0.470	0.038	0.000	-0.002	0.439	-0.070	0.262
Q9QZ23	Nfu1	0.022	0.094	0.000	0.235	-0.727	1.080	0.755	1.350
P51175	Ppox	0.909	1.000	0.000	0.082	-0.711	0.651	-0.730	-0.373
Q9JHR7	Ide	0.004	0.036	0.000	0.341	-0.020	-0.764	-0.819	-0.576
Q9D1P0	Mrpl13	0.522	0.787	0.000	0.348	-0.702	0.959	-0.679	0.596
Q8K1M6	Dnm1l	0.892	1.000	0.042	0.000	-0.313	0.147	-0.185	-0.310
Q8K4X7	Agpat4	0.005	0.042	0.000	0.300	-0.338	1.030	0.953	1.130
Q9CZL5	Pcbd2	0.058	0.171	0.028	0.000	-0.711	0.373	0.407	0.453
P48771	Cox7a2	0.957	1.000	-0.456	0.000	0.309	0.089	-0.409	0.125
P70404	Idh3g	0.775	1.000	0.000	0.070	-0.248	0.756	-0.504	-0.078
Q9D6Y7	Msra	0.068	0.189	0.549	-0.217	0.000	-0.252	-0.768	-0.814
P40630	Tfam	0.889	1.000	0.483	0.000	-0.272	0.049	0.003	0.264
P97386	Lig3	0.578	0.849	0.068	0.000	-0.173	0.026	-0.596	0.058
Q4VAE3	Tmem65	0.014	0.072	0.000	0.487	-0.336	1.190	1.030	1.570
P56135	Atp5j2	0.005	0.040	0.000	0.393	-0.087	0.924	1.130	0.968
Q9DCM2	Gstk1	0.701	0.977	0.010	0.000	-0.212	0.377	-0.571	-0.378
Q9D0C4	Trmt5	0.109	0.260	-0.090	0.320	0.000	-0.850	-4.670	-1.540
Q924L1	Letmd1	0.672	0.950	-1.210	0.847	0.000	-1.630	0.966	-1.040
Q9D8S4	Rexo2	0.107	0.257	-0.191	0.000	0.052	0.356	0.007	0.431
Q7TSQ8	Pdpr	0.166	0.347	0.000	0.234	-0.035	1.070	0.066	0.599
Q9D7B6	Acad8	0.170	0.353	0.000	-1.970	0.001	1.380	0.114	0.357
Q8K370	Acad10	0.053	0.162	0.324	0.000	-0.339	0.796	0.651	0.382
P70677	Casp3	0.003	0.030	-0.016	0.138	0.000	-1.190	-2.040	-1.570
P61922	Abat	0.014	0.073	0.000	1.570	-1.050	4.160	3.100	3.540
Q9CQZ6	Ndufb3	0.002	0.025	-0.037	0.054	0.000	0.800	0.535	0.580
Q9D6M3	Slc25a22	0.001	0.016	0.000	0.088	-0.280	1.510	1.170	1.410
Q9D2R6	Coa3	0.017	0.080	0.000	0.304	-0.248	1.120	0.611	0.904
P47934	Crat	0.395	0.644	0.000	-3.600	0.145	2.180	-1.640	0.743
Q91WK1	Spryd4	0.045	0.146	0.000	0.231	-0.354	0.951	0.398	0.566
Q9CQE1	Nipsnap3b	0.179	0.365	0.000	0.874	-0.677	0.769	0.963	0.692
Q9WVD5	Slc25a15	0.005	0.042	-0.508	0.364	0.000	1.270	1.750	1.660
Q91Z53	Grhpr	0.060	0.176	0.000	-0.087	0.077	-0.125	-0.652	-0.656
Q91VA6	Poldip2	0.121	0.278	0.000	0.211	-1.280	1.200	0.544	0.335
Q9Z1P6	Ndufa7	0.004	0.037	-0.044	0.000	0.010	1.000	0.554	0.732
P58281	Opa1	0.111	0.263	-0.010	0.051	0.000	-0.089	-0.563	-0.194
Q8VDT9	Mrpl50	0.179	0.365	0.195	-2.670	0.000	0.890	0.464	0.716

Q8K215	Lyrm4	0.019	0.086	0.000	0.224	-0.231	0.718	0.439	0.602
Q9JLZ3	Auh	0.243	0.453	0.028	0.000	-0.092	0.540	-0.170	0.570
Q8BGA9	Oxa1l	0.039	0.133	0.000	-1.550	0.191	1.400	1.020	1.330
Q8BUY5	Timmdc1	0.012	0.067	0.000	0.616	-0.099	1.080	1.290	1.470
Q9ERB0	Snap29	0.440	0.697	0.870	-3.570	0.000	0.006	0.284	0.520
O54918	Bcl2l11	0.580	0.851	0.000	0.199	-0.024	0.457	-0.129	0.176
Q9D8Y1	Tmem126a	0.000	0.011	0.000	0.009	-0.058	1.380	1.100	1.350
Q3TL44	Nlrx1	0.072	0.196	0.000	0.222	-0.158	0.479	0.242	0.303
Q9CZN8	Qrsl1	0.705	0.982	0.000	0.121	-0.527	0.510	-0.341	-0.174
Q91VN4	Chchd6	0.012	0.068	0.000	0.253	-1.110	1.520	1.500	1.590
Q9WU56	Pus1	0.903	1.000	2.900	-0.702	0.000	2.620	0.251	-1.290
Q71RI9	Kyat3	0.016	0.079	0.000	0.041	-0.711	0.821	0.680	0.805
O88587	Comt	0.014	0.072	-0.457	0.392	0.000	1.030	0.947	1.110
Q9D338	Mrpl19	0.721	1.000	0.000	-0.168	0.031	1.100	-0.582	-0.080
Q8BIP0	Dars2	0.009	0.056	0.571	-0.292	0.000	1.550	1.440	2.180
Q99LB2	Dhrs4	0.046	0.147	0.000	0.173	-0.424	1.020	0.369	0.601
Q8C5H8	Nadk2	0.914	1.000	0.228	0.000	-0.004	0.494	-0.258	-0.095
Q9CQE3	Mrps17	0.067	0.187	0.000	1.020	-0.199	0.968	1.420	1.540
Q9JKL4	Ndufaf3	0.124	0.284	0.000	-1.040	0.623	0.737	0.694	1.040
Q8BHC4	Dcakd	0.017	0.081	0.466	0.000	-1.560	2.210	1.810	2.370
Q9D1I6	Mrpl14	0.431	0.687	0.279	0.000	-0.206	0.925	-0.016	0.044
P41216	Acsl1	0.926	1.000	0.000	0.371	-0.869	0.044	0.090	-0.768
P52503	Ndufs6	0.095	0.237	-0.325	0.000	0.739	0.967	0.626	1.040
Q3U186	Rars2	0.906	1.000	0.398	-0.283	0.000	1.060	-0.833	-0.334
Q3U5Q7	Cmpk2	0.171	0.354	0.545	0.000	-0.063	0.143	-0.649	-0.640
Q8BK08	Tmem11	0.001	0.019	-0.043	0.285	0.000	1.080	0.954	1.080
Q60649	Clpb	0.990	1.000	0.421	0.000	-0.108	0.340	-0.304	0.289
Q3TC33	Ccdc127	0.031	0.114	-0.180	0.197	0.000	0.651	0.308	0.506
Q9CY73	Mrpl44	0.009	0.057	0.000	0.358	-0.175	0.827	0.770	0.815
Q80U63	Mfn2	1.000	1.000	0.000	0.057	-0.064	-0.674	0.298	0.369
Q9DC71	Mrps15	0.711	0.987	-0.194	0.000	0.044	0.841	-0.657	0.193
Q9CR59	Gadd45gip1	0.130	0.293	0.000	0.151	-0.194	0.895	0.031	0.578
Q8BVU5	Nudt9	0.155	0.330	0.000	-0.351	0.224	0.896	2.140	0.088
Q2TPA8	Hsdl2	0.861	1.000	0.190	-0.464	0.000	0.705	-0.463	-0.284
Q9D8S9	Bola1	0.460	0.719	0.000	-2.370	0.187	1.050	-0.214	-0.646
Q9CR68	Uqcrfs1	0.007	0.048	0.000	0.074	-0.106	0.656	0.355	0.524
Q66GT5	Ptpmt1	0.058	0.172	0.000	0.711	-0.229	1.030	0.782	0.979
Q9CQZ5	Ndufa6	0.233	0.438	0.000	0.678	-0.132	0.410	0.479	0.879
Q99N89	Mrpl43	0.003	0.030	0.000	0.185	-0.319	1.180	0.974	1.330
P56382	Atp5e	0.000	0.013	0.000	0.115	-0.081	0.914	0.754	0.858
Q9WV84	Nme4	0.027	0.105	1.300	-1.640	0.000	3.340	2.630	2.720
Q9D1B9	Mrpl28	0.304	0.534	0.000	0.671	-1.410	0.836	0.095	0.635
Q8BIG7	Comtd1	0.937	1.000	0.000	0.166	-0.276	0.673	-0.609	-0.276
Q5IRJ6	Slc30a9	0.003	0.030	0.000	0.577	-0.728	2.360	2.540	2.810
Q924D0	Rtn4ip1	0.540	0.807	0.000	0.155	-0.927	0.162	-2.980	-0.090

Q9D023	Mpc2	0.034	0.121	0.000	0.091	-0.908	0.954	0.558	0.976
Q8K2Y7	Mrpl47	0.048	0.152	0.000	0.273	-0.157	1.070	0.895	0.325
Q9CPQ1	Cox6c	0.008	0.052	0.000	0.148	-0.102	0.358	0.542	0.504
Q99N85	Mrps18a	0.010	0.060	0.176	-0.091	0.000	0.951	0.506	0.708
P63030	Mpc1	0.002	0.028	0.158	-0.024	0.000	1.540	0.979	1.210
Q921N7	Tmem70	0.029	0.111	-0.295	3.890	0.000	5.300	5.780	6.340
Q9CYK1	Wars2	0.461	0.720	-0.361	0.518	0.000	0.617	-0.291	0.913
Q61586	Gpam	0.000	0.012	0.000	-0.259	0.263	2.000	1.940	2.100
Q8BYL4	Yars2	0.539	0.807	0.319	-1.240	0.000	0.125	-1.890	-0.671
Q9ERI6	Rdh14	0.189	0.379	0.000	0.132	-0.126	-0.072	-0.191	-0.680
Q9D6U8	Fam162a	0.000	0.013	-0.044	0.195	0.000	1.030	0.901	0.963
Q9D125	Mrps25	0.125	0.285	5.570	-3.410	0.000	6.160	5.650	5.610
Q9DC29	Abcb6	0.117	0.272	0.022	-0.201	0.000	-0.174	-0.821	-0.399
Q9CZ57	Nsun4	0.430	0.686	0.129	-1.190	0.000	0.559	-0.895	1.310
Q9DAT5	Trmu	0.965	1.000	0.330	-0.121	0.000	0.746	-0.391	-0.095
Q9D1R1	Tmem126b	0.441	0.698	0.146	-0.371	0.000	-0.573	0.779	0.798
Q3TQB2	Foxred1	0.796	1.000	-0.086	0.930	0.000	0.212	0.095	0.873
Q9CQ91	Ndufa3	0.595	0.868	-0.286	0.062	0.000	0.320	-0.326	0.166
Q99N95	Mrpl3	0.067	0.187	0.000	0.558	-0.395	1.000	0.576	0.857
Q9DB10	Smdt1	0.087	0.224	-0.402	0.296	0.000	0.541	0.458	0.326

Supp. Table 2. Mitochondrial proteome was detected in $CD4^+$ T cells isolated from old mice after mito-transfer and in non-manipulated $CD4^+$ T cells from old mice. $CD4^+$ T cells from young and old mice, and from old mice after mito-transfer were cultured for 4 h before processing for mass spectrometry analysis. Data expressed as median protein Log2 fold change of $CD4^+$ T cells from old mice, from 3 individual old mice (paired experiment)

Uniprot.ID	Gene.ID	P. Val	FDR	O1	O2	O3	OM1	OM2	OM3
Q8JZN5	Acad9	0.215	0.412	0.000	0.150	-0.210	0.570	0.120	0.080
Q9Z0X1	Aifm1	0.917	1.000	0.000	0.040	-0.030	0.160	-0.130	0.010
Q3TQB2	Foxred1	0.796	1.000	-0.090	0.930	0.000	0.210	0.100	0.870
Q99LC3	Ndufa10	0.006	0.047	0.000	0.010	-0.250	0.720	0.460	0.860
Q7TMF3	Ndufa12	0.011	0.064	-0.160	0.000	0.140	0.790	0.550	1.110
Q9ERS2	Ndufa13	0.056	0.168	0.040	-0.180	0.000	0.650	0.140	0.880
Q9CQ75	Ndufa2	0.016	0.078	-0.060	0.190	0.000	0.740	0.370	0.640

Q9CQ91	Ndufa3	0.595	0.868	-0.290	0.060	0.000	0.320	-0.330	0.170
Q9CPP6	Ndufa5	0.245	0.456	-0.540	0.560	0.000	0.690	0.150	0.650
Q9CQZ5	Ndufa6	0.233	0.438	0.000	0.680	-0.130	0.410	0.480	0.880
Q9Z1P6	Ndufa7	0.004	0.037	-0.040	0.000	0.010	1.000	0.550	0.730
Q9DCJ5	Ndufa8	0.075	0.202	0.000	1.300	-0.140	1.220	1.620	2.010
Q9DC69	Ndufa9	0.004	0.037	-0.070	0.100	0.000	0.740	0.440	0.640
Q9JKL4	Ndufaf3	0.124	0.284	0.000	-1.040	0.620	0.740	0.690	1.040
Q9DCS9	Ndufb10	0.006	0.043	0.000	0.250	-0.110	0.630	0.920	0.810
O09111	Ndufb11	0.001	0.018	0.020	-0.200	0.000	0.580	0.570	0.650
Q9CQZ6	Ndufb3	0.002	0.025	-0.040	0.050	0.000	0.800	0.540	0.580
Q9CQC7	Ndufb4	0.005	0.039	0.000	0.250	-0.030	0.720	0.760	0.570
Q9CQH3	Ndufb5	0.003	0.032	0.000	0.200	-0.150	0.680	0.680	0.810
Q9CR61	Ndufb7	0.020	0.088	0.000	-0.040	0.110	0.720	0.440	1.080
Q9D6J5	Ndufb8	0.039	0.132	-0.880	0.150	0.000	0.960	0.800	0.600
Q9CQJ8	Ndufb9	0.003	0.033	-0.200	0.220	0.000	0.740	0.740	0.810
Q9CQ54	Ndufc2	0.001	0.022	0.040	0.000	-0.180	0.890	0.650	0.920
Q91VD9	Ndufs1	0.002	0.025	0.000	0.200	-0.070	0.850	0.650	0.790
Q91WD5	Ndufs2	0.006	0.045	0.000	0.410	-0.120	0.950	0.910	1.040
Q9DCT2	Ndufs3	0.021	0.090	-0.340	0.080	0.000	0.600	0.510	1.070
Q9CXZ1	Ndufs4	0.012	0.067	-0.110	0.320	0.000	0.880	0.660	1.120
P52503	Ndufs6	0.095	0.237	-0.330	0.000	0.740	0.970	0.630	1.040
Q9DC70	Ndufs7	0.005	0.040	0.000	0.110	-0.180	0.680	0.470	0.570
Q8K3J1	Ndufs8	0.002	0.025	0.000	0.080	-0.030	0.750	0.500	0.550
Q91YT0	Ndufv1	0.001	0.019	0.000	0.030	-0.080	0.820	0.550	0.690
Q9D6J6	Ndufv2	0.049	0.154	0.000	0.340	-0.180	0.720	0.360	0.860
Q8BUY5	Timmdc1	0.012	0.067	0.000	0.620	-0.100	1.080	1.290	1.470
Q9D8Y1	Tmem126a	0.000	0.011	0.000	0.010	-0.060	1.380	1.100	1.350
Q9D1R1	Tmem126b	0.441	0.698	0.150	-0.370	0.000	-0.570	0.780	0.800
Q921N7	Tmem70	0.029	0.111	-0.290	3.890	0.000	5.300	5.780	6.340
Q8K2B3	Sdha	0.017	0.081	0.000	0.000	-0.200	0.720	0.300	0.450
Q9CQA3	Sdhb	0.005	0.042	0.000	0.130	-0.140	0.650	0.430	0.550
Q9D0M3	Cyc1	0.192	0.384	0.240	0.000	-0.040	0.020	0.590	0.600
Q9D855	Uqcrb	0.013	0.069	0.000	0.170	-0.230	0.670	0.450	0.550
Q9CZ13	Uqcrc1	0.015	0.076	0.080	0.000	-0.050	0.660	0.290	0.460
Q9DB77	Uqcrc2	0.140	0.306	0.000	0.130	-0.100	0.560	0.050	0.310
Q9CR68	Uqcrfs1	0.007	0.048	0.000	0.070	-0.110	0.660	0.350	0.520
Q9CQ69	Uqcrq	0.004	0.038	0.000	0.170	-0.020	0.640	0.470	0.460
Q9D2R6	Coa3	0.017	0.080	0.000	0.300	-0.250	1.120	0.610	0.900
Q8BJ03	Cox15	0.015	0.075	0.000	-0.640	0.350	1.240	1.100	1.810
P19783	Cox4i1	0.004	0.038	0.100	-0.020	0.000	0.710	0.420	0.700
P12787	Cox5a	0.002	0.028	0.000	0.140	-0.030	0.630	0.450	0.630
P19536	Cox5b	0.287	0.512	-0.200	0.100	0.000	0.200	-0.050	0.220
P56391	Cox6b1	0.015	0.076	0.030	0.000	-0.080	0.410	0.170	0.410
Q9CPQ1	Cox6c	0.008	0.052	0.000	0.150	-0.100	0.360	0.540	0.500
P48771	Cox7a2	0.957	1.000	-0.460	0.000	0.310	0.090	-0.410	0.130

Q62425	Ndufa4	0.219	0.419	-0.210	0.210	0.000	0.200	0.070	0.540
P09925	Surf1	0.000	0.013	0.070	0.000	-0.070	0.680	0.590	0.720
Q03265	Atp5a1	0.002	0.025	0.000	0.050	-0.110	0.800	0.540	0.810
P56480	Atp5b	0.009	0.057	0.000	0.260	-0.160	0.720	0.570	0.810
Q91VR2	Atp5c1	0.035	0.125	0.130	0.000	-0.030	1.150	0.540	0.470
Q9D3D9	Atp5d	0.126	0.287	-0.220	0.090	0.000	0.570	0.060	0.270
P56382	Atp5e	0.000	0.013	0.000	0.120	-0.080	0.910	0.750	0.860
Q9DCX2	Atp5h	0.025	0.101	0.000	0.470	-0.340	1.070	1.120	0.720
P97450	Atp5j	0.033	0.121	0.000	0.130	-0.630	1.010	0.420	1.140
P56135	Atp5j2	0.005	0.040	0.000	0.390	-0.090	0.920	1.130	0.970
Q9CPQ8	Atp5l	0.001	0.022	-0.230	0.080	0.000	0.680	0.760	0.800
Q9DB20	Atp5o	0.001	0.019	0.000	0.130	-0.070	0.900	0.670	0.900
O35143	Atpif1	0.013	0.069	0.260	0.000	-0.320	1.590	1.150	0.810
Q921N7	Tmem70	0.029	0.111	-0.290	3.890	0.000	5.300	5.780	6.340

Supp. Table 3. Proteins related to ETC were detected in $CD4^+$ T cells isolated from old mice after mito-transfer and in non-manipulated $CD4^+$ T cells from old mice. $CD4^+$ T cells from young and old mice, and from old mice after mito-transfer were cultured for 4 h before processing for mass spectrometry analysis. Data expressed as median protein Log2 fold change of $CD4^+$ T cells from old mice, from 3 individual old mice (paired experiment)

Uniprot ID	Gene ID	P.Val	FDR	O1	O2	O3	OM1	OM2	OM3
Q9R1C7	Prpf40a	0.057	0.169	0.000	0.036	-0.175	-0.196	-0.679	-0.769
Q9ES52	Inpp5d	0.069	0.191	-0.054	0.183	0.000	-0.248	-0.967	-0.380
Q9ERK4	Cse1l	0.041	0.138	0.073	-0.029	0.000	-0.350	-1.430	-0.960
Q9DBG6	Rpn2	0.000	0.012	0.000	0.145	-0.216	1.580	1.360	1.520
Q9D358	Acp1	0.010	0.060	0.000	0.034	-0.377	-0.763	-1.300	-1.250
Q9CX99	Grap	0.077	0.207	-0.922	0.152	0.000	-1.990	-2.090	-0.687
Q99L45	Eif2s2	0.540	0.807	0.342	-0.259	0.000	0.266	-0.631	-0.179
Q99JR1	Sfxn1	0.018	0.083	0.000	0.180	-0.179	0.403	0.408	0.393
Q99JF8	Psip1	0.090	0.230	-0.095	0.000	0.152	-0.474	-0.546	-0.054
Q921F2	Tardbp	0.080	0.211	0.004	0.000	-0.021	-0.142	-0.728	-0.349
Q8QZY9	Sf3b4	0.531	0.798	-2.010	0.478	0.000	-3.370	-0.510	-0.237
Q8K4I3	Arhgef6	0.010	0.058	-0.259	0.000	0.183	-0.812	-1.510	-1.100

Q8K2Z4	Ncapd2	0.437	0.694	0.059	-0.356	0.000	0.217	-0.607	-0.761
Q8K1I7	Wipf1	0.146	0.315	-0.001	0.000	0.402	-0.311	-0.419	0.062
Q8CC88	Vwa8	0.942	1.000	0.000	0.045	-0.313	0.847	-0.752	-0.481
Q8C3J5	Dock2	0.006	0.047	0.009	0.000	-0.011	-0.628	-1.100	-0.665
Q8C2K5	Rasal3	0.018	0.083	-0.082	0.141	0.000	-0.512	-1.320	-0.924
Q8BZN6	Dock10	0.210	0.406	-0.532	0.000	0.228	-0.481	-1.600	-0.303
Q8BK67	Rcc2	0.253	0.466	0.487	-0.092	0.000	0.079	-0.473	-0.172
Q8BH59	Slc25a12	0.037	0.127	-0.084	0.153	0.000	0.368	0.204	0.480
Q8BGW0	Themis	0.127	0.288	-1.320	0.000	0.443	-1.890	-1.260	-1.100
Q80SU7	Gvin1	0.117	0.273	0.231	0.000	-0.019	0.045	-0.881	-0.733
Q78ZA7	Nap1l4	0.009	0.056	-0.293	0.000	0.003	-0.919	-1.530	-0.967
Q6ZQ38	Cand1	0.009	0.057	-0.021	0.028	0.000	-0.389	-0.813	-0.557
Q6PDI5	Ecm29	0.133	0.297	0.000	-0.153	0.001	0.008	-1.570	-1.600
Q6PB66	Lrpprc	0.035	0.125	0.000	0.121	-0.292	0.941	0.428	0.430
Q62351	Tfrc	0.848	1.000	1.330	0.000	-0.491	1.130	-0.397	-0.350
Q62077	Plcg1	0.003	0.033	-0.125	0.000	0.471	-1.190	-1.370	-1.750
Q61823	Pdcd4	0.011	0.065	-0.098	0.000	0.177	-1.090	-2.030	-1.100
Q61081	Cdc37	0.002	0.027	0.019	0.000	-0.009	-0.837	-1.370	-1.050
Q60932	Vdac1	0.006	0.046	0.000	0.313	-0.052	1.240	1.010	1.700
Q60931	Vdac3	0.007	0.050	0.000	0.252	-0.058	1.080	0.902	1.570
Q60787	Lcp2	0.009	0.057	-0.096	0.845	0.000	-1.390	-1.550	-1.040
Q60631	Grb2	0.005	0.041	-0.091	0.403	0.000	-1.080	-1.510	-0.944
Q3UUV5	Skap1	0.002	0.023	-0.314	0.000	0.236	-1.930	-2.300	-1.630
Q3UPF5	Zc3hav1	0.070	0.193	-0.342	0.000	0.012	-0.376	-0.579	-0.367
Q3UND0	Skap2	0.206	0.403	0.518	0.000	-0.624	-0.258	-0.599	-1.130
Q3TBT3	Tmem173	0.649	0.925	-0.395	0.164	0.000	-0.291	-0.323	0.074
Q1HFZ0	Nsun2	0.102	0.247	0.289	0.000	-0.086	-0.029	-1.110	-0.849
Q03526	Itk	0.005	0.041	0.620	-0.355	0.000	-2.150	-1.480	-1.840
Q01965	Ly9	0.539	0.807	0.248	-0.106	0.000	-0.213	-0.306	0.254
P97370	Atp1b3	0.009	0.056	0.000	0.096	-0.048	0.414	0.419	0.703
P70218	Map4k1	0.001	0.015	-0.001	0.000	0.020	-0.901	-1.290	-1.110
P70168	Kpnb1	0.204	0.400	-0.040	0.088	0.000	-0.081	-0.545	-0.064
P68254	Ywhaq	0.006	0.046	-0.139	0.000	0.050	-0.858	-1.630	-1.230
P63101	Ywhaz	0.001	0.015	0.000	-0.021	0.113	-1.140	-1.610	-1.370
P63037	Dnaja1	0.340	0.580	0.072	0.000	-0.107	0.131	-0.492	-0.294
P62259	Ywhae	0.027	0.105	0.000	0.068	-0.183	-0.420	-1.160	-0.884
P61982	Ywhag	0.016	0.078	0.076	0.000	-0.065	-0.399	-0.977	-0.678
P61290	Psme3	0.001	0.021	0.000	0.420	-0.049	-1.120	-1.150	-1.340
P54775	Psmc4	0.018	0.083	-0.123	0.000	0.106	-0.391	-0.884	-0.580
P49718	Mcm5	0.432	0.688	0.140	0.000	-0.032	0.135	-0.802	-0.001
P43404	Zap70	0.038	0.131	-0.465	0.041	0.000	-0.669	-0.946	-0.589
P42227	Stat3	0.103	0.250	0.000	-0.155	0.131	-0.089	-0.977	-0.688

P42225	Stat1	0.005	0.039	-0.079	0.271	0.000	-0.603	-0.992	-0.866
P39688	Fyn	0.582	0.853	-0.633	0.103	0.000	-0.287	-0.529	-0.169
P39054	Dnm2	0.326	0.562	0.075	-0.001	0.000	0.448	-0.098	0.271
P36371	Tap2	0.787	1.000	-0.225	0.273	0.000	-0.153	-0.078	0.133
P27870	Vav1	0.049	0.154	0.325	0.000	-0.114	-0.272	-1.240	-1.350
P26450	Pik3r1	0.468	0.727	0.000	0.958	-0.100	-0.021	0.030	0.038
P26039	Tln1	0.041	0.137	0.059	0.000	-0.282	-0.358	-1.020	-1.000
P25206	Mcm3	0.066	0.185	0.280	0.000	-0.196	-0.205	-1.110	-0.943
P24161	Cd247	0.811	1.000	-0.617	0.000	0.247	-0.627	0.147	0.420
P24063	Itgal	0.054	0.163	-0.246	0.010	0.000	-0.641	-0.514	-0.247
P22682	Cbl	0.000	0.013	-0.024	0.000	0.154	-1.190	-1.550	-1.380
P22646	Cd3e	0.501	0.766	-0.349	0.000	0.371	-0.475	-0.277	0.156
P19783	Cox4i1	0.004	0.038	0.100	-0.024	0.000	0.711	0.422	0.696
P11942	Cd3g	0.167	0.349	-0.367	0.000	0.062	-0.670	-0.495	-0.158
P11352	Gpx1	0.131	0.294	0.457	0.000	-0.235	-0.028	-0.804	-0.877
P08113	Hsp90b1	0.004	0.035	0.176	0.000	-0.151	1.090	0.696	0.949
P04235	Cd3d	0.281	0.504	-0.353	0.097	0.000	-0.435	-0.393	-0.084
P01851	Tcb2	0.061	0.176	-0.290	0.000	0.247	-0.718	-0.420	-0.372
O89100	Grap2	0.049	0.154	-0.257	0.110	0.000	-0.559	-2.360	-1.760
O54957	Lat	0.507	0.771	-0.255	0.567	0.000	0.081	0.134	0.862
O54734	Ddost	0.002	0.025	0.000	0.042	-0.469	1.490	1.120	1.220

Supp. Table 4. Proteins related to TCR signalosome were detected in $CD4^+$ T cells isolated from old mice after mito-transfer and in non-manipulated $CD4^+$ T cells from old mice. $CD4^+$ T cells from young and old mice, and from old mice after mito-transfer were cultured for 4 h before processing for mass spectrometry analysis. Data expressed as median protein Log2 fold change of $CD4^+$ T cells from old mice, from 3 individual old mice (paired experiment)